EUB/AGS Earth Sciences Report 2006-04

Structure Mapping for the Clear Hills–Smoky River Region Using Well-Log Data and Geostatistical Analysis

Alberta Energy and Utilities Board
Alberta Geological Survey

AGS

EUB/AGS Earth Sciences Report 2006-04

Structure Mapping for the Clear Hills–Smoky River Region Using Well-Log Data and Geostatistical Analysis

S. Mei

Alberta Geological Survey

May 2006

ISBN 0-7785-3842-7

Mei, S. (2006): Structure mapping for the Clear Hills–Smoky River region using well-log data and geostatistical analysis; Alberta Energy and Utilities Board, EUB/AGS Earth Sciences Report 2006-04, 89 p.

Published May 2006 by:
Alberta Energy and Utilities Board
Alberta Geological Survey
4th Floor, Twin Atria Building
4999 – 98th Avenue
Edmonton, Alberta
T6B 2X3
Canada

Tel: (780) 422-3767 (Information Sales)
Fax: (780) 422-1918
E-mail: EUB.AGS-Infosales@gov.ab.ca
Website: www.ags.gov.ab.ca

Contents

Tables

Figures

Acknowledgments

The author thanks Reg Olson for constant understanding, encouragement and support of this study, and Kevin Parks for support of advanced study in geostatistics. The Applied Stratigraphy Research Group (ASRG) of University of Calgary provided refined formation picks for Montney and Belloy formations. The author has benefited from discussions with Charles Henderson from the University of Calgary and Alberta Geological Survey colleagues Willem Langenberg, Matt Grobe, Roy Eccles and Laurence Andriashek during the course of the project. Reg Olson and Jill Weiss provided opportunities for observing the regional geology; Desmond Wynne and Andre Lytviak provided assistance with access to the AGS well log database. Charles Henderson and Willem Langenberg are thanked for scientific review and Bob Davie of RnD Technical for editorial review.

Abstract

The present study was initiated to provide updated information on subsurface structures for the region of the Clear Hills (Peace River) ironstone deposits in northwestern Alberta. The objectives were to

- develop an effective structure-mapping methodology for the Alberta Basin using large well-log datasets and geostatistical analysis; and
- provide a refined structure framework for the region of the Clear Hills ironstone deposits.

The methodology developed is a refined approach to the mapping of subsurface structures that incorporates trend-surface analysis and surface-fitting techniques into the conventional well-log interpretation workflow. The trend-surface analysis is first used to separate formation picks into a component of regional dip/trend and a residual component of local structures using polynomial regression. Then, the residuals are fitted by a representative surface using kriging. In both steps, existing geological knowledge about the regional and local structures is incorporated as constraints in both modelling the trend and interpolation of the residual surface. Finally, the linear patterns of formation-top offset are extracted from the residual surface using a moving window neighbourhood statistics method. Lineaments are then interpreted and digitized from the resultant maps. The trend-surface analysis is also applied to the isopach data calculated from two sets of formation-top picks, in order to differentiate syndepositional faults from postdepositional faults.

The methodology developed has a higher resolution in detecting formation-top offsets and higher accuracy in digitizing fault locations compared the conventional contour-map, seismic-section and aeromagnetic-data interpretation techniques in structure mapping for the sedimentary cover. The result is a significant update to the structure framework of the Peace River Arch region, which has been the focus of structure study for decades. Lineaments, interpreted from the linear offset pattern of formation tops extracted with the refined approach, have been identified from each of 14 formation tops (including the Precambrian top) and traced through most of the sedimentary cover. Many of these lineaments were found to be associated with known major faults that had been previously interpreted from well-log and seismic interpretations. This suggests that the linear offset patterns extracted with the refined approach in the study area are related mainly to faults rather than differential compactions. The effect of the possible differential compaction has been mostly removed with the trend. The Dawson Creek Graben Complex (DCGC) has been reinterpreted using this new approach. A different structure pattern was identified from the Triassic and Lower Jurassic formation tops. Activation of the DCGC in the Late Cretaceous has been identified with direct evidence. Some of the faults (e.g., Josephine Creek, Farmington, Gordondale, Belloy (Dunvegan), Fairview, Bluesky, Berwyn, Normandville (Tangent), Whitemud, Hines Creek and Beaton Creek faults) were identified as steep and/or listric faults and have offset formation tops from the Upper Cretaceous through the Paleozoic and down to the top of Precambrian. They could be the possible pathways/conduits for the hydrothermal venting hypothesis for the origin of the ooidal ironstone deposit.

1 Introduction

In 2004, the Alberta Geological Survey (AGS) launched a project to study the geology, metallurgy and economics of the Clear Hills (Peace River) ooidal ironstone deposits within the Upper Cretaceous Bad Heart Formation, which is the largest undeveloped iron resource in western Canada. The Clear Hills ironstone deposits overlap the well-known Peace River Arch (PRA) region, which is characterized by a long-lived zone of structural disturbance in the Western Canada Sedimentary Basin (WCSB) that affected sedimentation and the resulting subsurface stratigraphy (e.g., Pană et al., 2001). Previous study suggested that basement faults have commonly influenced the distribution of hydrocarbon traps and mineralization zones in the WCSB (Lyatsky et al., 1998, 1999; Edwards et al., 1998), and that Precambrian faults may have reactivated during the Cretaceous (O'Connell et al., 1990; O'Connell, 1994; Eccles et al., 2002). Reactivated Precambrian faults may have controlled the deposition, geometry and grades of the Upper Cretaceous Bad Heart Formation ooidal ironstones (e.g., Donaldson et al., 1998, 1999; Clear Hills–Spirit River–Smoky River, Bad Heart Formation Ooidal Ironstone, Field Trip Guidebook, R.A. Olson et al., work in progress, 2005). It has also been postulated that upward movement of hypersaline brines and related hydrothermal venting along reactivated Precambrian faults may have resulted in the local deposition of the ferruginous ooidal facies (Olson et al., 1999; Collom, 2001; Collom and Johnston, 2001). The present study was therefore initiated as a structure component of the AGS Clear Hills project to provide information on subsurface structure that may be critical in characterization of the Clear Hills iron deposits.

Basement structures of the WCSB, detected mainly through the use of potential-field geophysical data, were differentiated by Lyatsky et al. (1999) into

- Archean and Early Proterozoic ductile orogenic structures, and
- Middle Proterozoic to Recent brittle cratonic structures

Although the ancient ductile basement structures predominate in potential-field maps, it is the brittle, high-angle and block-bounding faults that had the most influence on the evolution of the WCSB. The brittle faults partly follow the older ductile orogenic structures, but also commonly cut across them. These steep, brittle basement faults are much more subtle and less easily detectable in potential-field maps; many of them are below the resolution of seismic-data (Lyatsky et al., 1999). Ross and Eaton (1999) differentiated the basement faults based on differences in their magnetic and seismic expression into the following two types:

- Precambrian faults that were reactivated during the Phanerozoic and are recognized by a close correlation with basement magnetic and seismic data are referred to as "intrabasement" faults
- Phanerozoic faults that show no correlation with basement magnetics and seismic reflection data are referred to as "suprabasement" faults

The ultimate test of the basement reactivation comes from geological evidence from the sedimentary cover. It is necessary to trace extension or influence of the basement faults in the sedimentary cover so as to identify those that could be related to the deposition of the Bad Heart Formation ooidal ironstones. As a result, the present study is focused on structure mapping of the sedimentary cover.

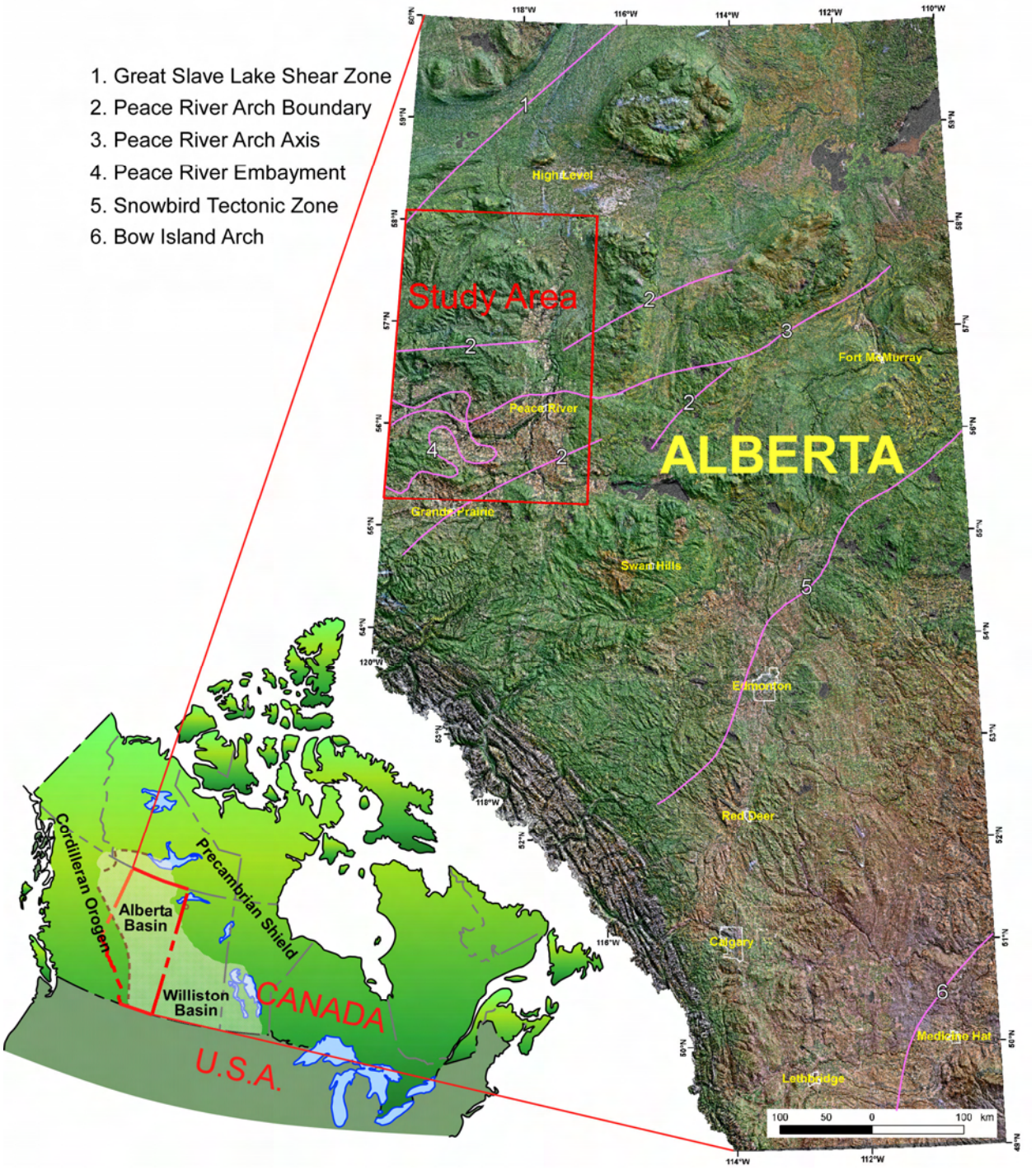

Figure 1. Location of the study area. The image of Alberta is created by fusing a Landsat image with a sunshade relief image of digital elevation model (DEM) from the Shuttle Radar Topography Mission (SRTM). Labelled structure elements are from Wright et al. (1994) and O'Connell (1994). The Landsat image used was provided by PhotoSat Information Ltd. and the SRTM data used were provided by the Earth Resources Observation and Science (EROS) Data Center, United States Geological Survey.

The study area represents part of the Alberta Basin in the WCSB, which is almost entirely covered by Pleistocene glacial drift and boreal forestry (Figure 1). As a result, the understanding of the bedrock geology of the Alberta Basin is based mainly on information from well-logs and drillcores. Formation

picks, interpreted from well-logs, are routinely used to construct structure-top and isopach contour maps for structure interpretation (e.g., Mossop and Shetsen, 1994). This is often augmented with seismic data when available. Although numerous subsurface faults were previously interpreted for the sedimentary cover, they were interpreted from separated stratigraphic horizons, using different data spacings and by different authors at different times. A compilation of the faults of northern Alberta (Pană et al., 2001) indicates that some of the faults interpreted from different stratigraphic horizons may represent the same or reactivated faults. According to the compilation, most of the Phanerozoic faults were interpreted from Palaeozoic strata, and only two of the faults were from the Lower Cretaceous and four were from the Upper Cretaceous Bad Heart Formation, which is the target of the present study. It is not clear which of these faults interpreted from the older strata were still active, and/or whether additional new faults existed, around the time of deposition of the Bad Heart Formation.

The AGS has access to the well-log database of the Alberta Energy and Utilities Board (EUB) for the Alberta Basin, with numerous picks for geological formations that have been generated, refined and accumulated by industry, university and government organizations, including the AGS itself, for decades. One of the crucial signatures of or clues to faults in the sedimentary cover is significant offsets in the formation tops and the resulting changes in formation thickness, which can be detected by conventional well-log and seismic interpretation approach. The formation picks, however, also contain a great deal of information on minor and subtle offsets in formation picks that are often caused by faults at different scales but are beyond the resolution of conventional well-log and seismic interpretation technique. Much of the information on faults associated with small offsets in formation tops remains buried in vast datasets of well-log data. It is these faults, however, that are probably more closely related to the Clear Hill ooidal ironstone deposits (e.g., Donaldson et al., 1999). Even with minor offsets and subresolution seismically, Precambrian brittle faults and block movements may exert considerable syn- and postdepositional influence on the sedimentary cover. Basement control on the sedimentary cover might be episodic, locally variable and commonly indirect, and even unreactivated brittle faults with minor to zero offsets might have affected fluid flow, salt dissolution and carbonate alteration. Thus, identification of such local faults in the sedimentary cover has mineral exploration significance. The present study attempts to apply geostatistical analysis to resolve this information. Determination of such information on offsets in different formation tops throughout the sedimentary section provides a direct and effective means of mapping and tracing faults throughout the sedimentary cover. This study therefore has two objectives:

- Develop an effective structure-mapping methodology for the Alberta Basin, using large well-log datasets and geostatistical analysis
- Provide a refined structure framework for characterizing the Clear Hills iron deposit

2 Study Area

The study area (Figure 2) extends from 55.3°N to 58.1°N (i.e., from the southern margin of Twp 74 north to the northern margin of Twp 105) and from 116.5° W to 120.2°W (i.e., from the eastern margin of Rge. 16, W 5^{th} Mer. west to the Alberta–British Columbia border, roughly the western margin of Rge. 13, W 6^{th} Mer.). This area includes the Clear Hills and the Halverson Ridge as the core area, the Chinchaga River valley to the northwest of the Halverson Ridge, and the Peace River valley to the east and south of the Clear Hills. To the northwest of the Chinchaga River valley is the Chinchaga Hills, which forms the northwestern corner of the study area. To the south of the Peace River are the Saddle Hills, forming the southwestern corner of the study area, and the Smoky River and the Little Smoky River, forming the Southeastern corner. Except for the farmlands along the Peace River valley, the study area is covered by boreal forest.

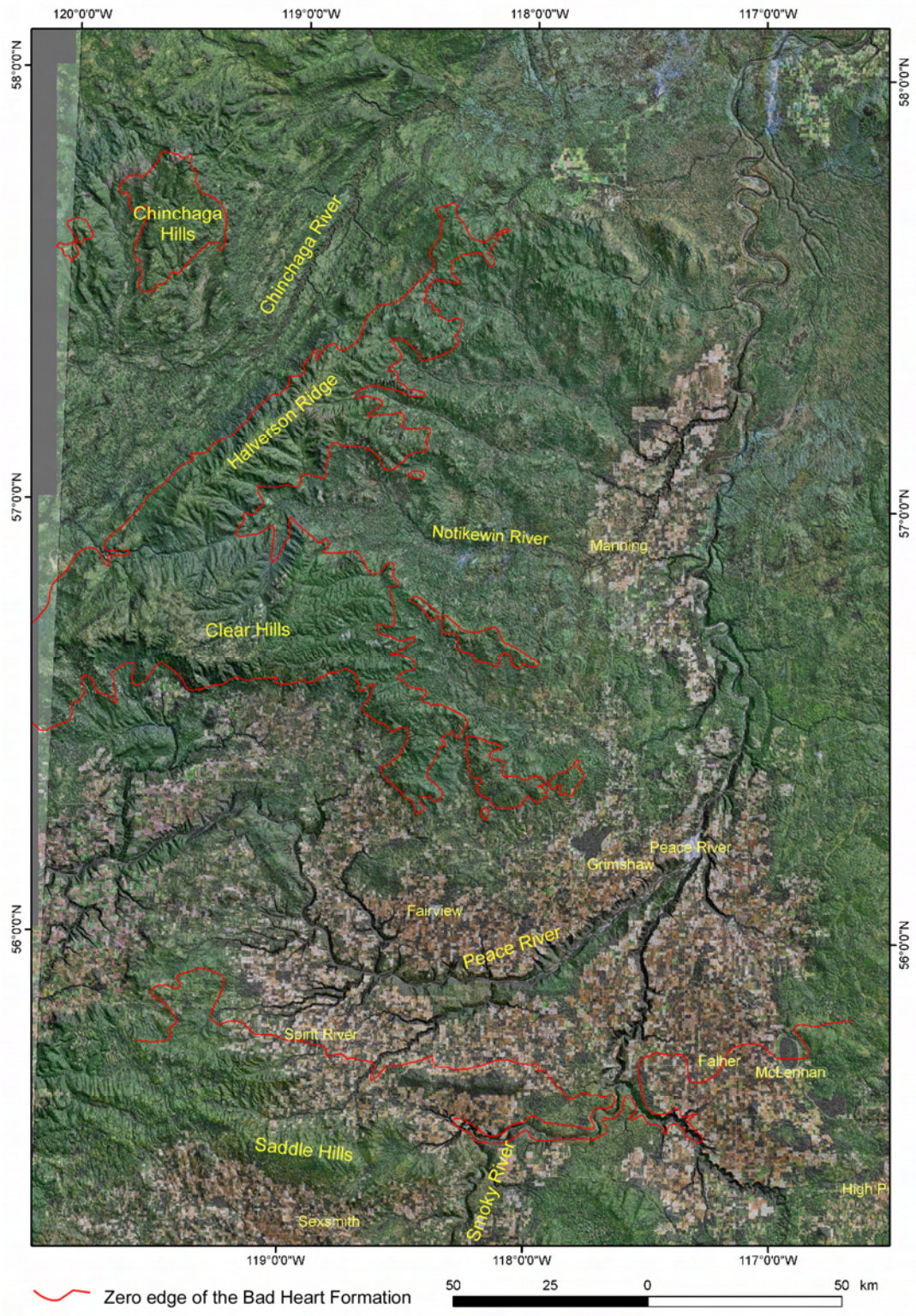

Figure 2. Satellite image of the study area created by fusing a Landsat image with a sunshade relief image from the Shuttle Radar Topography Mission (SRTM). The Landsat image was provided by PhotoSat Information Ltd. and the SRTM data were provided by the Earth Resources Observation and Science (EROS) Data Center, United States Geological Survey.

The Clear Hills and the Halverson Ridge originated as post-Cretaceous monadnocks, and the former dissected upland is now mantled by Pleistocene unconsolidated glacial and alluvial deposits (Hamilton, 1980). The glacial deposits range in thickness from zero to 20 m and consist largely of pebbly clay till in ground moraine or hummocky disintegration moraine in the highland area, and glaciolacustrine clay with sparse pebbles in the farmed lowland area (Green and Mellon, 1962). The glaciolacustrine sediments were deposited by glacial Lake Peace, which was formed as a large proglacial lake during deglaciation along the retreating ice margin (Mathews, 1980; Lemmen et al., 1994; Dyke, 2004).

Bedrock immediately underlying the glacial deposits is Cretaceous marine and non-marine sandstone, alternating with marine mudstone or shale. The formations are nearly flat lying, with a gentle regional dip to the southwest. Figure 3 shows the bedrock geology of the study area and the adjacent portion of British Columbia, which extends from 120ºW to 122ºW. The oldest rocks in this region are shale and sandstone of the Lower Cretaceous Loon River Formation and Peace River Group in the northeast, and sandstone and shale of the Upper Jurassic to Lower Cretaceous Minnes Group and Lower Cretaceous Bullhead and Fort St. John groups in the southwest. The Shaftesbury Formation represents the base of the Upper Cretaceous and underlies the lowlands adjacent to Hay River in the northwest, and Chinchaga River and Peace River in the northeast and southwest, respectively. It consists of dark grey marine shale with laminated siltstone interbeds that increase near the top of the sequence, and increases in thickness toward the east in the Clear Hills area (Green and Mellon, 1962, 1970). Overlying the Shaftesbury Formation is the Dunvegan Formation, which consists of carbonaceous, medium- to coarse-grained, crossbedded sandstone with interlayered siltstone and mudstone. It underlies the lower slopes of the Chinchaga and Milligan hills, and the lowlands adjacent to the Chinchaga, Notikewin and Peace rivers in Alberta. Overlying the Dunvegan Formation. is the Smoky Group, comprising a thick sequence of predominantly shale. It underlies the upper part of the Milligan and Chinchaga hills, the upper slope of the Halverson Ridge and the Clear Hills, and Peace River and Smoky River valleys to the south of the Clear Hills. In the Clear Hills and Halverson Ridge area, the Smoky Group consists of, in ascending order, the Kaskapau Formation (60-120 m of predominately marine mudstone), the Bad Heart Formation (5-9 m of argillaceous quartzose sandstone and/or ferruginous ooidal ironstone) and the Puskwaskau Formation (about 90-180 m of predominately marine dark grey mudstone). The youngest rocks in the region are referred to as the Wapiti Formation, which consists of nonmarine sandstone and shale and forms the caps of Halverson Ridge, Clear Hills and Saddle Hills.

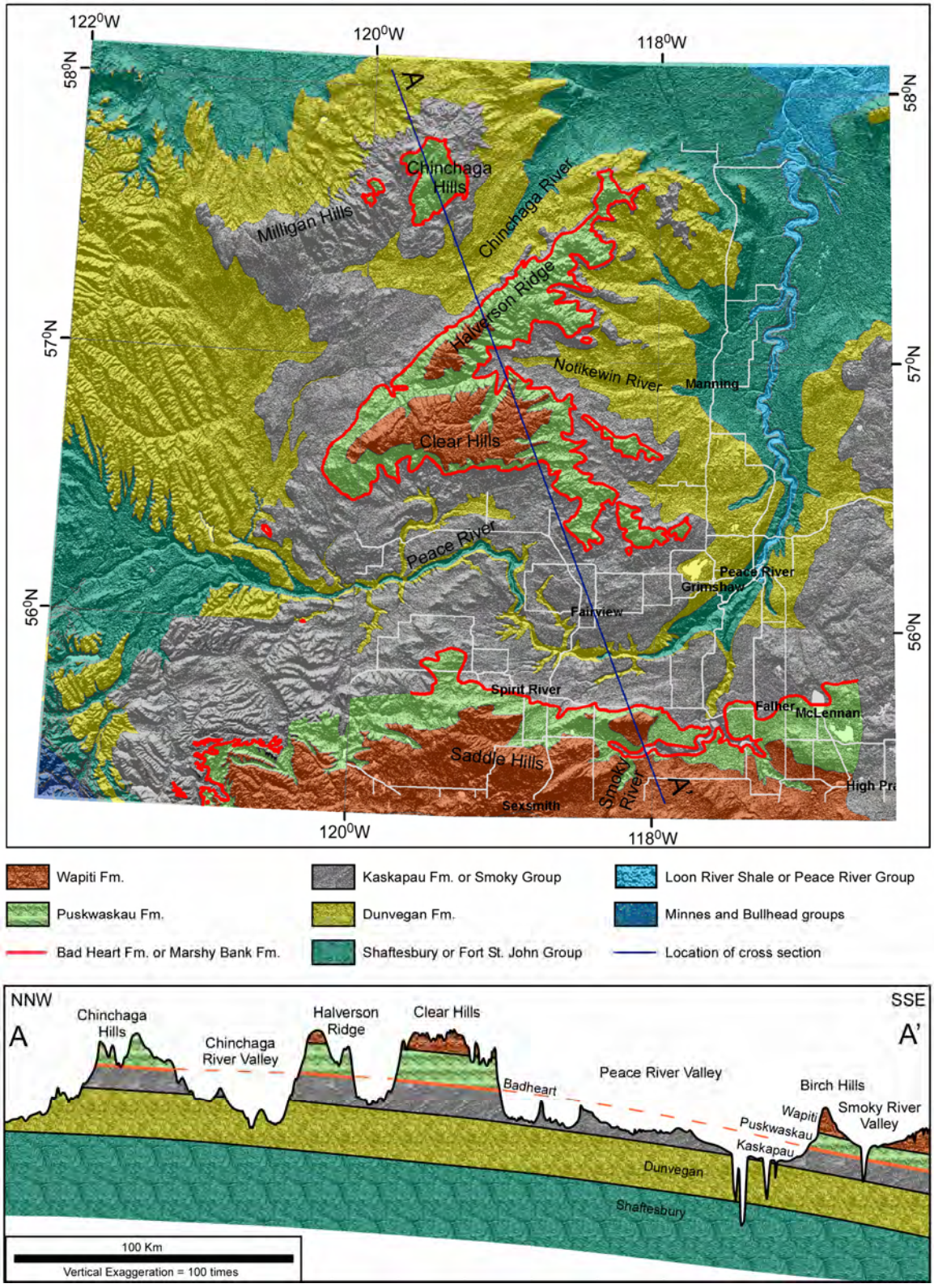

Figure 3. Bedrock geology of the study area and adjacent portion of British Columbia (west of 120⁰W) compiled from the Geological Map of Alberta (Hamilton et al., 1999) and the Digital Geology Map of British Columbia (Massey et al., 2005); (downloaded from http://www.em.gov.bc.ca/Mining/Geolsurv/Publications/catalog/bcgeolmap.htm).

3 Previous Work

The ancestral western continental shelf of North America is separated into at least six major blocks by northeast-trending linear features, which are interpreted to represent ancestral strike-slip or transfer faults (Cecile et al., 1997). Each of these blocks has an independent tectonic history. Among them is the Alberta block, which is bordered to the north by the Hay River–Great Slave Lake tectonic zone and to the south by the Moyie and Dibble Creek faults near the Alberta-Montana border. The Alberta block is further divided into the Peace River sub-block and the Southern Prairies sub-block along the Rimbey Magnetic and Snowbird Tectonic zones (Cecile et al., 1997). The study area lies within the Peace River sub-block.

The geological history of the Alberta Basin has been divided into three main tectonic phases (e.g., Price, 1994; Ross and Eaton, 1999). The first phase is Late Proterozoic to early Paleozoic extension and continental break-up, and is represented by passive margin deposition with periodic exposure up to the Late Silurian. The second phase consists of several loosely constrained tectonic environments during the Devonian to Early Jurassic, including the Devonian–Early Carboniferous development and collapse of the Peace River Arch, which is contemporaneous with the Antler Orogeny in the Great Basin of the united States. The third phase begins with deposition of Jurassic Fernie Group turbidites, and is represented by Jurassic to Eocene foreland-basin development during formation of the Cordilleran fold-and-thrust belt, which is followed by isostatic recovery and erosion throughout the Tertiary.

The Peace River Arch (PRA) region is a roughly east-northeast-striking zone cutting across the WCSB in which a long history of tectonic activity in the WCSB has been recorded. It was suggested that basement faults were active over an extended period of time or reactivated episodically through time, and controlled the Phanerozoic sedimentary patterns in this region (e.g., Cant, 1988; Pană et al., 2001). The tectonic evolution of this region has been divided into three distinct phases (Cant, 1988; O'Connell et al., 1990): pre-Late Devonian Peace River Arch (PRA, sensu stricto), Carboniferous to Triassic Peace River Embayment (PRE), and Jurassic and Cretaceous downwarping.

The pre-Late Devonian PRA formed a topographic high throughout the early Paleozoic and served as the source of clastic sediments that were deposited within and along the Cordilleran miogeocline (McMechan, 1990; Norford, 1990; Ross et al., 1993; Gehrels et al., 1995; Ross and Villeneuve, 1997; Gehrels and Ross, 1998). The PRA reached a maximum width of 140 km at the sixth meridian (118ºW) and a maximum elevation of about 1000 m above the surrounding WCSB (Cant, 1988; O'Connell et al., 1990). It was an asymmetrical structure with a steeply dipping northern flank and a more gently dipping southern slope (O'Connell et al., 1990). The total deposition immediately north of the arch was several hundred metres thicker than it was to the south.

The Peace River Embayment (PRE) was initiated during the Early Carboniferous when an elongated zone of maximum subsidence formed along the northern margin of the Devonian PRA. It marked a stage beginning with topographic reversal from a highland arch to an embayment, and experienced enhanced subsidence relative to other parts of the WCSB that persisted at least through the Triassic (e.g., Beaumont et al., 1993). The continued tectonic inversion during the Late Carboniferous resulted in localized subsidence along the former axis of the Devonian PRA, forming a system of grabens referred to as the Dawson Creek Graben Complex (DCGC) (Barclay et al., 1990; Richards et al., 1994). The DCGC consists of the Fort St. John Graben, the principal seaward opening in the west, and the Hines Creek, Whitelaw and Cindy satellite grabens in the east. The Carboniferous DCGC was followed by more widespread subsidence during the Permian and Triassic.

The PRE was followed by a downwarping phase during the Jurassic and Cretaceous that is coeval with the initiation and evolution of thrust loading (Columbian and Laramide orogenies) in the Cordilleran Orogen (O'Connell et al., 1990). This phase is represented by overall enhanced subsidence. It has been suggested that many minor structural offsets within units throughout the Cretaceous may have been

caused by reactivation of the underlying PRA-DCGC structure (Cant, 1988; Hart and Plint, 1990). It is also noteworthy that evidence from thickness and facies variation throughout Jurassic and Cretaceous strata indicates that the subsidence may be controlled by the underlying DCGC structures. Poulton et al. (1990) reported that minor thickness variation in Jurassic strata coincides geographically with the axis of the Fort St. John and Hines Creek grabens. A northeast-trending thickening within the Gething Formation of the Lower Mannville Group coincides with the location and orientation of the underlying DCGC (Stott, 1973; Smith et al., 1984; Gibson, 1992; Cant and Abrahamson, 1996). A large northeast-trending sand body within the Bluesky Formation at the base of the Upper Mannville Group was found to be contained within the structural boundaries of the DCGC, suggesting that renewed subsidence of the DCGC resulted in the preferential preservation of this sand unit (O'Connell et al., 1990; O'Connell, 1992). Additional post-Mannville-equivalent strata (Harmon and Cadotte members of the Lower Cretaceous Peace River Formation) are preserved beneath the post-Mannville unconformity in the area of the PRA-PRE, which was attributed to a mild downwarping of the PRE subsequent to deposition of the Mannville Group (Smith, 1994). The PRA-PRE area also served as a boundary area, during the deposition of the Upper Mannville Group and the Peace River Formation, with different facies to the north and south (e.g., Smith, 1994). During deposition of the Upper Mannville, an area of enhanced subsidence developed parallel to the trend of the DCGC and overlies its southern margin. At the southern edge of the basin, a series of the Upper Mannville Group shoreline units are stacked one on top of one another (Cant, 1984; Smith et al., 1984), suggesting that rapid subsidence prohibited the northward progradation of these shorelines (Cant, 1984, 1988; Leckie, 1986). Within the Cadotte Member, an abrupt transition from shoreline sandstone to offshore shale was found to overlap with a hinge that extends from the axis of the Fort St. John graben to the axis of Hines Creek graben (Leckie et al., 1990). This shoreline is also paralleled by an incised fluvial-estuarine system at the base of the overlying Paddy Member. A detailed lithostratigraphic study in the Saddle Hills area suggests that the Gordondale, Rycroft and Dunvegan faults of the DCGC appear to have been reactivated during deposition of the Lower Kaskapau Formation (Kiernan, 1996).

Numerous lineaments and/or faults have been interpreted as resulting from the long-lived tectonic activity in the PRA-PRE area. The term 'lineaments' is used herein to denote any linear feature interpreted from structure-top contour, isopach contour and facies maps, and the term 'faults' is used herein to include the lineaments that have been confirmed to have real structural offset. The previously interpreted lineaments have been compiled into GIS format by the AGS (Pană et al., 2001). Figure 4 shows lineaments that are believed to be related to the Precambrian basement in the study area. These lineaments include those interpreted from structure contour maps of Devonian formations (Barss et al., 1970; Cant, 1988; O'Connell, 1994), geophysical logs (Sikabonyi and Rodgers, 1959; Cant, 1988; Burwash et al., 1994), aeromagnetic potential field data (Ross et al., 1994; Geiger and Cook, 2001), magnetotelluric data (Boerner et al., 1997) and oxygen isotope anomalies in the Precambrian basement (Burwash et al., 2000).

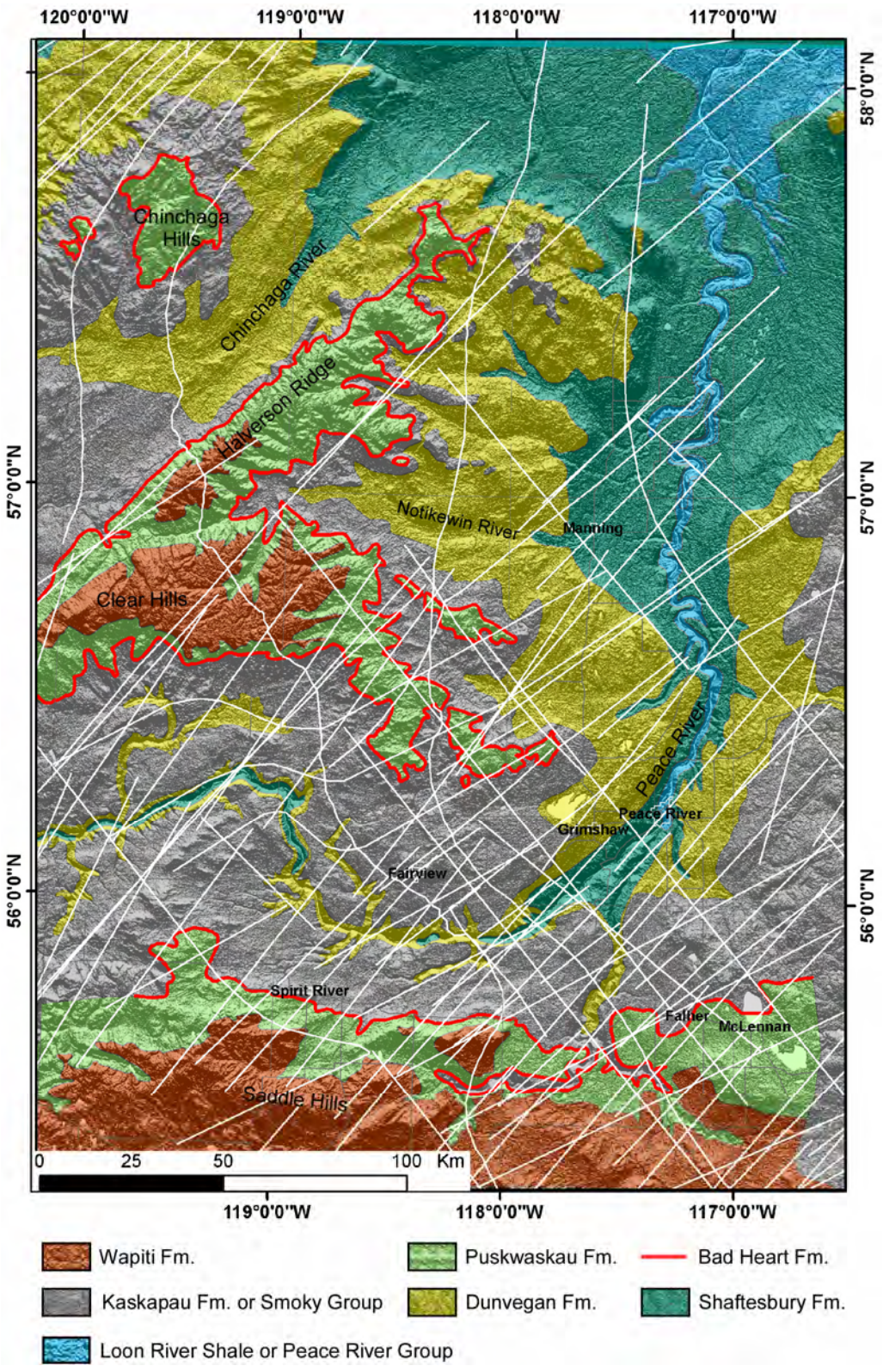

Figure 4. Previously interpreted Precambrian lineaments (indicated by white lines; from Pană et al. (2001), superimposed on the bedrock geology map.

Figure 5 shows lineaments previously interpreted from the Devonian Strata. These lineaments were interpreted from facies changes (Sikabonyi and Rodgers, 1959), geophysical logs and structure-contour maps (Jones, 1980; O'Connell, 1994).

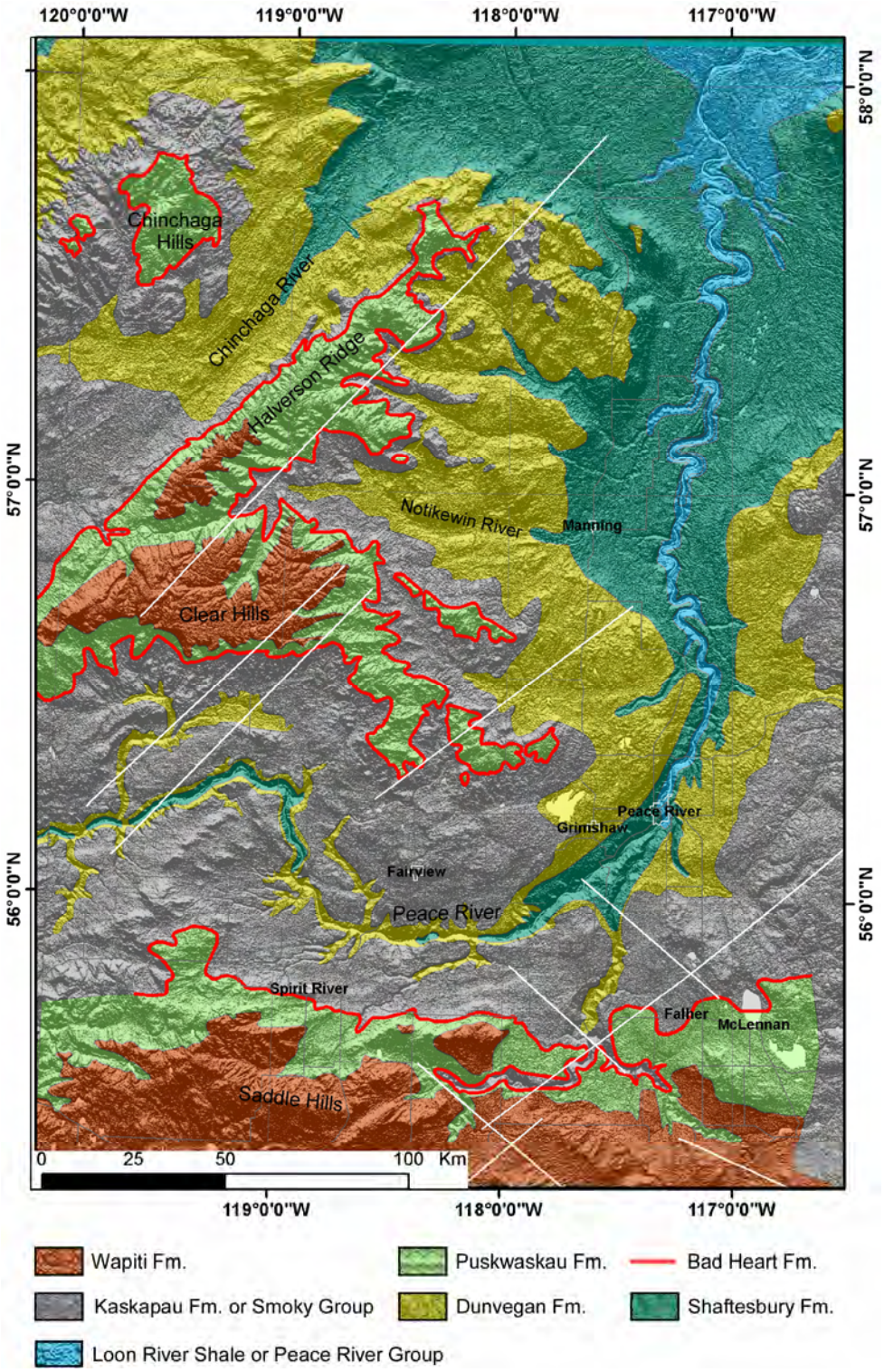

Figure 5. Previously interpreted Devonian lineaments (indicated by white lines; from Pană et al. (2001), superimposed on the bedrock geology map.

Figure 6 shows lineaments previously interpreted from Carboniferous and Permian strata. These lineaments were interpreted from structure-contour maps (Sikabonyi and Rodgers, 1959; Cant, 1988; O'Connell, 1994), geophysical logs (Barclay et al., 1990; Richards et al., 1994; Henderson et al., 1994) and facies changes (Sikabonyi and Rodgers, 1959). Some of them represent the same faults interpreted by different authors, at different times and with differing degrees of detail.

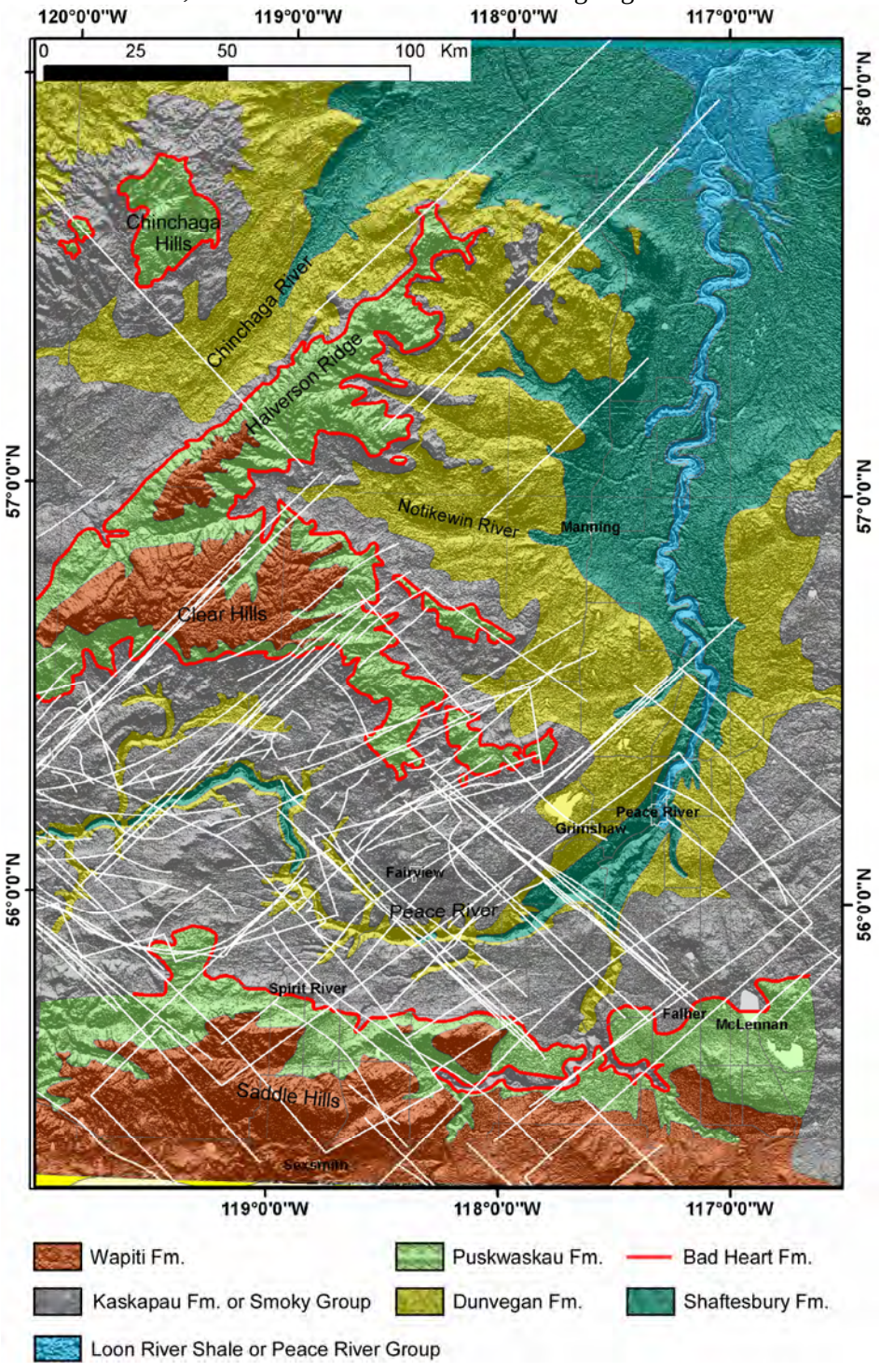

Figure 6. Previously interpreted Carboniferous and Permian lineaments (indicated by white lines; from Pană et al. (2001), superimposed on the bedrock geology map.

Figure 7 shows lineaments previously interpreted from the Lower Cretaceous Upper Mannville Group (O'Connell, 1994) and the Upper Cretaceous Bad Heart Formation (Donaldson et al., 1998). All the lineaments are interpreted from thickness changes.

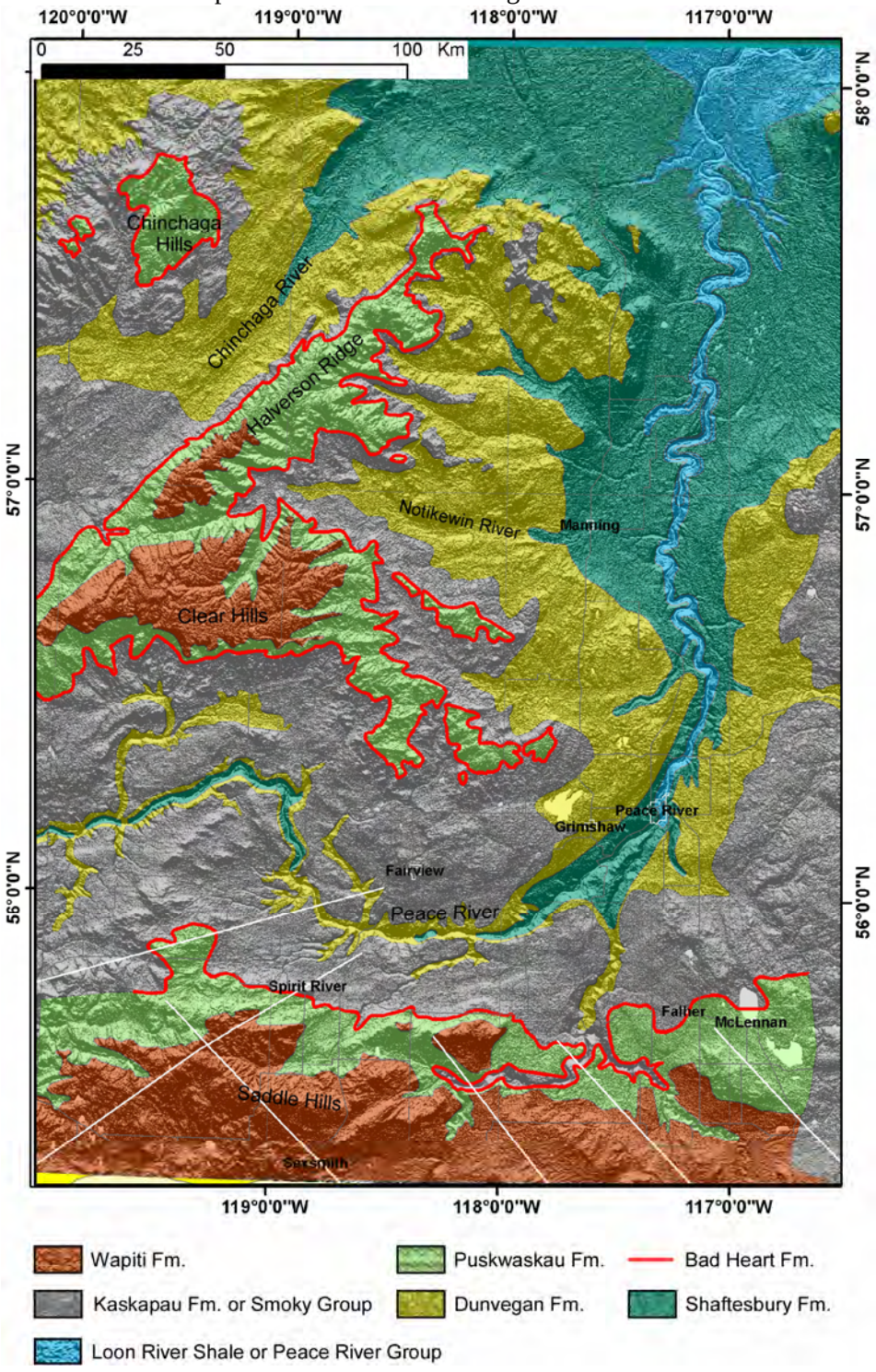

Figure 7. Previously interpreted Cretaceous lineaments (indicated by white lines; from Pană et al. (2001), superimposed on the bedrock geology map.

In summary, most of the lineaments previously interpreted from the sedimentary cover are from the Carboniferous and Permian, and related to the Dawson Creek Graben Complex (DCGC). It is noteworthy that only a very few lineaments are interpreted from Devonian strata and Cretaceous strata relative to those from Carboniferous and Permian strata. It remains unclear which of the DCGC-related faults are associated with the Precambrian lineaments and which of them were still active or were reactivated during the Cretaceous. It is also necessary to examine whether additional new faults were formed during the Columbian (Middle Jurassic–Early Cretaceous) and Laramide (Late Cretaceous–Paleogene) orogenies.

4 Methodology

In general, the conventional approach to structure study uses potential-field data, including aeromagnetic and gravity data, for detecting the basement structures, and geophysical well-log data (combined with seismic data when available) for interpreting the sedimentary cover structures. With respect to well-log data, the main approach is to interpret faults from isopach and structure-top contour maps. For example, descriptions of structures related to the PRA-PRE, as presented by DeMille (1958), Lavoie (1958), Williams (1958), Sikabonyi and Rodgers (1959), Jones (1980), Cant (1988), Barclay et al. (1990), Dix (1990), O'Connell et al. (1990) and O'Connell (1994), are all based on use of well-log and sedimentological data to identify fault locations and trends, as well as magnitudes and types of offset.

The conventional well-log and seismic interpretation techniques have achieved varying success in detecting regional structure and major faults. However, the structure-top contour maps are usually characterized by a regional trend for numerous examples, see Mossop and Shetsen, 1994), and this trend can mask local structure and faults that cause only minor offset (e.g., a few metres). Variations at such a metre-scale dimension on the structure-top contour map usually show as subtle irregularities in contour lines or subtle variations in the spacing of contour lines and are therefore difficult to interpret. In addition, the location of faults can only be poorly defined on the contour maps (e.g., cf. Barclay et al., 1990's Figure 6 with Figure 7). As a result, it is difficult to interpret faults with small offsets by using the conventional structural-top contour approach. These faults are usually beneath the detection resolution of seismic data. The present study attempts to develop a new approach to detecting faults with small offsets using formation picks data, based on trend-surface analysis. It goes one step beyond the conventional approach by incorporating advanced geostatistics for modelling residuals and extracting, from residual surfaces, information on formation-top offset patterns that could be caused by faults.

Similarly, except in a few cases of extensive growth faulting such as the DCGC, the conventional isopach map is usually controlled by a regional subsidence trend (for numerous examples, see Mossop and Shetsen, 1994). The conventional isopach map is useful for identifying regional features such as depositional centres and associated major growth faults. However, most of the growth faults may cause only subtle local subsidence compared to the regional basin subsidence. As a result, the local subsidence caused by local growth faults could be masked by the regional subsidence trend on the conventional isopach contour map. The approach developed in this study applies trend-surface analysis to formation-thickness data to differentiate between a regional subsidence component and a local subsidence component. The local subsidence is then compared to the local formation-top offset pattern to infer whether the interpreted faults are syndepositional growth faults (and have influenced the formation thickness) or postdepositional faults.

4.1 Refined Trend-surface Analysis

Trend-surface analysis has been used by geologists for years to separate an observed contour map into two components: a regional trend and a local fluctuation component (Davis, 1973, 1986, 2002). A vast literature on the application of trend-surface analysis in geology appeared in the 1960s and 1970s (e.g., Krumbein, 1962; Forgotson, 1963; Merriam, 1964; Elliot, 1965; Merriam and Lippert, 1966; Read and

Merriam, 1966; Cook, 1969; Burk, 1970; Doveton, 1970; Stevenson, 1970; Davis, 1973; O'Connor and Gretener, 1974), and several major oil fields related to the Devonian Leduc reefs were discovered in Alberta using this exploration technique (Davis, 1986). This technique appears, however, to have been somehow underutilized in recent years (Evenick et al., 2005). Present-day observed elevations of formation tops resulted from both regional and local processes. In the Alberta Basin, the regional processes are related to the Jurassic to Eocene foreland-basin development during formation of the Cordilleran fold-and-thrust belt, and the local processes are largely related to faults formed throughout the geological history of Western Canada Sedimentary Basin. Trend-surface analysis has been successfully applied in the Alberta Basin to isolate local drape structures on Cretaceous formation tops over the deeply buried Devonian reefs by removal of regional trend (O'Connor and Gretener, 1974; Davis, 1986). With advances in geostatistical analysis and computation capacity, the old trend-surface analysis can be refined for highlighting small offsets that could be related to local-scale faults. The present study uses ArcGIS Geostatistical Analyst™ to achieve this goal.

It is necessary to point out that trend-surface analysis, as practised by geologists, constitutes only a segment of the larger statistical field of regression analysis. It is often confused with the technique of surface fitting or surface modelling. These two applications differ in objectives and underlying assumptions, but their common methodology has obscured these differences. On one hand, trend-surface analysis is designed to separate observed data into regional and residual components: the regional component expresses the large-scale effect or trend influencing the entire map area whereas the residual component is the difference between the observed values and the trend, and represents local effects or anomalies that influence only parts of the map area. In this case, it is assumed that the residual component is largely due to the local structure. The focus is on the local structure and the regional trend component is only of incidental interest. On the other hand, the process of surface fitting is to generate a mathematical surface that fits the observed data as close as possible. The goal is to generate a representative surface of the data that was not obvious because of noise in the data. In this case, the resultant residual component is assumed to represent error or noise, and the goal is to filter it out.

The methodology developed in the present study combines the use of both trend-surface analysis and surface fitting. The trend-surface analysis is used first to separate formation picks into a component of regional dip/trend and a residual component of local structures, using polynomial regression. Then, the residuals are fitted by a representative surface using kriging. In both steps, existing knowledge about the regional and local structures is incorporated as constraints in both modelling the trend and interpolation of the residual surface. Finally, the local variation patterns are extracted from the residual surface using a moving-window neighbourhood statistics method. Lineaments are then interpreted from the resultant maps with local variations in formation tops highlighted.

The steps in this refined trend-surface analysis are demonstrated below using the Upper Cretaceous Basal Fish Scale Zone (BFSZ) as an example. The Basal Fish Scale Zone is a basin-wide log marker that is located near the boundary between the Lower and Upper Cretaceous. It derives its name from the abundant fish remains (scales and skeletal material) it contains. The BFSC can be picked with exceptional consistency on log traces because of the pronounced high gamma response. Figure 8 shows the distribution of about 7600 wells that penetrate the Basal Fish Scale Zone. The wells cover the entire study area except the northeastern part. Figure 9 shows a conventional example of the structure-contour map for the BFSZ, with an interpolated surface as the background. It is dominated by a northeast to southwest regional dip, and this regional feature masks local variations.

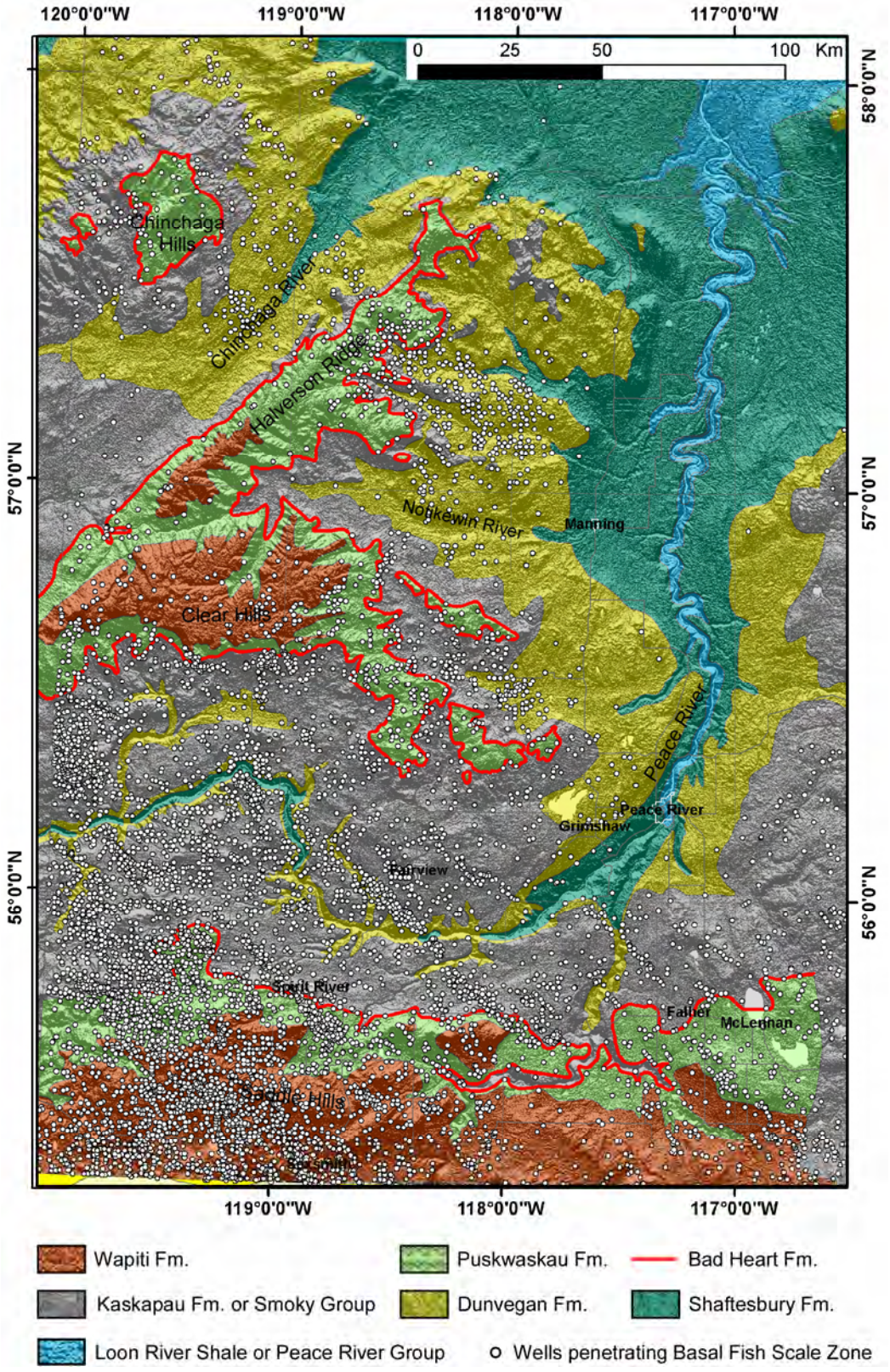

Figure 8. Wells (about 7600 wells in total) that penetrate the Basal Fish Scale Zone (BFSZ), superimposed on the bedrock geology map.

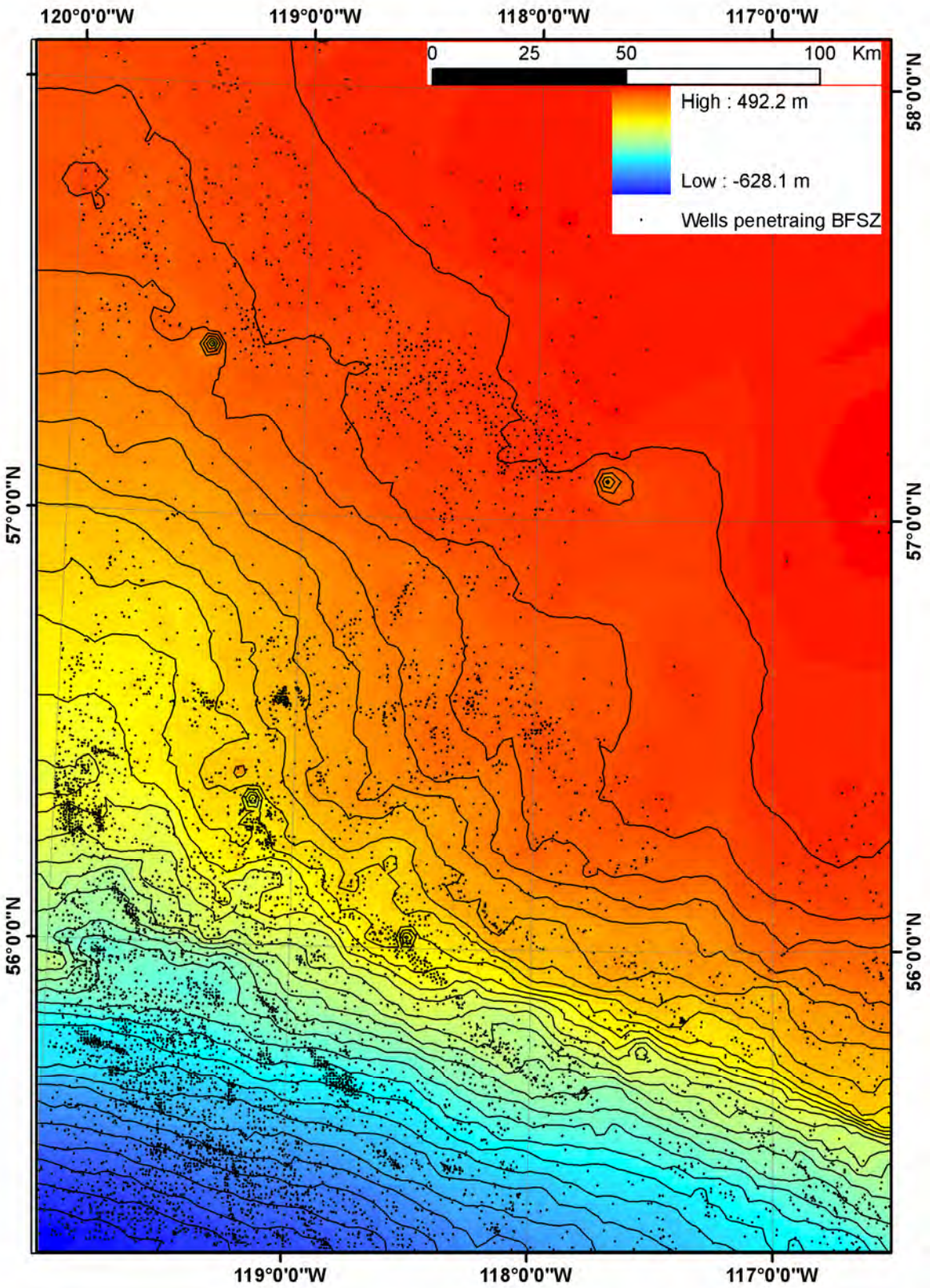

Figure 9. Structure-contour map on the Basal Fish Scale Zone (BFSZ), created using inverse distance weighting (IDW) with a power parameter of 2. Note the dominant regional dip toward the southwest.

4.1.1 Data Cleaning and/or Removal of Outliers

The first step is to prepare the data by dealing with outliers. A global outlier is a measured sample point that has a very high or very low value relative to all values in a dataset. A local outlier is a measured sample point with a value that is within the normal range for the entire dataset but unusually high or low compared to the surrounding points. Outliers, if they are caused by errors, can have several detrimental effects on the interpolated surface and trend-surface modelling. They should either be corrected or removed before creating a surface. A variety of methods, including examining neighbourhood statistics, histogram, semivariogram/covariance cloud and Voronoi maps, is available with ArcGIS for identifying outliers. In addition, the inverse distance weighted (IDW) interpolation method is found to be useful for locating the outlier data points, which appear as bull's-eyes on the interpolated map (e.g., Figure 9). Outliers are repeatedly examined during the course of both modelling the trend and fitting the residuals. In the present study, it was found that the ArcGIS Geostatistical Analyst extension could be used effectively to locate outliers by examining the residuals. This tool allows the user to select those data points with extremely high and low residual values.

4.1.2 Modelling the Trend

The second step is to model the regional features or regional dip or basinal configuration. The objective of modelling the trend is to closely simulate the regional features of the structure-top map so that subtraction of the trend will remove the regional component of structure. In effect, the modelled trend surface is used as a high-pass filter that removes the large-scale structure variation from the map and leaves behind or highlights the small-scale features. Modelling the trend is the most crucial task, as it determines whether the desired information will be best highlighted in the resultant residual map. Separation of the data into regional and local components is entirely subjective, and it is challenging to find the optimal division. Improper decomposition of trend and residual components would result in a residual map that is dominated either by noisy signals (random errors) due to over-removal of trend or by a remaining trend that still masks local features due to under-removal of trend. The process to obtain the best trend surface is the craft of the researcher, their knowledge of the phenomenon being analyzed, and the reasons and goals for the modelling. Modelling of the trend in the present study is constrained by the following considerations:

- **Existing knowledge about the regional features:** Although existing knowledge is limited, the study area is known to be characterized by a northeast to southwest regional dip of the strata in the WCSB, with the Peace River Arch (PRA) superimposed on the regional dip.

- **Size of the regional feature:** The Peace River Arch (PRA)-related feature is about half the size of the study area. This feature can be accounted by the regional compaction over the hard metamorphic rock of PRA.

- **Targeted feature and its size:** The goal is to extract information about local faults, which are represented by offsets on the formation top (i.e., the BFSZ in this example). The fault itself is a linear feature, but its impression on the formation top is usually an elongate zone that is about 1-2 Km wide and extends for up to dozens of kilometres.

- **Scale of the residual to be modelled:** The vertical offset of the formation top caused by faults in the study area is on the order of several to dozens of metres, depending on the stratigraphic horizon, and mostly from a few metres to about 20 metres in Cretaceous formations.

- **Smoothness of the trend surface:** The vertical offset of the formation top caused by faults is represented by relatively abrupt and localized undulations on the formation top. As a result, the

modelled trend surface should be a smooth surface, so that the local nonsmooth undulations can be highlighted.

Among a variety of available interpolation methods, polynomial regression and moving-average techniques, including Kriging, can be used for modelling the trend. Conventionally, global polynomial interpolation has been widely used for geological trend analysis merely as a matter of convenience, because it is straightforward and easy to use, and the polynomial functions can be solved quickly by computer. In addition, only one parameter needs to be decided for trend modelling (i.e., the power value of the polynomial regression). Global polynomial interpolation, however, fits a smooth surface to the entire dataset or study area. As a result, it is not good for modelling subregional trend features that are larger than the local features of interest but smaller than the regional trend for the entire study area. To overcome this limitation, the local polynomial interpolation tool in ArcGIS Geostatistical Analyst fits many polynomials to the data, each within specified overlapping neighbourhoods. Thus, it produces trend surfaces that account for more subregional variation. Since the objective of this study was to extract local offsets possibly caused by faults, local polynomial interpolation was chosen for modelling and removing both regional and subregional trend features. It is flexible because it allows the user to define the size and shape of neighbourhoods, number of points to be included and a power parameter for polynomial regression.

Based on the above-mentioned geological knowledge and constraints, a neighbourhood with a search distance of 76 km and a second-power polynomial were chosen for the BFSZ. A cross-validation of the interpolation yielded a regression line of $y = 1.00x - 0.094$, and a root-mean-square error (RMSE) of 12.79 m. The trend surface modelled for the BFSZ is shown in Figure 10. The two major regional and subregional features, the Western Canada Sedimentary Basin regional dip and the Peace River Arch-related positive feature, are clearly represented. In fact, the modelled surface gives a more realistic picture of the regional features than previously obtained by showing the subtle undulations within the regional and subregional features. The regression line indicates that the interpolation model is unbiased (i.e., it does not underpredict large values or overpredict small values). The RMSE defines roughly the order of average offsets in formation tops that are subsequently going to be modelled. The interest in this application is not statistical estimation, but rather a close simulation of the regional features. As a result, a statistical test of significance on the trend surface is not applicable.

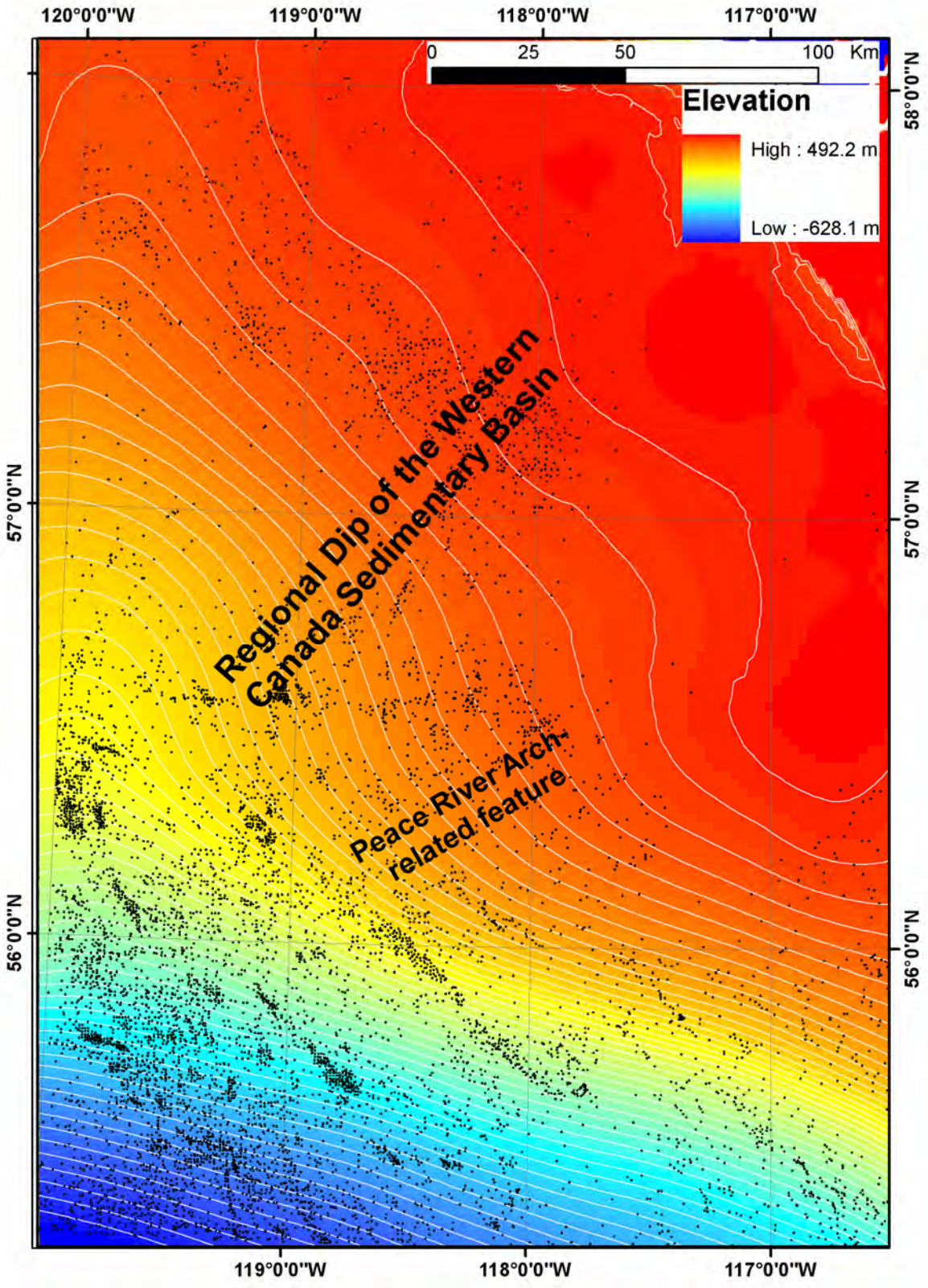

Figure 10. Trend surface modelled for the top of Basal Fish Scale Zone (BFSZ) using local polynomial regression with a search distance of 76 km and a power of 2. Controlling wells are shown as dots.

4.1.3 Fitting the Residual Surface

The third step is to fit the residual surface. The histogram of the residuals resulting from the trend modelling is shown in Figure 11. Most of the values are centred around –3 m and range from –50 m to +45 m.

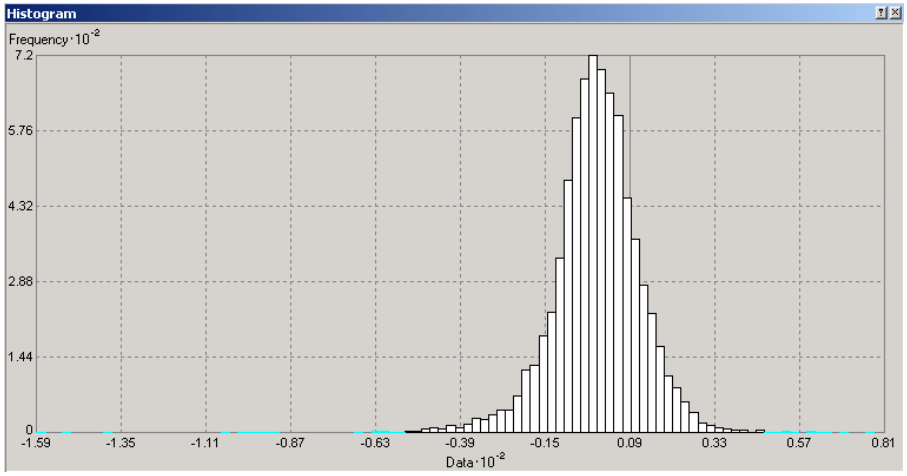

Figure 11. Histogram of the residuals for the Basal Fish Scale Zone (BFSZ).

A few extremely low and high values (17 in total), marked by cyan colour in Figure 11, needed to be checked for outliers. Those outliers that were found to be due to error were removed and the resultant histogram is replotted in Figure 12. Most of the residuals are centered around 1.9 m and range from –40 m to +30 m after removal of the outliers.

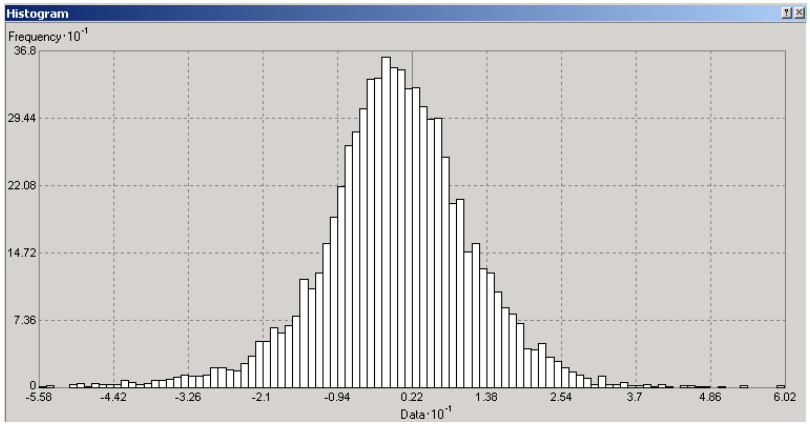

Figure 12. Histogram of the residuals for the Basal Fish Scale Zone (BFSZ) after removal of erroneous outliers.

A variety of stochastic and deterministic interpolation methods is available for fitting the residuals. Unlike trend modelling, the aim of this application is to fit a surface to the residuals as closely as possible. As a result, a statistical test of significance of the fitted surface is relevant. In the present study, different spatial interpolation techniques, including inverse-distance-weighted interpolation (IDW), spline interpolation, local polynomial interpolation and kriging, were first compared on the basis of mean error (ME), root mean squared error (RSME) and the regression slope of predicted versus measured values. As the true surface was not known, the comparison statistics were obtained using cross validation, where one data point is withheld and the remaining data points are used to predict at the withheld point. To obtain the cross-validation statistics, the technique is repeated 'n' times, where 'n' represents the total sample

number. Summary statistics were used to determine if any method was significantly better than the other methods tested on the basis of ME, RMSE and the regression slope. These summary statistics were also used to determine if any set of parameters chosen for a specific interpolation technique were better than other sets of parameters. The value of ME is related to whether the estimation is globally unbiased, and a value of zero indicates that the estimation is globally unbiased. The value of RMSE indicates how close the prediction is to the measurement. The smaller the RMSE, the closer the predictions are to the measurements. The regression slope indicates whether the estimation is conditionally unbiased. It is desirable to have the slope as close to 1 as possible. Table 1 shows an example of the cross-validation summary statistics from different interpolation techniques applied to the residuals of BFSZ. The parameters for each technique were chosen in an attempt to achieve a good estimation. The example in Table 1 shows that simple kriging is the best among the tested techniques. The results cannot be conclusively regarded with confidence, however, as the accuracy of the method also depends on the data and selection of parameters, which are subjective. Generally speaking for the BFSZ dataset, IDW and kriging are similar in RMSE and can reach a lower RSME than spline and local polynomial interpolations. Ultimately, the surfaces from different interpolation techniques will have to be evaluated on the basis of geology (i.e., whether the desired local variations can be extracted effectively from the interpolated surfaces).

Table 1. Comparison of cross-validation summary statistics

Workflow	Conventional approach	Refined approach
Identify syndepositional faults	Isopach contour map (e.g., Barclay, 1990, Fig. 6)	Residual Isopach (differential subsidence) surface (e.g., this report, Fig. 42, 45 and 48)
Identify postdepositional faults	Structure-top contour map (e.g., Barclay, 1990, Fig. 7)	Residual formation-top surface (e.g., this report, Fig. 41, 44, 47 and 50)
Trace offset of a fault vertically	Cross-section, seismic-section (e.g., Richards et al., 1994, Fig. 14.6; Hope et al., 1999, Fig. 8; Eaton et al., 1999, Fig. 4)	Slices from multiple formation tops (e.g., this report, Fig. 56)
Digitizing fault locations	Faults drawn by hand from contour maps	Linear offset pattern extracted statistically (e.g., this report, Fig. 40, 43, 46 and 49)

The underlying interpolation algorithm for each technique was also examined in the context of geological validation. Inverse-distance-weighted interpolation (IDW) is a weighted-average interpolation technique that assumes that values closer to the predicted location are more representative of the value to be estimated than values of the samples farther away. The weights decrease with distance and the spatial arrangement of the samples does not affect the weights. A power parameter controls how fast the weight decreases with distance. Natural-neighbours interpolation is another weighted-average interpolation that uses only the closest samples around the interpolation point, and the weight of each neighbour is determined by the proportionate area of its Thiessen/Voronoi polygon that overlaps with the Thiessen/Voronoi polygon of the newly added location to be estimated. Spline interpolation is a deterministic technique to estimate values using a mathematical function that minimizes overall surface curvature. Local polynomial uses a least-squares regression fit, which results in a surface that minimizes the variance of the surface in relation to the input values. Kriging is also a weighted-average interpolation with an assumption that the distance and direction between sample points reflects a spatial correlation that can be used to explain variation in the surface. The weights are based on spatial correlation and arrangement of the samples.

Among these techniques, IDW, local polynomial and kriging allow for incorporating existing knowledge about directional influence within the data, to various extents, by defining the shape of the search neighbourhood. Among these three techniques, kriging is the best for quantifying spatial continuity of

data through semivariogram modelling. Semivariogram modelling gives more flexibility for incorporating existing knowledge into the model. Kriging is also the most complicated of these techniques, however, and requires a thorough comprehension of geostatistics to understand the underlying interpolation algorithm and select optimal parameters. The natural-neighbours interpolation is the simplest technique in that only one parameter (i.e., cell size) needs to be decided. If the data are accurate, unevenly distributed and without distinct anisotropy, it can achieve comparable results. It has the advantage of capturing local variation, which is desired by the present study, through the use of a least number of neighbourhood points. In the present study, simple kriging was chosen for fitting the residual surface and natural neighbour interpolation was sometimes used for general exploration and comparison (*see* below).

For simple kriging, the parameters that need to be defined include log size, nugget effect, sill, range, semivariogram model function and anisotropy for the semivariogram modelling, and shape, geometry and minimum and maximum number of points to use for the search-neighbourhood strategy. Selection of these parameters is flexible and subjective, and therefore very challenging. It relies heavily on the available knowledge of the phenomenon being analyzed and sample data, the experience of the operator and the objective of the modelling. The selection of these parameters was repeatedly checked with the resultant summary statistics of cross validation so as to find the optimal set of parameters. Semivariogram modelling for the BFSZ residuals is shown in Figure 13. A log distance of 1 km was chosen and spatial continuity was modelled within a distance of 20 km. These parameters were based on the low range of sample separation and an estimate of the dimension of offset patterns to be modelled. Anisotropy was modelled as an ellipse with a semi-major axis of 25 km, a semi-minor axis of 10 km and a direction of 113.2°. This was based on the goal to focus on modelling the spatial continuity within about 10 km. The selected direction can be validated by the fact that the study area is dominated by northwest-trending features, including faults. It should be pointed out that one limitation with the application of kriging in the current version of ArcGIS Geostatistical Analyst is that only one dominant anisotropy direction can be specified for semivariogram modelling. In the study area, however, there are two dominant trends of faults, northeast and northwest. As a result, natural neighbour interpolation is sometimes used for comparison.

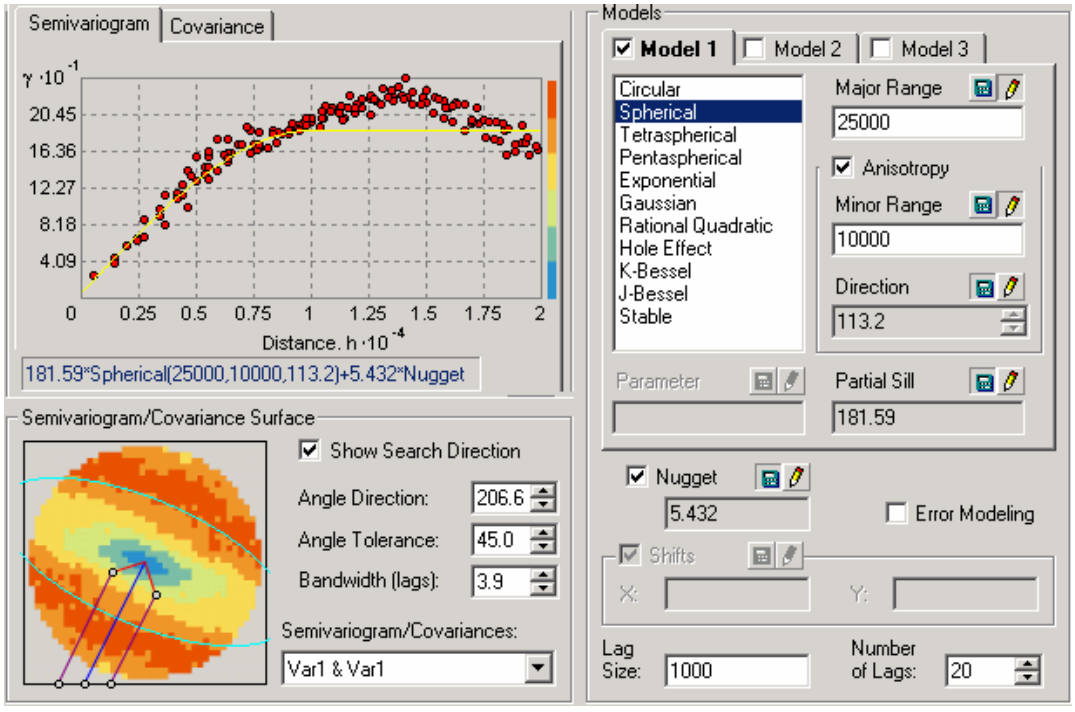

Figure 13. Parameters used for semivariogram modelling of Basal Fish Scale Zone (BFSZ) residuals.

The ellipse of anisotropy used for semivariogram modelling was also used for defining the shape of the search neighbourhood. The search neighbourhood was divided into four sectors and, for each sector, the number of data points used was confined to a minimum of two and a maximum of 5 (Figure 14). The division of the search neighbourhood avoids bias in a particular direction. The selection of the maximum number of data points helps to control the extent to which the resultant surface captures local variations.

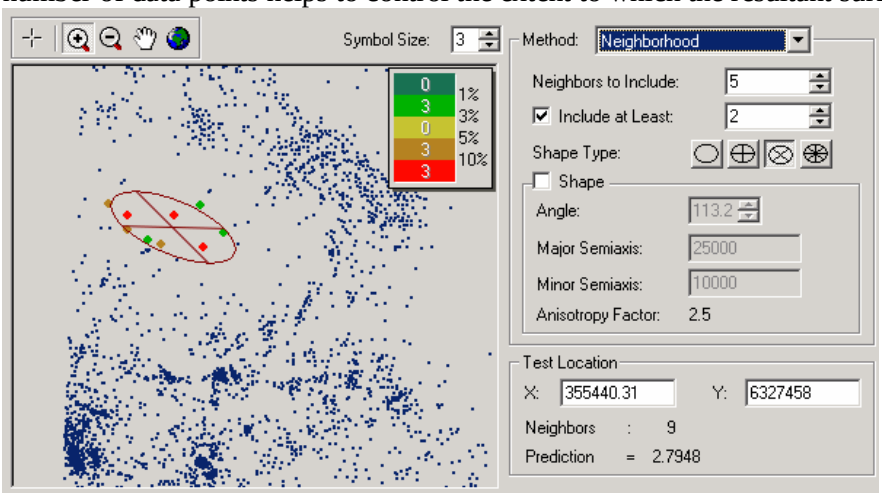

Figure 14. Parameters of the search neighbourhood for interpolation of the Basal Fish Scale Zone (BFSZ) residual surface.

The resultant summary statistics of cross validation are shown in Figure 15. It is desirable that the plot of predicted versus measured values scatters around the 1:1 line (the dashed line), although the regression slope is usually less than one (in this case, 0.864). This is a property of kriging that tends to underpredict large values and overpredict small values, which is also known as conditional bias. Globally, the prediction is nearly unbiased, as the mean prediction error (0.02773) is close to zero. The prediction error can be standardized by dividing it by the estimated kriging standard error, and the mean standardized error (0.0007946) further suggests the global unbiasedness. The statistics also suggest that the assessment of uncertainty, or the estimated prediction standard error, is valid, as the average kriging standard error (5.34) is close to the root-mean-squared prediction error (5.554). A root-mean-squared standard error close to 1 also indicates that the estimation of variance in the prediction is valid.

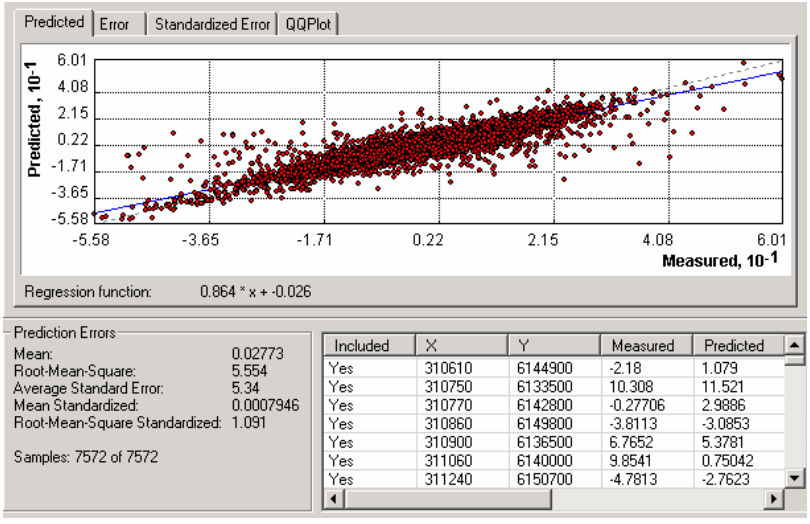

Figure 15. Summary statistics of cross validation for fitting the residual surface for the Basal Fish Scale Zone (BFSZ).

The resulting fitted residual surface for BFSZ is shown in Figure 16. Residuals within two standard deviation units range roughly from –15 m to +15 m. Local features are much better highlighted in the modelled residual surface than on the conventional structure-top contour map of the of BFSZ (Figure 9).

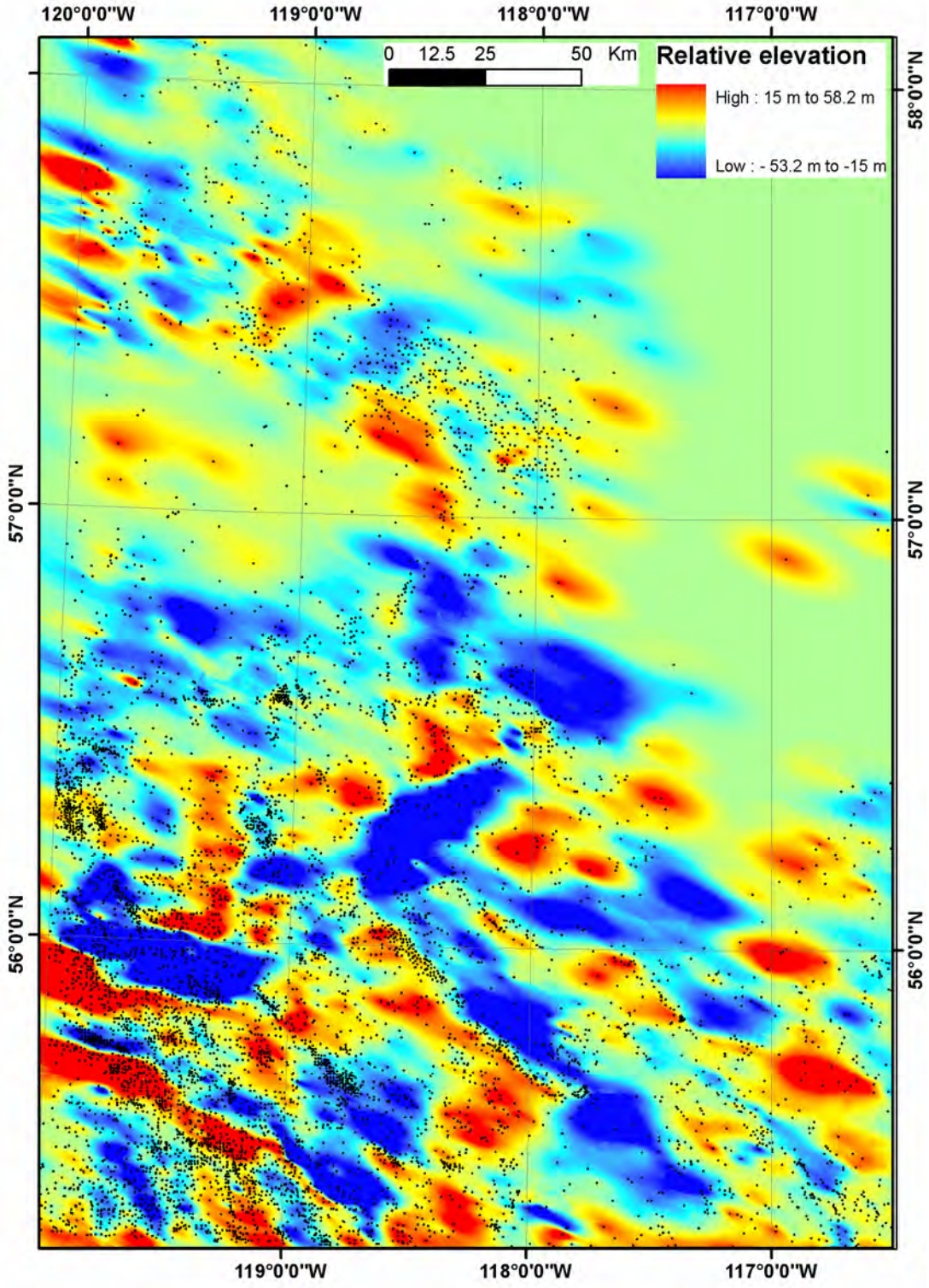

Figure 16. Residual surface fitted for the Basal Fish Scale Zone (BFSZ) using simple kriging. Controlling wells are shown as dots.

For comparison, Figure 17 shows the fitted residual surface using natural-neighbours interpolation. It is noteworthy that the residual map from kriging emphasizes more of the northwest-trending features than that from natural-neighbours interpolation due to the ability of the former technique to model anisotropy.

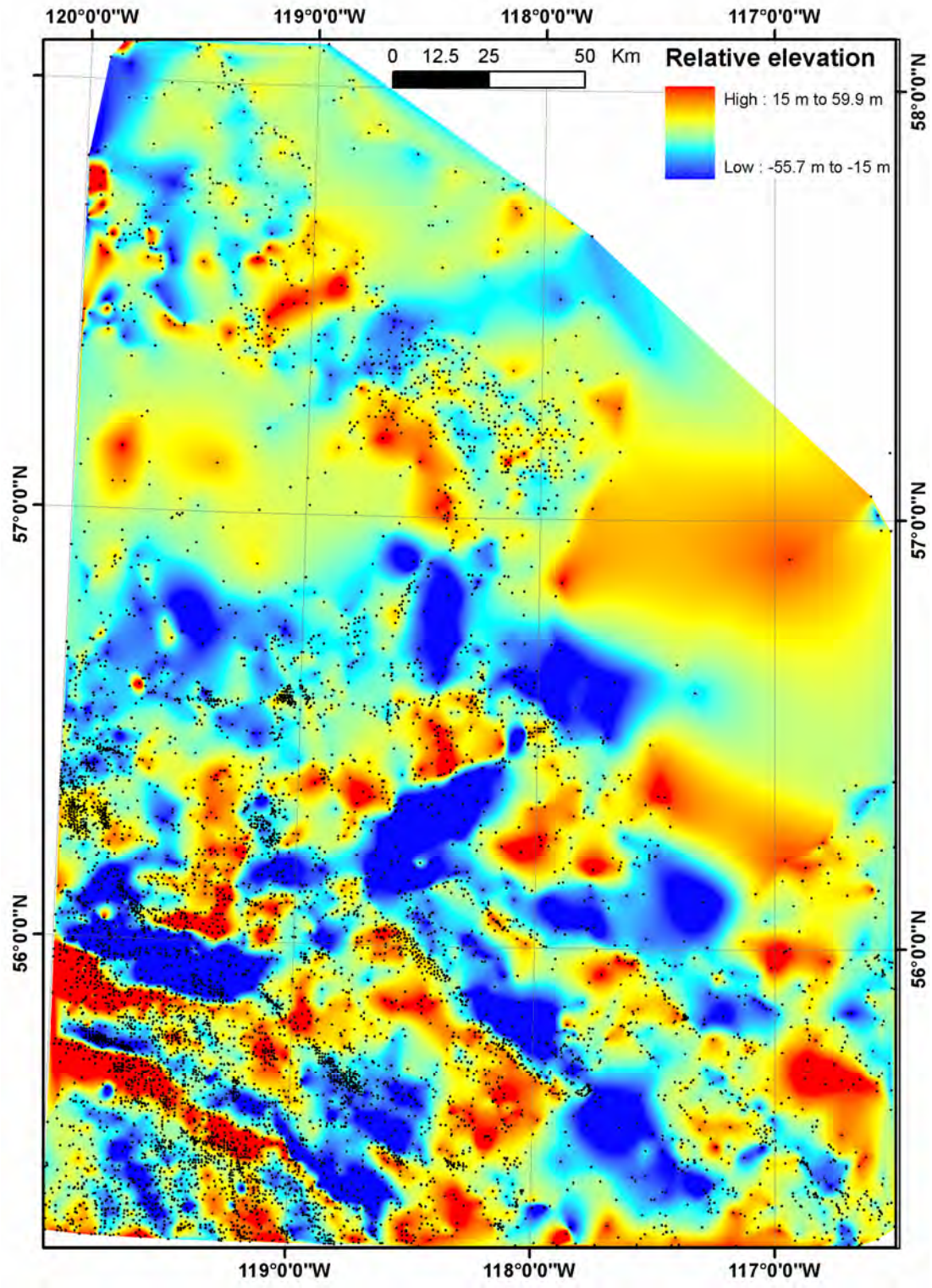

Figure 17. Residual surface of BFSZ fitted with natural-neighbours interpolation. Controlling wells are shown as dots.

4.1.4 Trend-Surface Analysis Applied to Formation Thickness

Trend-surface analysis can also be applied to formation-thickness data to decompose the associated subsidence into regional and local components. Figure 18 shows the isopach map of the interval from the BFSZ to the top of the Peace River Formation. It was created using inverse-distance-weighting interpolation, and serves as an example of a conventional isopach-contour map (*see* also Leckie et al., 1990, Figure 10 for comparison). Figure 19 shows the associated regional subsidence trend and Figure 20 shows the relative local subsidence after the removal of the regional subsidence trend. Comparing Figures 18 with 20, it can be seen that Figure 20 clearly highlights the local relative subsidence associated with the deposition from the top of the Peace River Formation to the BFSZ. A northeast trending zone of high relative subsidence is clearly highlighted near the middle of the map, as is its southeastern bank of low subsidence. The boundary between the two coincides with the northern depositional limit of the underlying Paddy and Cadotte members as defined by Leckie et al. (1990).

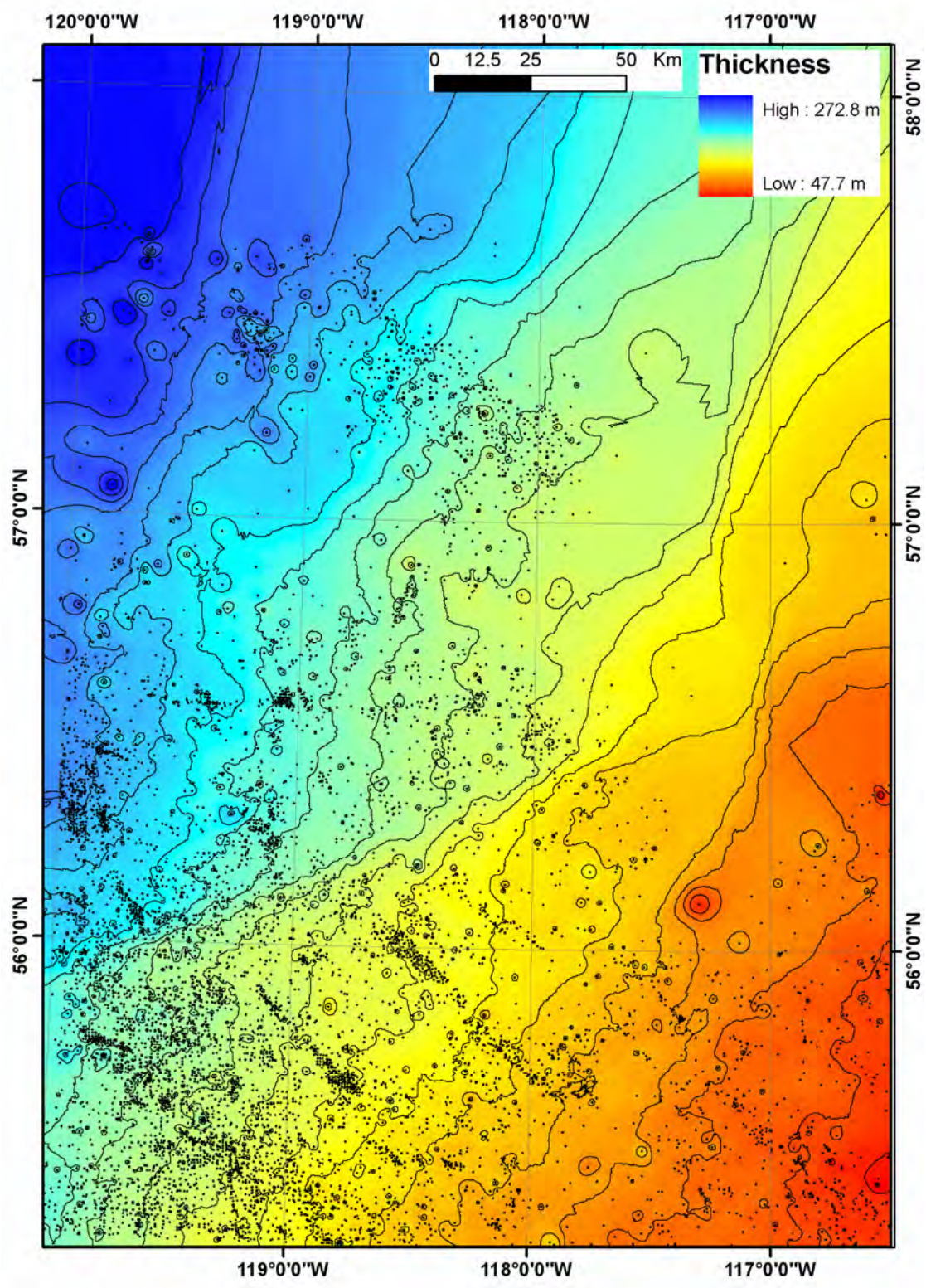

Figure 18. An example of the conventional isopach contour map of the interval from the top of the Peace River Formation to the Basal Fish Scale Zone (BFSZ) created using inverse distance weighting (IDW). Contour interval is 10 m and controlling wells are displayed as black points.

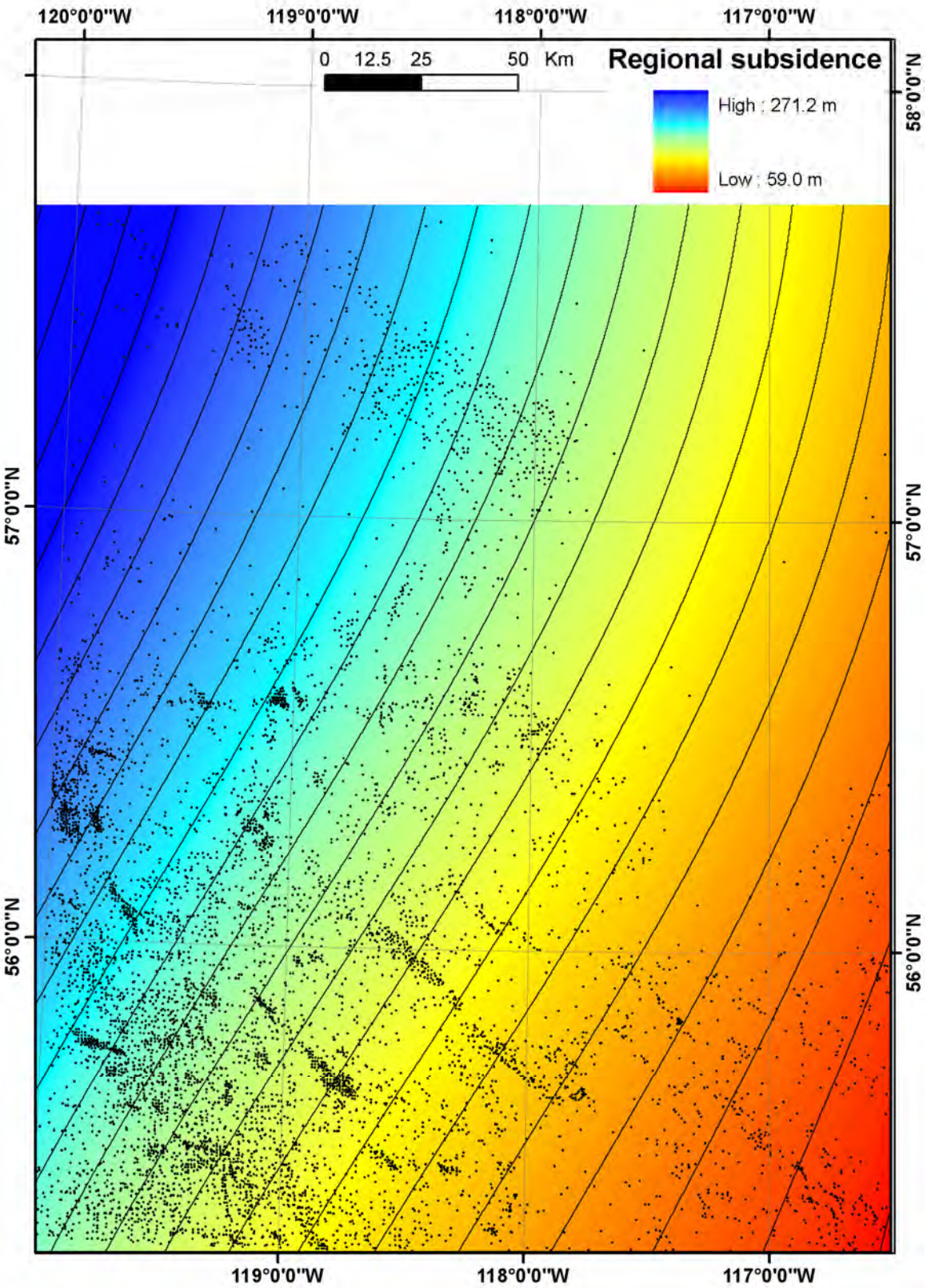

Figure 19. Modelled regional subsidence trend in response to the deposition of the interval from the top of the Peace River formation to the Basal Fish Scale Zone (BFSZ). Contour interval is 10 m and controlling wells are displayed as black points.

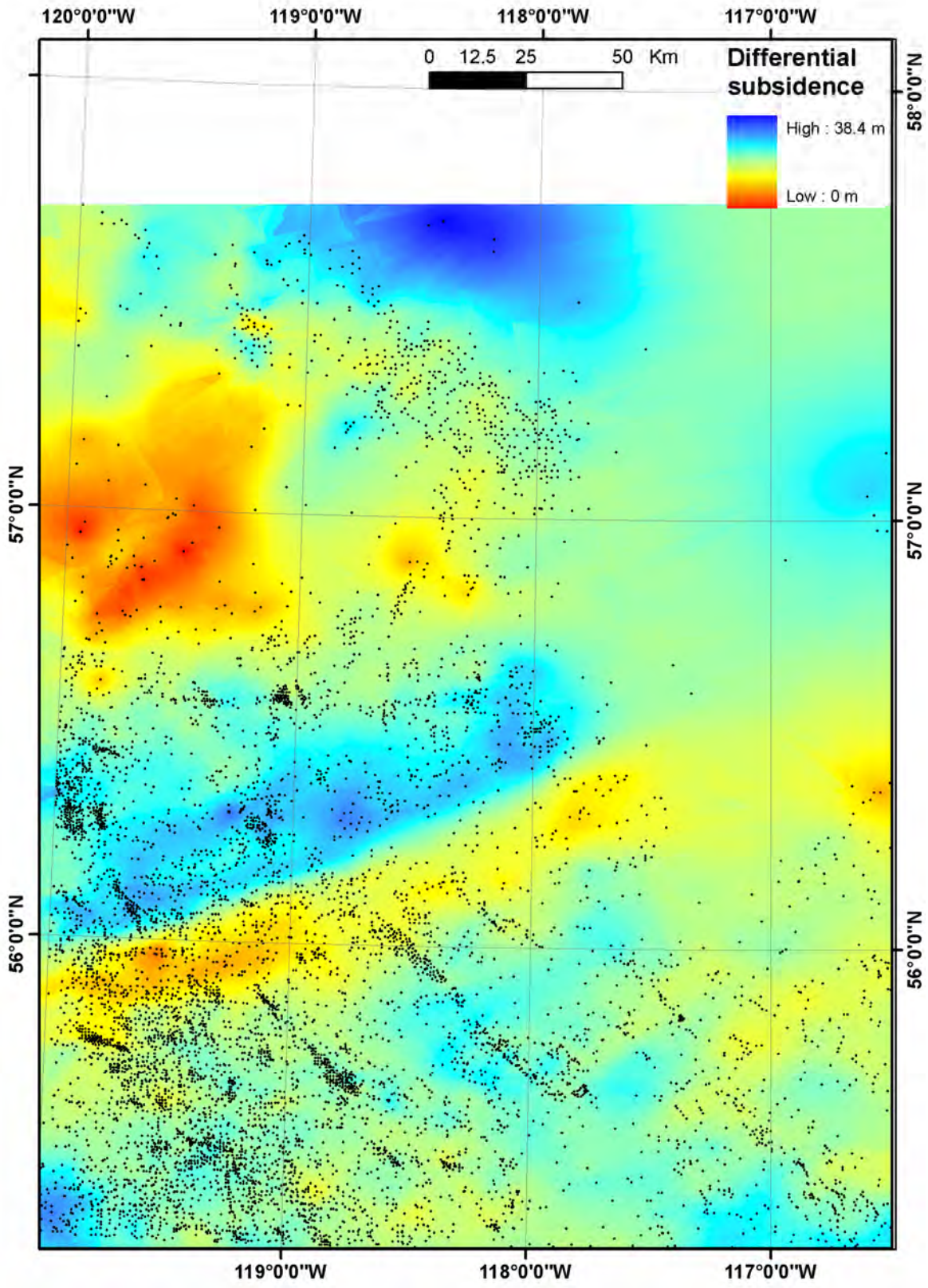

Figure 20. Differential subsidence map during deposition of the interval from the top of the Peace River Formation to the Basal Fish Scale Zone (BFSZ). Controlling wells are displayed as black points.

4.2 Extracting Linear Patterns of Formation-Top Offset from the Residual Surface

Conventionally, faults and other structures are visually interpreted and digitized directly from the contour maps. In the present study, a geostatistical method was employed to quantitatively extract the offset information from the modelled residual surface. The terms 'offset' or 'offset pattern' are used hereafter to refer to the systematic change in the elevation of formation top along a linear pattern. It could be caused by a fault, a change in slope or a drape structure. A variety of image-processing techniques, including sunshade relief, slope analysis, neighbourhood statistics and data fusion, were examined for their potential to extract local variation and assist visual interpretation of structural lineaments from the modelled residual surface. Neighbourhood statistics, including range, standard deviation, variance and image texture indices (including contrast, entropy and correlation), were tested for capturing the local variation on the residual-surface image. For the present study, the neighbourhood statistic of range was found to be sufficient for capturing the local offset patterns possibly caused by faults. The residual surface previously modelled was interpolated based on a 250 m by 250 m cell size, which was chosen based on the low range of data separation distance and the desired resolution. The neighbourhood statistic of range was applied using a 3 pixel by 3 pixel window, which is a square measuring 0.75 km on each side and having a diagonal distance of 1.06 km. The window contains 9 pixels and the algorithm calculated the range of the 9 values held by the 9 pixels. The new range value was then assigned to the pixel at the middle of the window. After the window moved across the entire residual surface image, a new image was created with the range values. This image captured local variation by recording the total offset of formation picks within a square measuring 0.75 km on each side or, in other word, over a distance of about 1 km (i.e., close to the length of the diagonal of the square). Figure 21 shows the local variation map created by applying the neighbourhood statistic of range to the residual map of the BFSZ (Figure 16). The colour in the local offset map is related to the maximum vertical difference in the formation top over distances of up to one km. Large vertical differences over per unit distance (i.e., $\geq$5 m/km) are displayed as red, the intermediate differences as yellow and the small to zero differences as blue. Some linear offset patterns of formation top are clearly manifested on the local offset map (Figure 21). These linear patterns indicate where faults are likely present.

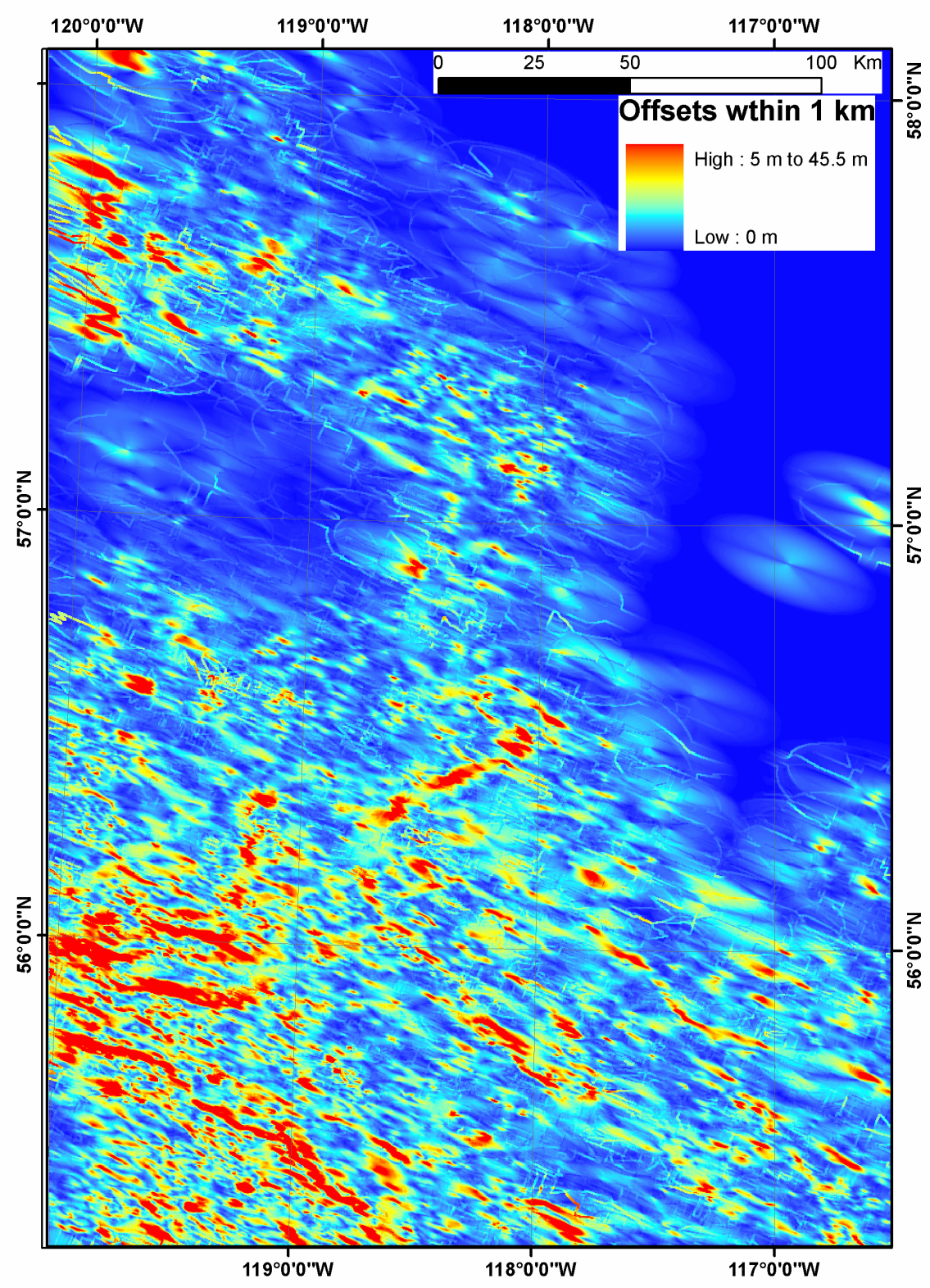

Figure 21. Local offset map created from the residual surface of the Basal Fish Scale Zone (BFSZ; Figure 16), using the range within a 750 m by 750 m neighbourhood.

To explain the linear offset pattern on the local offset map in more detail, Figure 22 shows a close-up look of the linear pattern located near the middle of Figure 21, with formation picks of BFSZ included as integer for each well for simplicity and explanation. The linear offset pattern is marked by a dashed line. A close examination of the formation picks yields the following observations:

- In general, the formation pick values increase systematically from southwest to northeast. This is also true if the picks on each side of the linear offset pattern are examined separately. This can be explained by the regional dip of the WCSB.

- Across the dashed line, the formation picks exhibit a systematic difference or offset across the linear pattern. The offset varies from about 19 to 40 m along the dashed lines, but the formation pick values on the southeast side of the linear pattern are systematically smaller than those on the northwest side if examined in the direction perpendicular to the dashed line.

- The offset along the linear pattern ranges from about 19 to 40 m over a distance of about 3.5 km across the dashed line, as indicated by the mostly yellow to red colour. This amount of offset is larger than that in areas either north or south of the dashed line, as indicated by mostly blue colour.

- The area away from the linear pattern is generally more homogeneous in light of offset pattern.

In summary, the local offset map obtained from the developed methodology is effective for capturing the linear pattern of formation-top offset. These patterns indicate the locations of potential faults. Compared to the residual map (Figures 16 and 17), the local offset map allows interpretation of lineaments/faults with a higher degree of accuracy and greater ease. Nevertheless, there are a few cases where the residual map also needs to be examined for those linear offset patterns that may not be clear on the local offset map due to wide data spacing (see below).

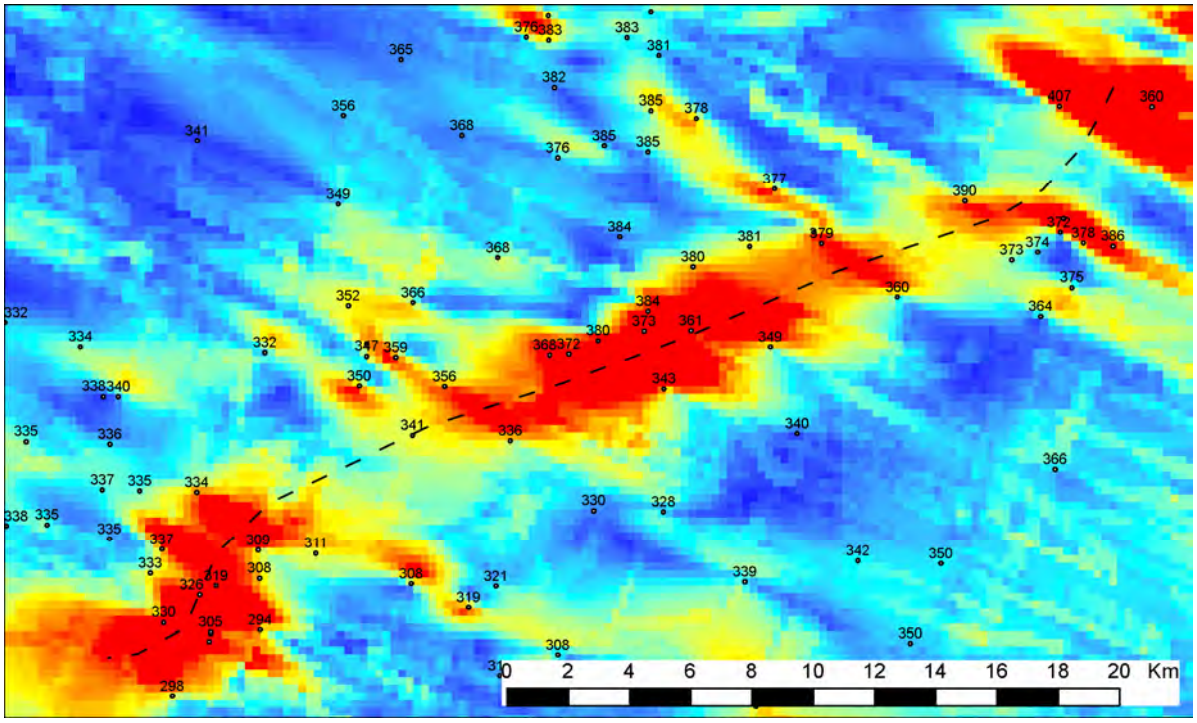

Figure 22. Close-up of the linear pattern of formation-top offset near the middle of the local offset map (see Figure 21 for location).

Lineaments are interpreted from both the local offset map, as described previously, and the residual map. Figure 23 shows the lineaments interpreted from the BFSZ superimposed on the local offset map, and Figure 24 shows these same lineaments superimposed on the residual map. Although a majority of faults can be more accurately located from the local offset map, some of the lineaments can be more easily inferred from the residual map.

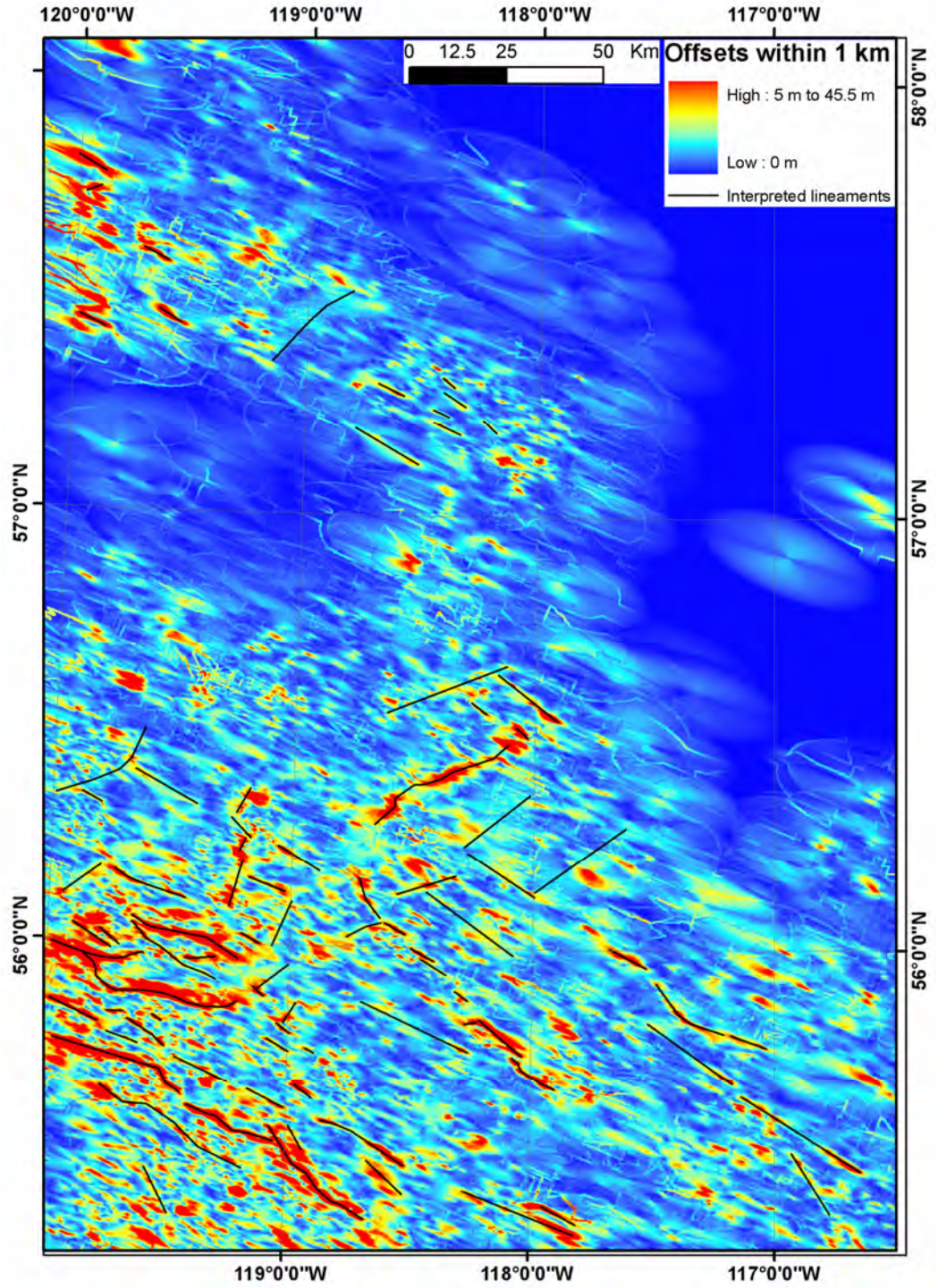

Figure 23. Lineaments interpreted from the Basal Fish Scale Zone (BFSZ), superimposed on the local offset map.

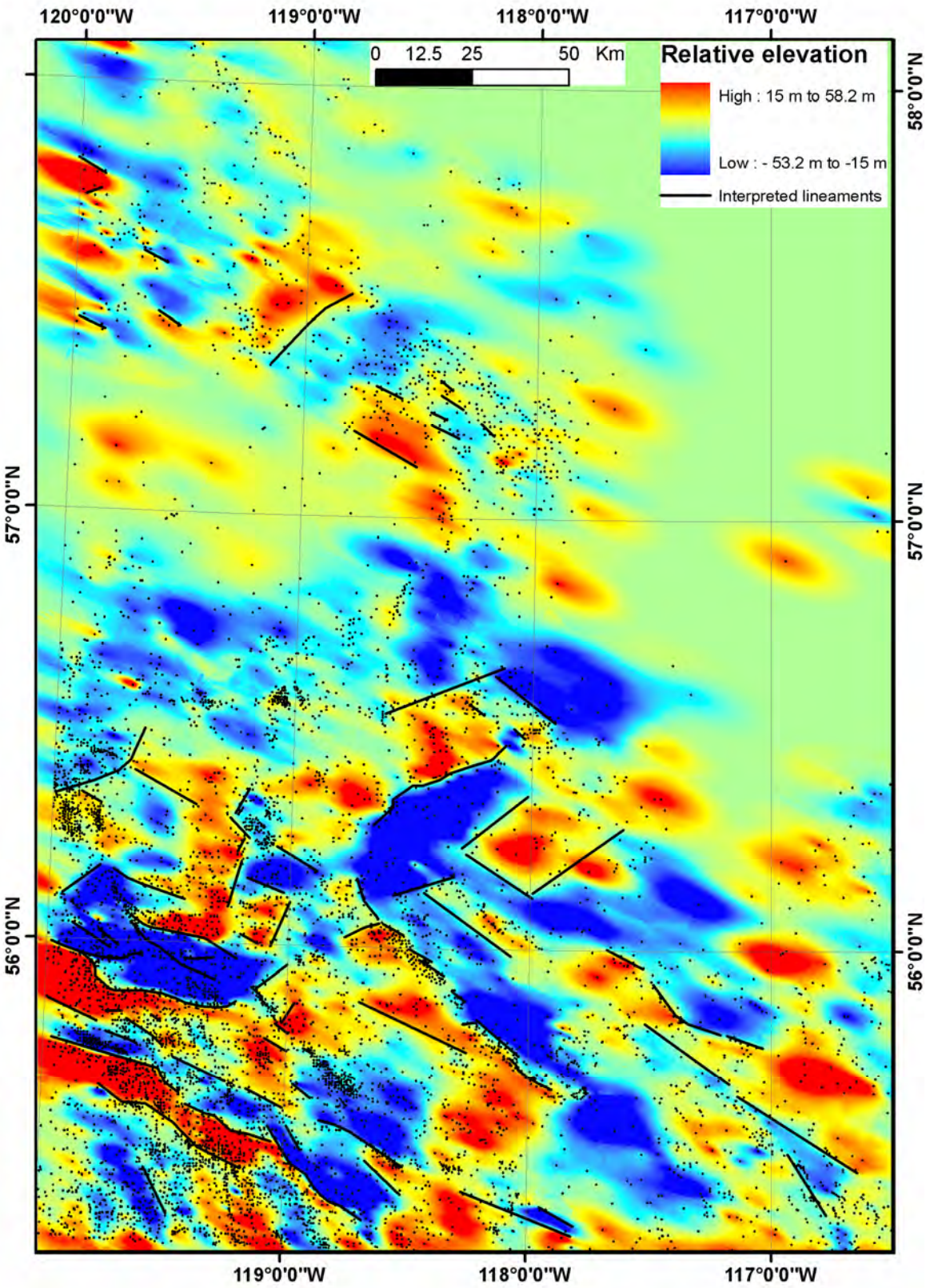

Figure 24. Lineaments interpreted from the Basal Fish Scale Zone (BFSZ), superimposed on the residual surface. Controlling wells are shown as black dots.

4.3 Comparison of Local Offset Patterns with Local Subsidence Patterns

Isopach maps have been routinely used to approximate basin subsidence patterns (*see* Mossop and Shetsen, 1994), assuming that the changes in thickness of the strata under consideration are due to lateral variations in subsidence rate during deposition. Isopach maps, however, do not usually record exactly the structural deformation of a basin between the time of deposition of the lowermost and uppermost strata of the interval examined because secondary factors, including compaction of the interval of interest, syndepositional compaction of the underlying units and the paleobathymetry of both included and bounding strata, are also involved (Calvert, 1974). When trend-surface analysis is applied to formation thickness data to decompose it into regional and local subsidence components, the effects of these secondary factors can be mainly removed with the trend and cancelled out in the resultant residual map, which represents differential local subsidence. The differential local subsidence can be associated mainly with growth faults, as in the case of the DCGC. As a result, comparison of the local subsidence pattern to the local formation-top offset pattern helps to identify whether the interpreted faults are syndepositional growth faults or postdepositional faults. Figure 25 shows the lineaments, interpreted from the local offset map, superimposed on the differential subsidence map. Except for a few lineaments that coincide with parts of the northern depositional limits of the underlying Paddy and Cadotte members (as defined by Leckie et al., 1990), it appears that most of the lineaments are postdepositional and not associated with syndepositional subsidence.

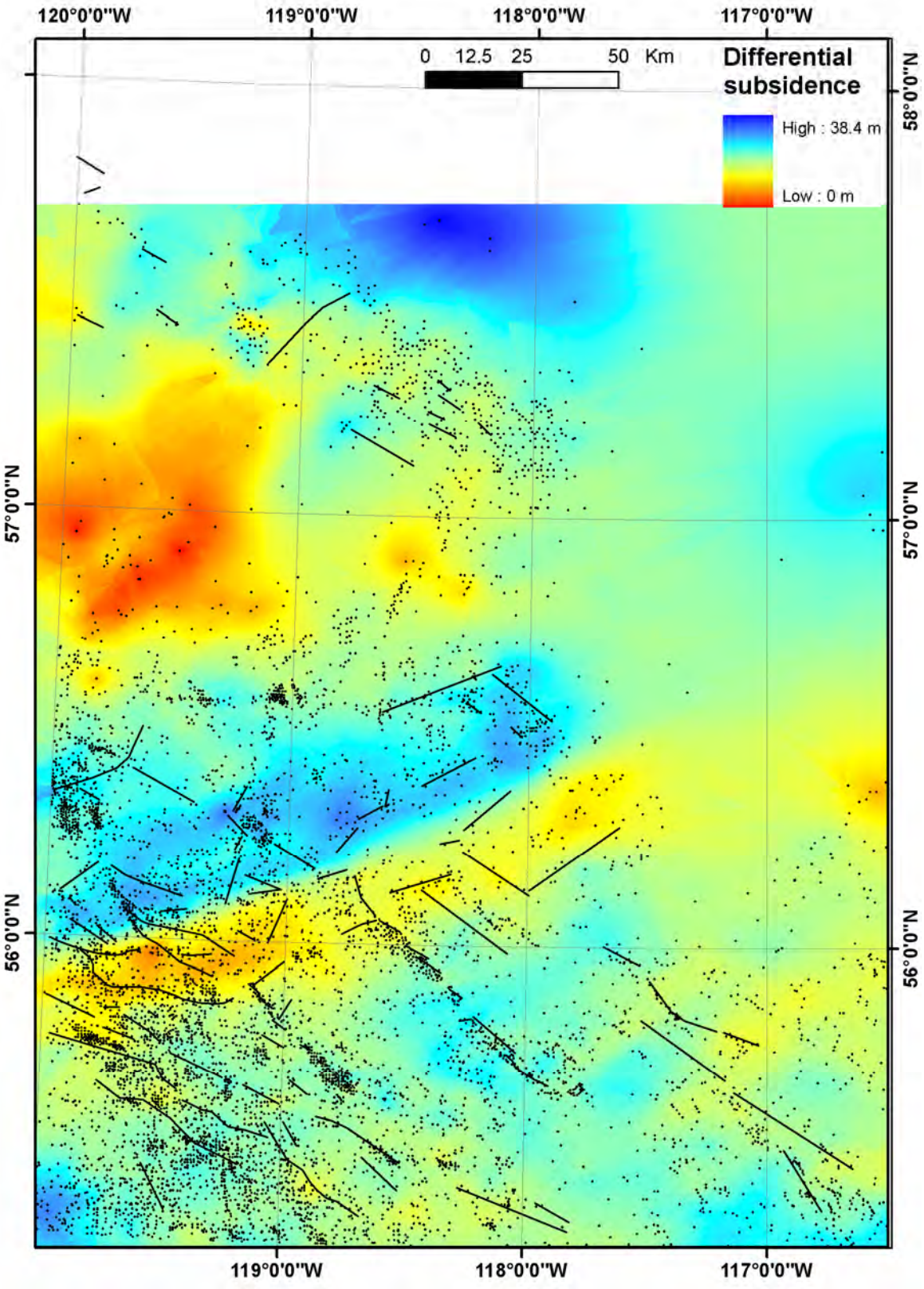

Figure 25. Interpreted lineaments superimposed on differential subsidence map during deposition of the interval from the top of the Peace River Formation to the Basal Fish Scale Zone (BFSZ). Controlling wells are shown as black points.

4.4 Tracing Linear Patterns of Formation-Top Offset Throughout the Sedimentary Section

The refined trend-surface analysis and extraction of linear offset patterns from the residual surface, as described above, were applied to multiple selected formation tops throughout the sedimentary section. Applying the analysis on multiple formation tops allows the trace of a linear pattern vertically throughout the sedimentary cover down to the top of the Precambrian. Previously, faults were interpreted from offset stratigraphic intervals in the sedimentary section. Tracing linear offset patterns throughout the sedimentary sections allows clarification of the relationships among faults previously interpreted from different stratigraphic intervals in the sedimentary section, which, in turn, helps to identify reactivation of basement faults. This also allows description of faults in three dimensions, as opposed to treating a fault as a linear feature on a two-dimensional map.

The formation tops used in this study were selected such that the penetrating wells have a good coverage and density; the top can be easily picked on the well-log; and the formation top represents more or less a synchronous surface. This ensures that the data have a fairly good quality. Nevertheless, the availability of formation tops for analysis is constrained by the fact that the deeper a formation top, the smaller the number of penetrating wells available. Figure 26 shows the selected formation tops for the study area.

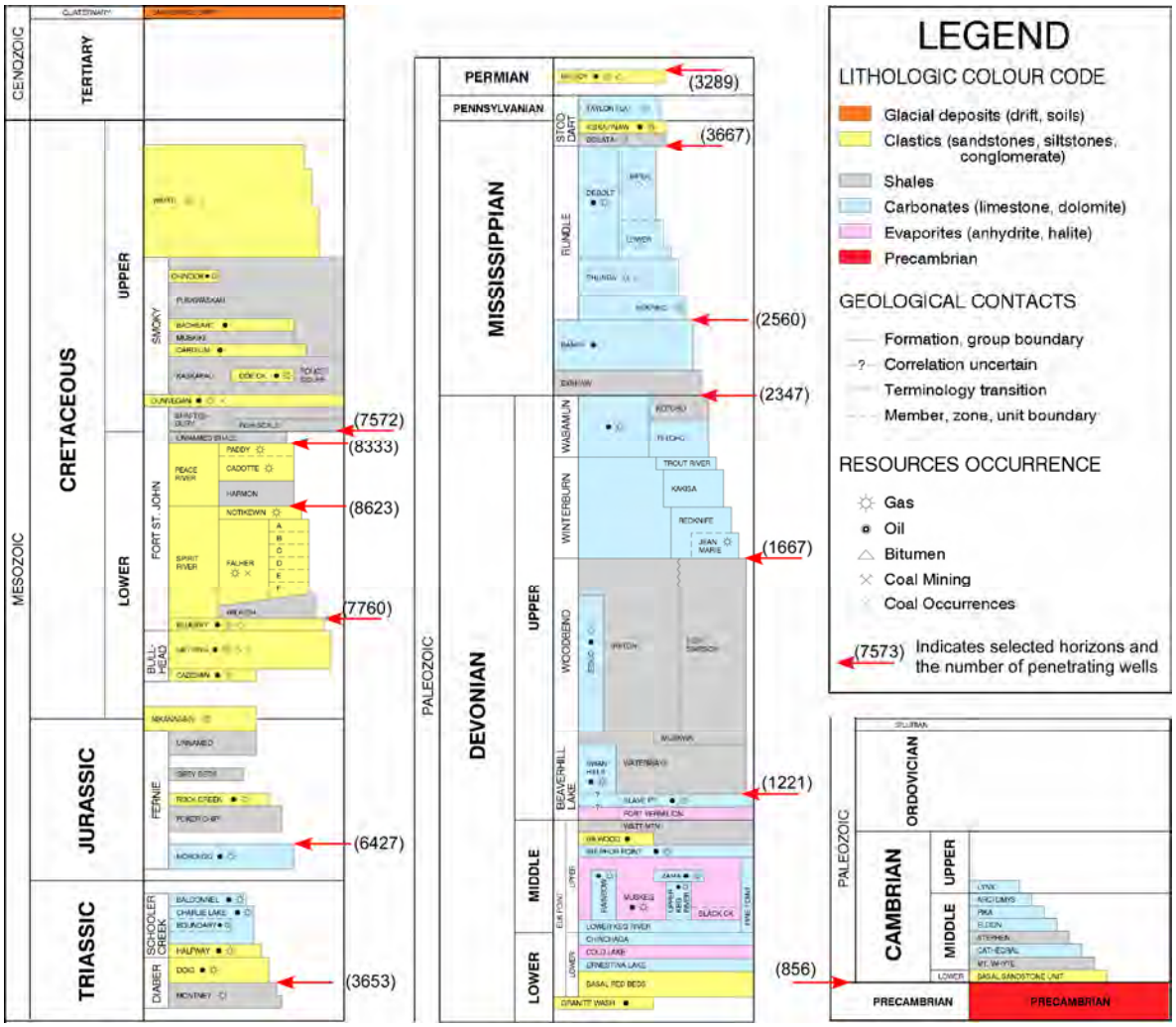

Figure 26. Stratigraphic column of the study area (from Alberta Energy and Utilities Board, 2002), selected formation tops and associated penetrating wells.

Figures 27 to 29 show lineaments interpreted from the top of the Paddy Member, Peace River Formation superimposed, respectively, on the local offset map of the top of the Paddy Member, Peace River Formation, the residual map of the top of the Paddy Member, Peace River Formation and the differential subsidence map of deposition from the top of the Notikewin Member, Spirit River Formation to the top of the Paddy Member, Peace River Formation. Figures 30 to 32 show lineaments interpreted from the top of the Notikewin Member, Spirit River Formation superimposed, respectively, on the local offset map of the top of the Notikewin Member, Spirit River Formation, the residual map of the top of the Notikewin Member, Spirit River Formation and the differential subsidence map of deposition from the top of the Bluesky Formation to the top of the Notikewin Member, Spirit River Formation. Figures 33 and 34 show lineaments interpreted from the top of the Bluesky Formation superimposed, respectively, on the local offset and residual maps of that top. They represent the downwarping stage of the Peace River Arch region. The two previously interpreted northeast-trending Cretaceous lineaments (*see* Figure 7), shown by O'Connell (1994, Figure 28.19) as the north and south boundaries of the axis of the Upper Mannville Group depositional basin, roughly overlap with the boundary of the local subsidence centre (see Figure 32).

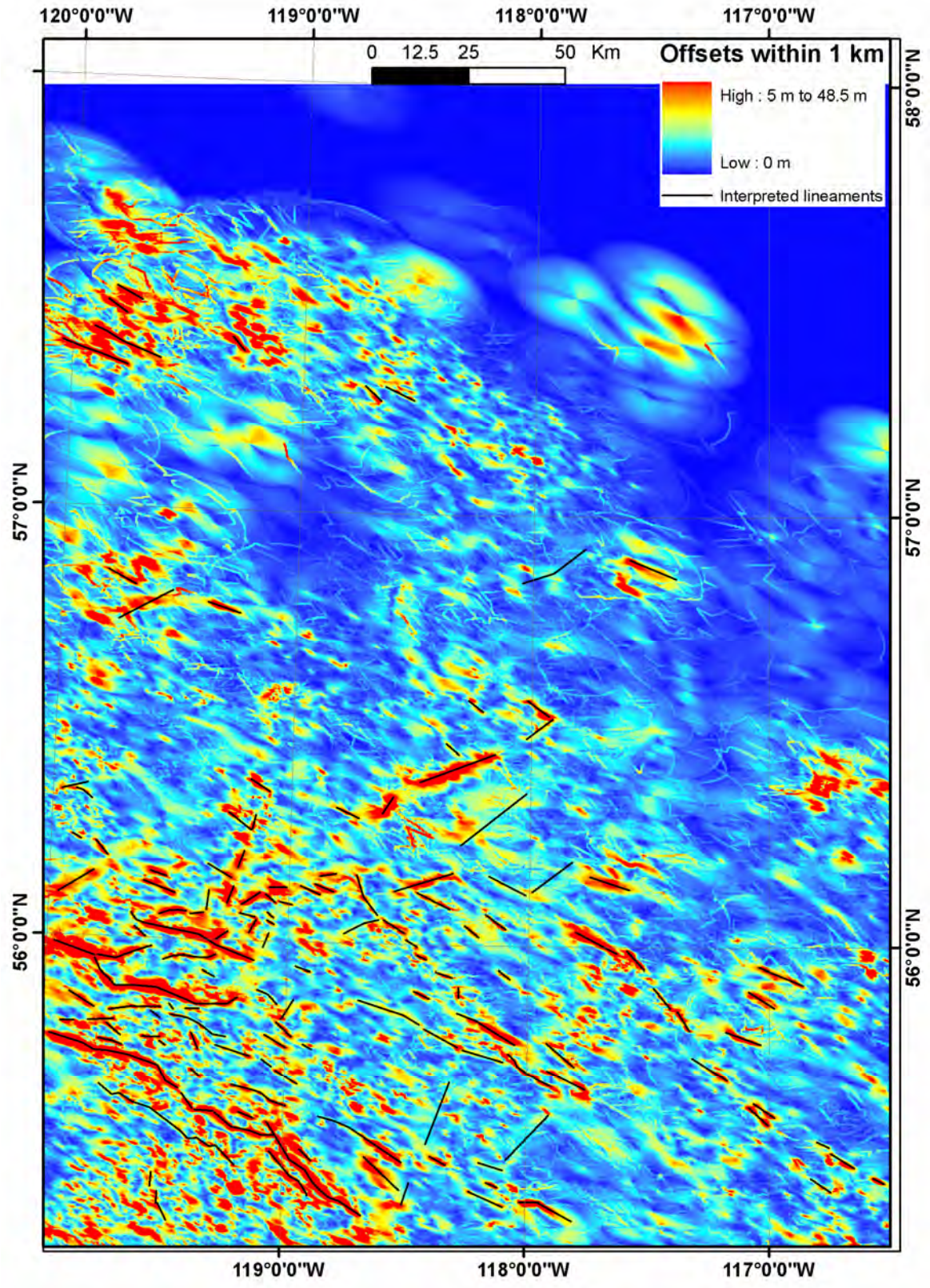

Figure 27. Lineaments interpreted from the top of the Paddy Member, Peace River Formation superimposed on the local offset map of the top of the Paddy Member, Peace River Formation.

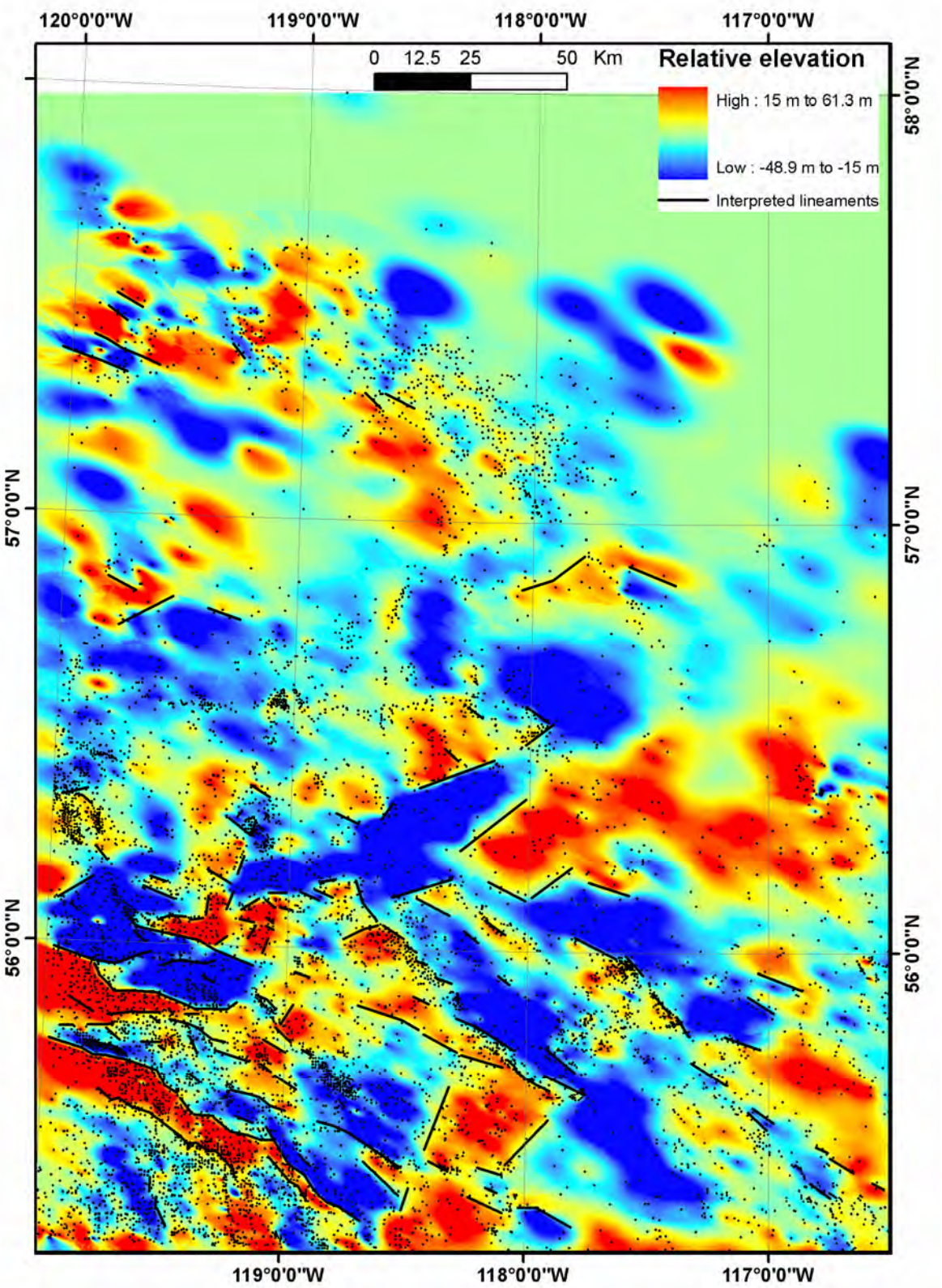

Figure 28. Lineaments interpreted from the top of the Paddy Member, Peace River Formation superimposed on the residual map of the top of the Paddy Member, Peace River Formation. Controlling wells are shown as black dots.

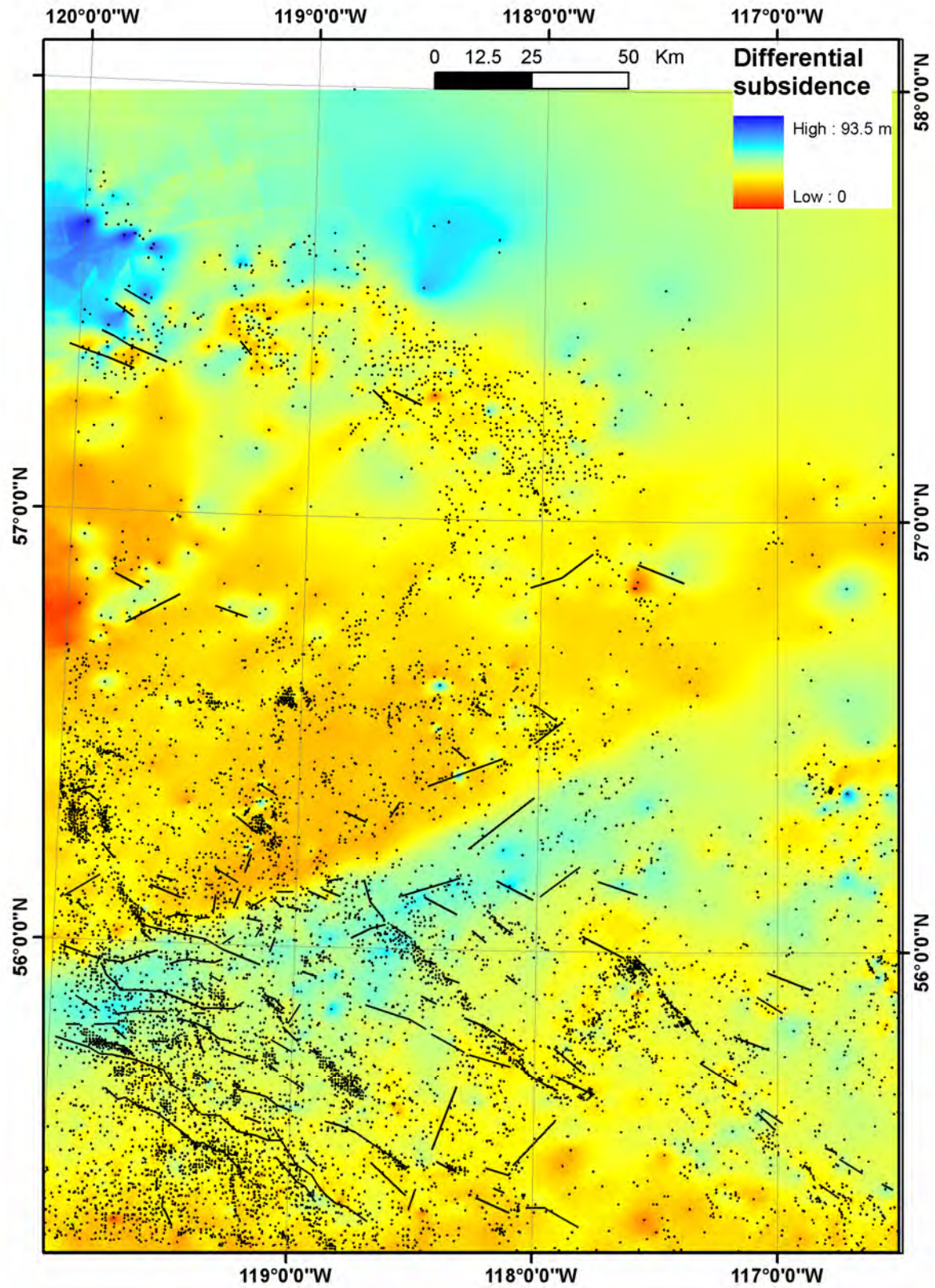

Figure 29. Lineaments interpreted from the top of the Paddy Member, Peace River Formation superimposed on the differential subsidence map of deposition from the top of the Notikewin Member, Spirit River Formation to the top of the Paddy Member, Peace River Formation. Controlling wells are displayed as black points.

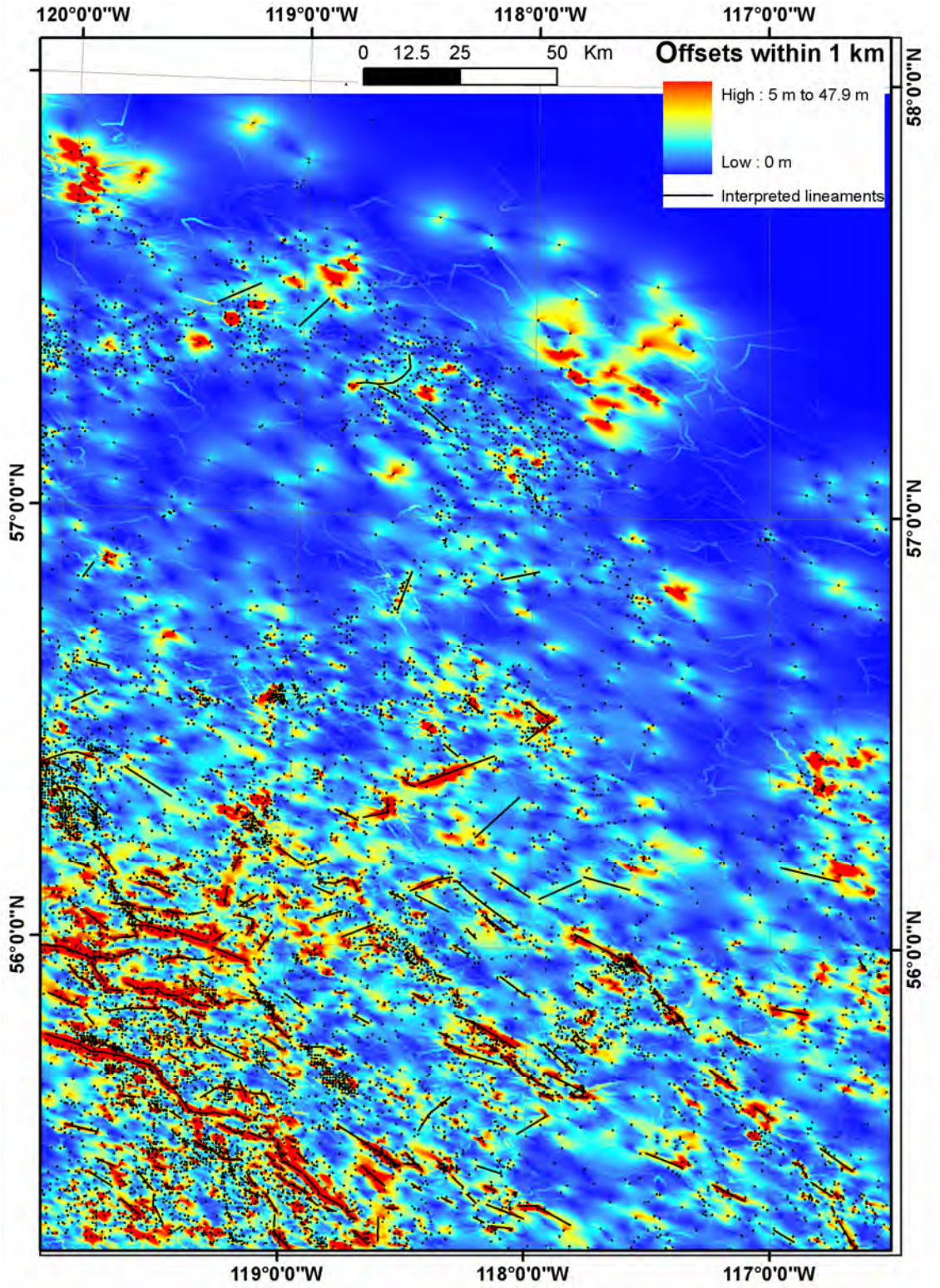

Figure 30. Lineaments interpreted from the top of the Notikewin Member, Spirit River Formation superimposed on the local offset map of the top of the Notikewin Member, Spirit River Formation. Controlling wells are displayed as black points.

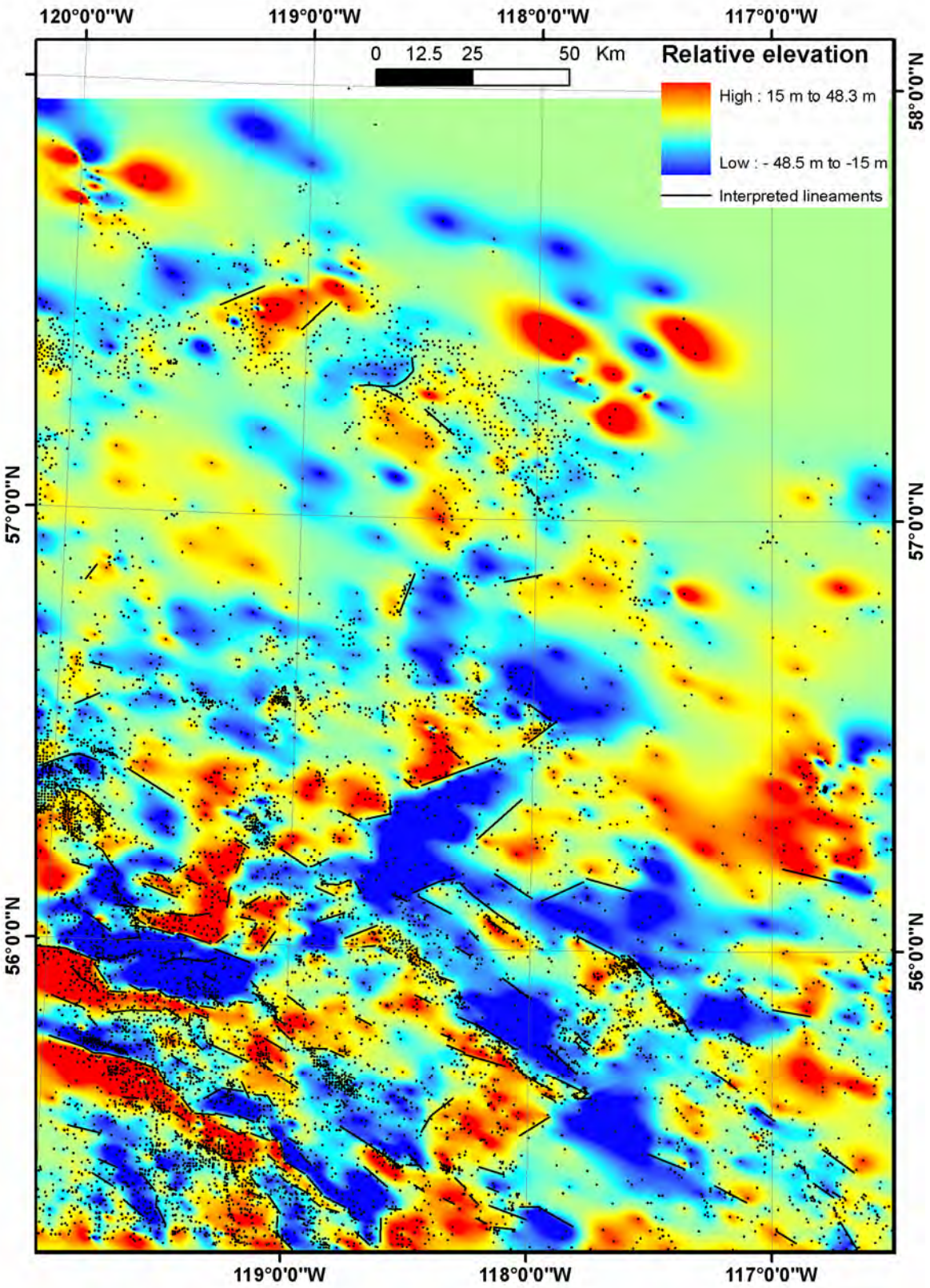

Figure 31. Lineaments interpreted from the top of the Notikewin Member, Spirit River Formation superimposed on the residual map of the top of the Notikewin Member, Spirit River Formation. Controlling wells are shown as black dots.

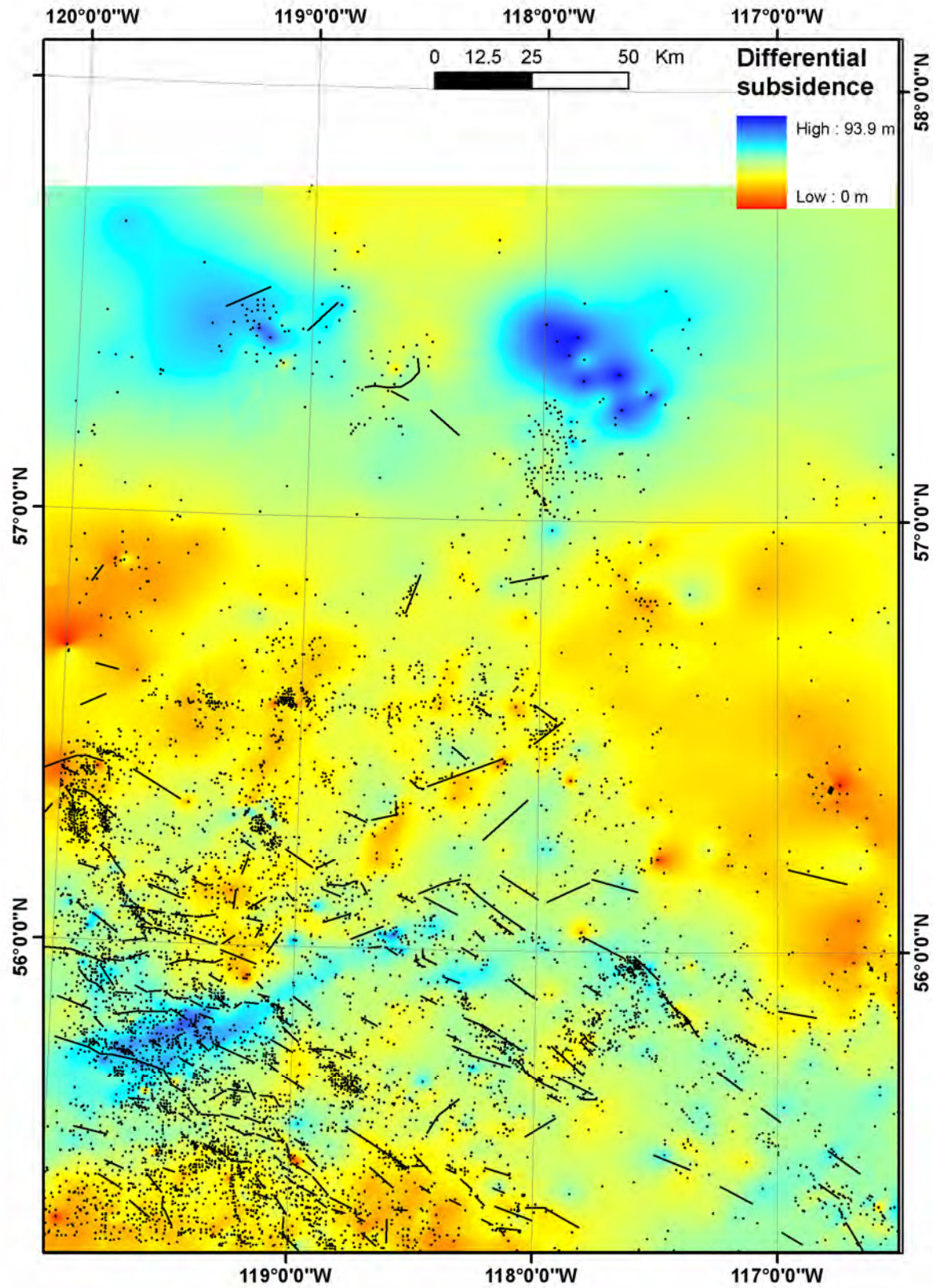

Figure 32. Lineaments interpreted from the top of the Notikewin Member, Spirit River Formation superimposed on the differential subsidence map of deposition from the top of the Bluesky Formation to the top of the Notikewin Member, Spirit River Formation. Controlling wells are displayed as black points.

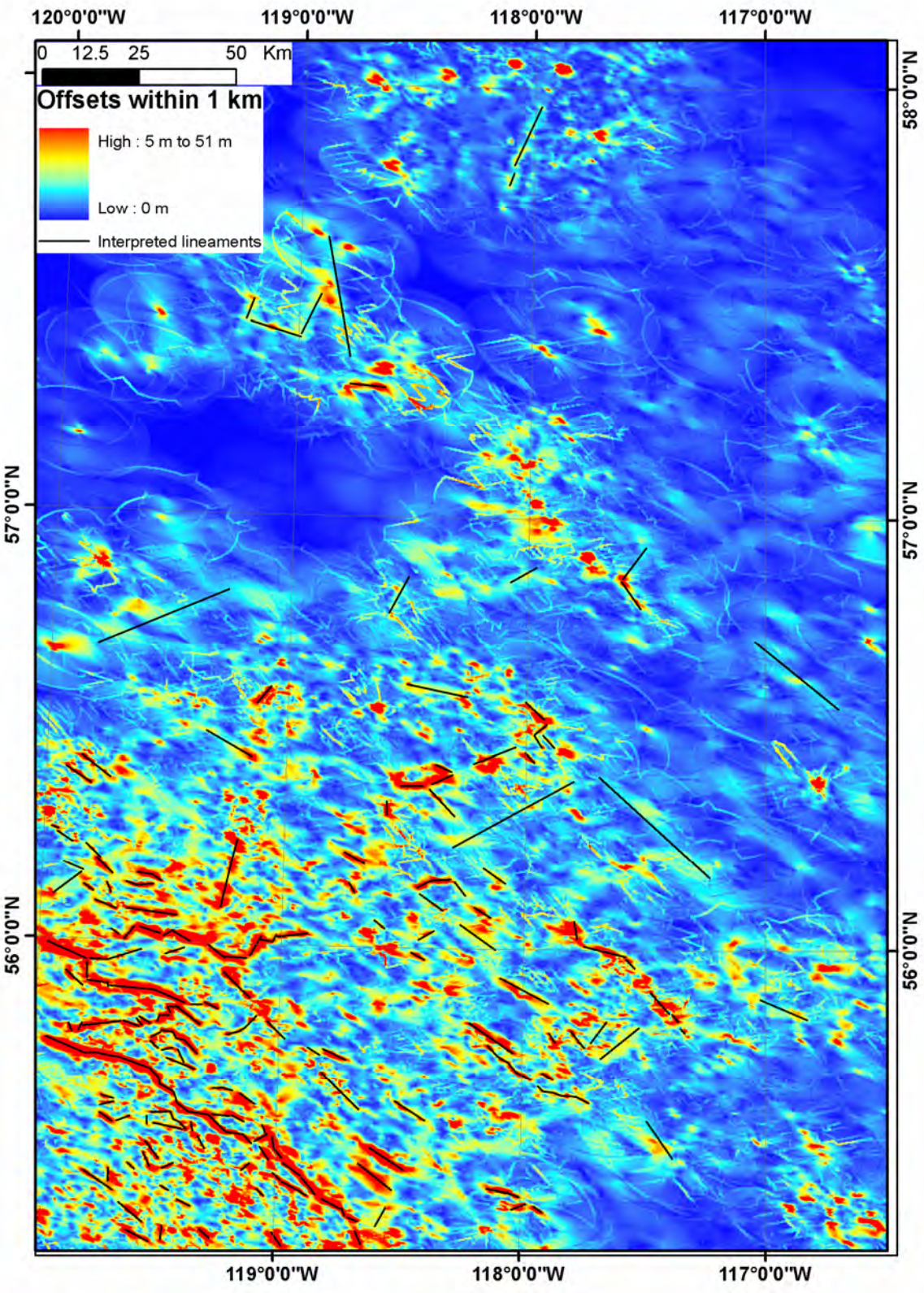

Figure 33. Lineaments interpreted from the top of the Bluesky Formation superimposed on the local offset map of the top of the Bluesky Formation.

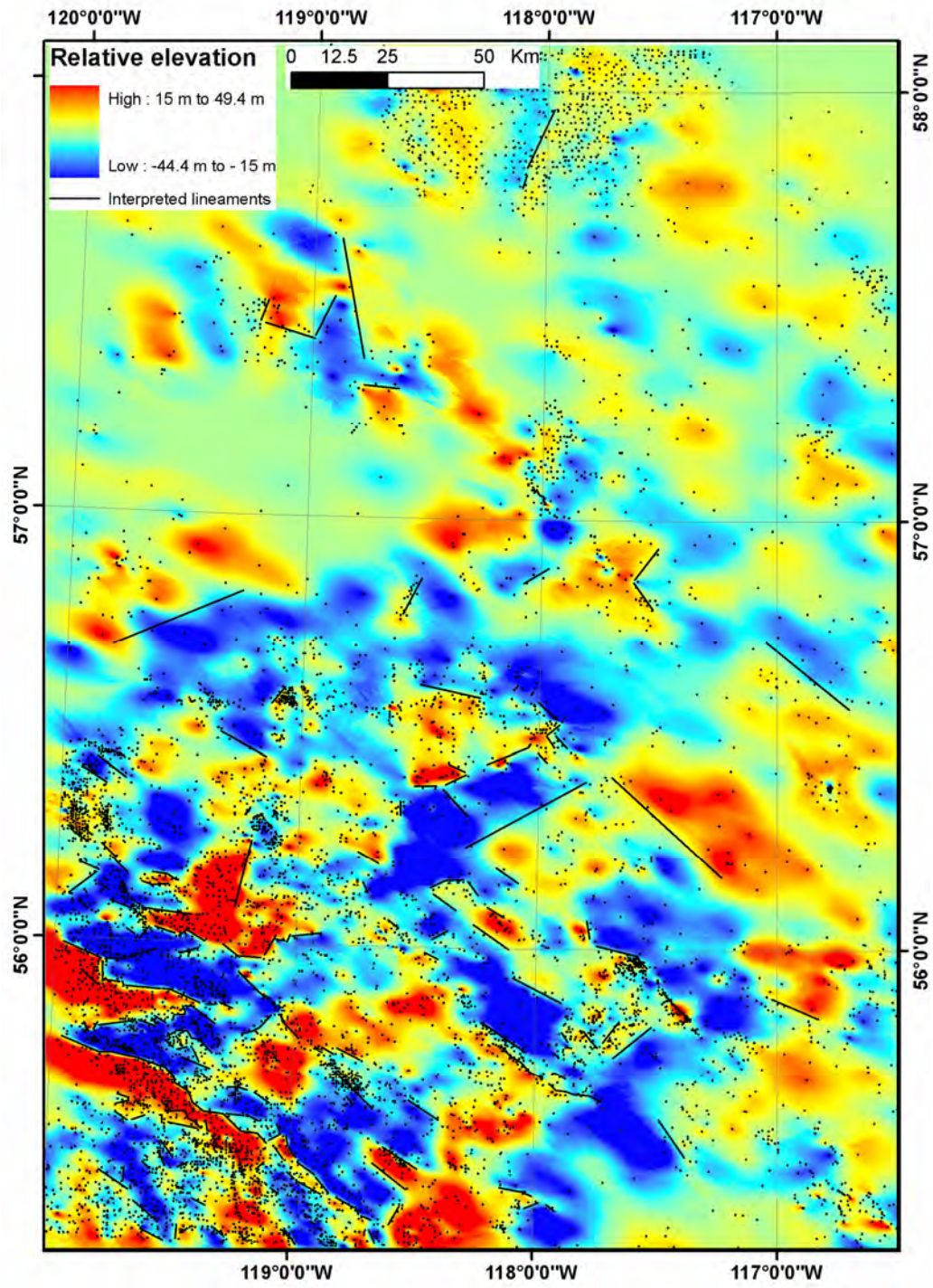

Figure 34. Lineaments interpreted from the top of the Bluesky Formation superimposed on the residual map of the top of the Bluesky Formation. Controlling wells are shown as black dots.

Figures 35 and 36 show lineaments interpreted from the top of the Jurassic Nordegg Formation superimposed, respectively, on local offset and residual maps of that top. Figures 37 to 39 show lineaments interpreted from the top of the Triassic Montney Formation superimposed, respectively, on local offset and residual maps of that top and the differential subsidence map of deposition from the top of the Belloy Formation to the top of the Montney Formation. The Nordegg and Montney formations occur

mainly in the southwestern half of the study area. They were deposited during the late stage of development of the Peace River Embayment.

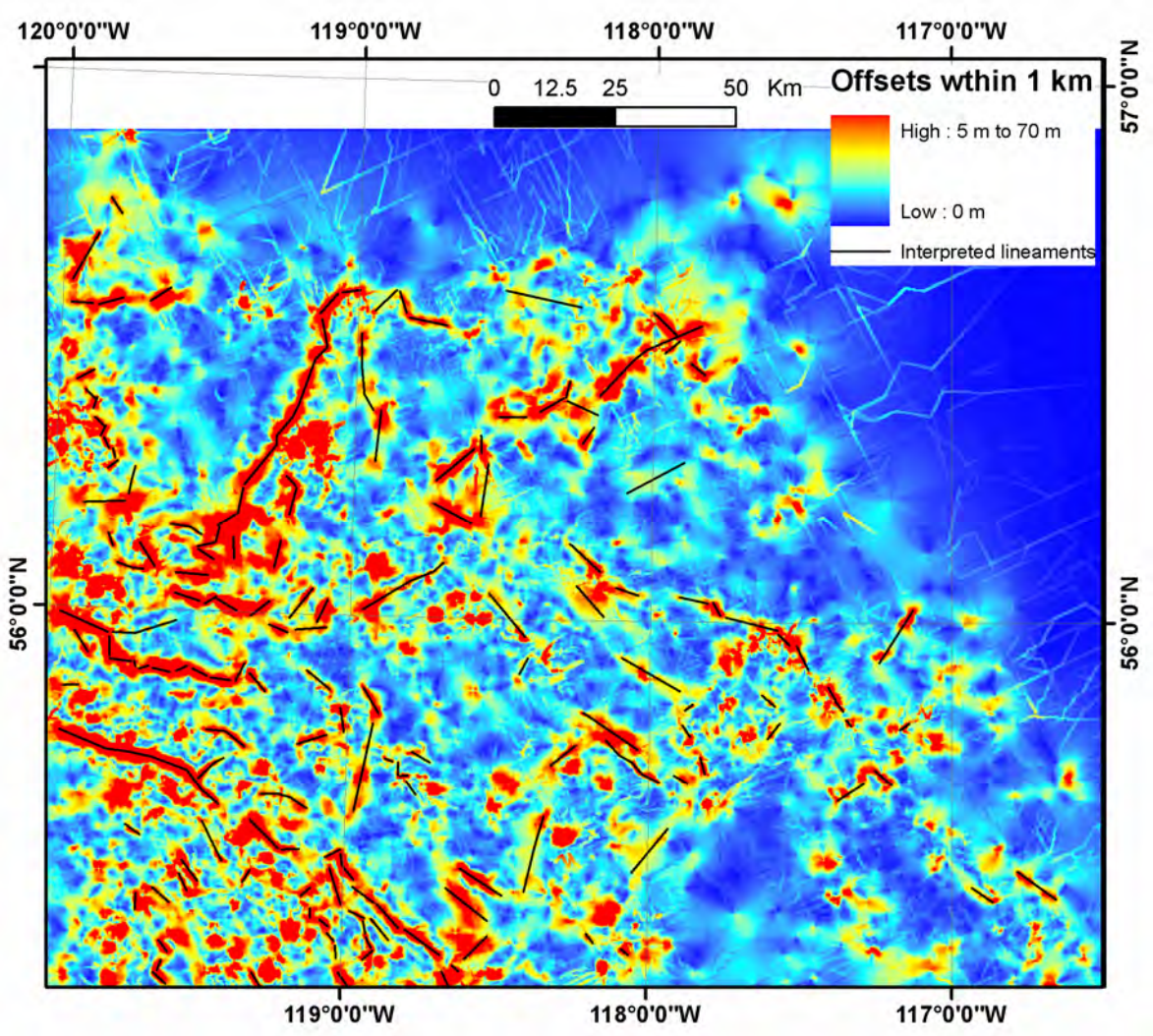

Figure 35. Lineaments interpreted from the top of the Jurassic Nordegg Formation superimposed on the local offset map of the top of the Nordegg Formation.

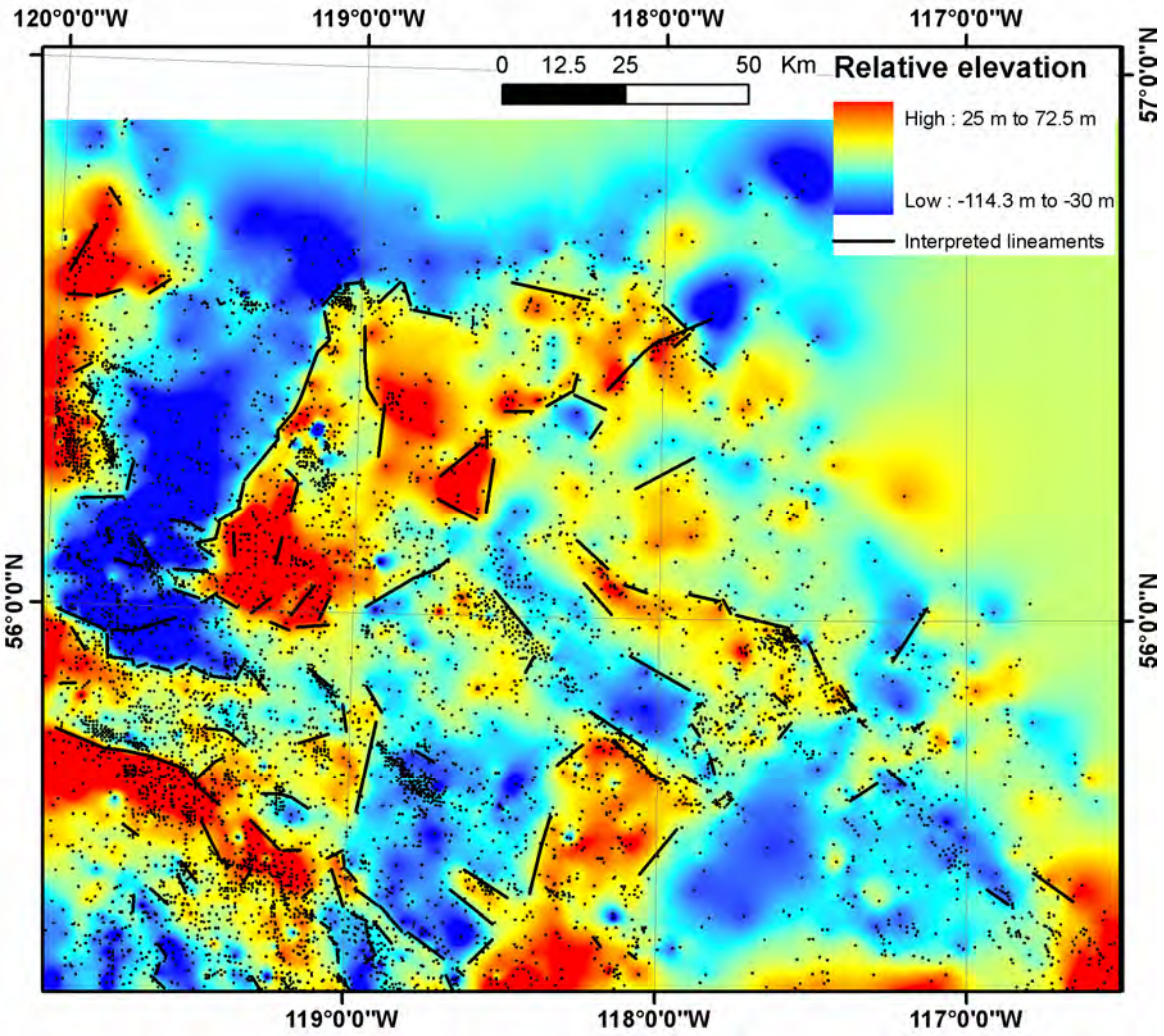

Figure 36. Lineaments interpreted from the top of the Jurassic Nordegg Formation superimposed on the residual map of the top of the Nordegg Formation. Controlling wells are shown as black dots.

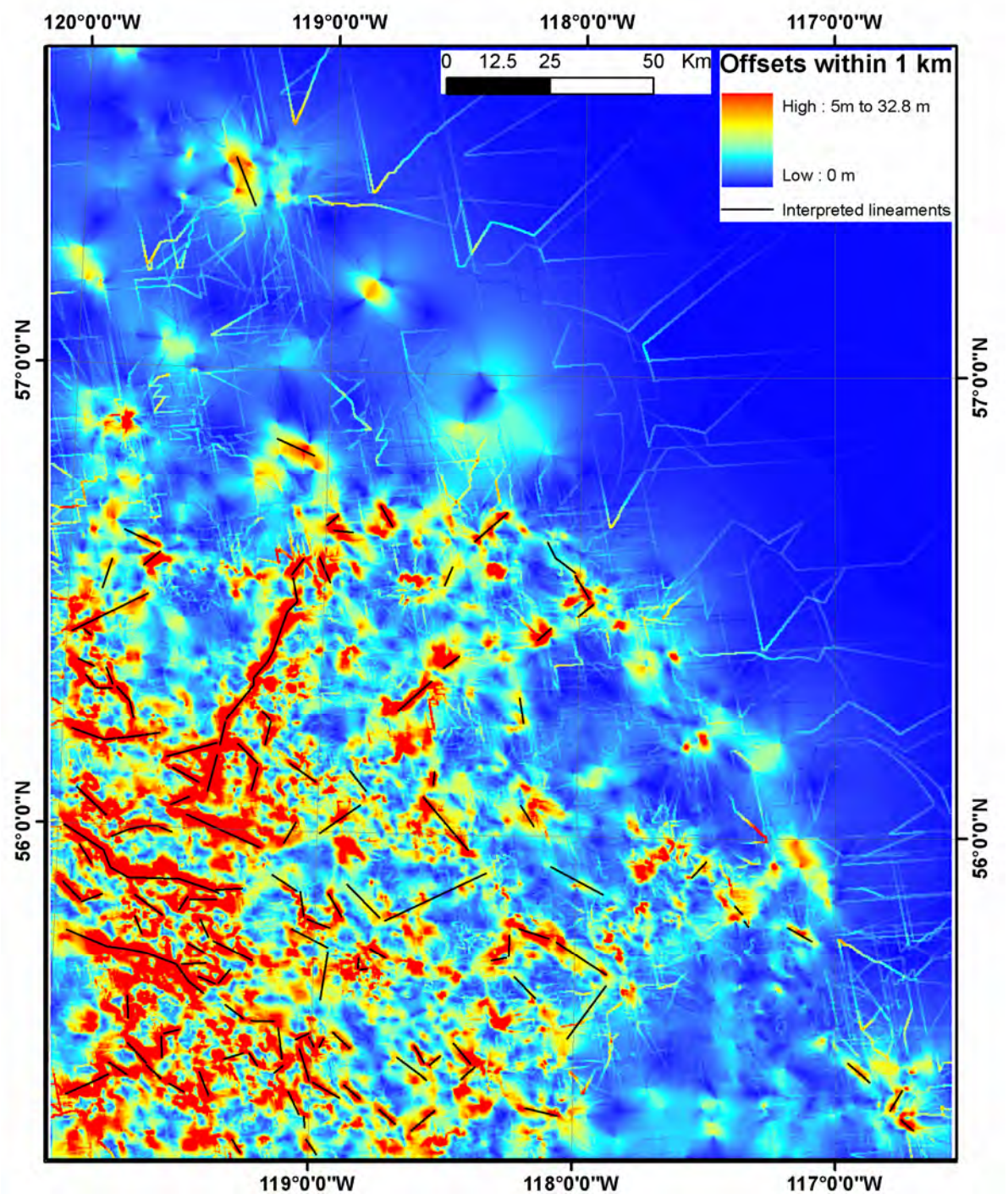

Figure 37. Lineaments interpreted from the top of the Triassic Montney Formation superimposed on the local offset map of the top of the Montney Formation.

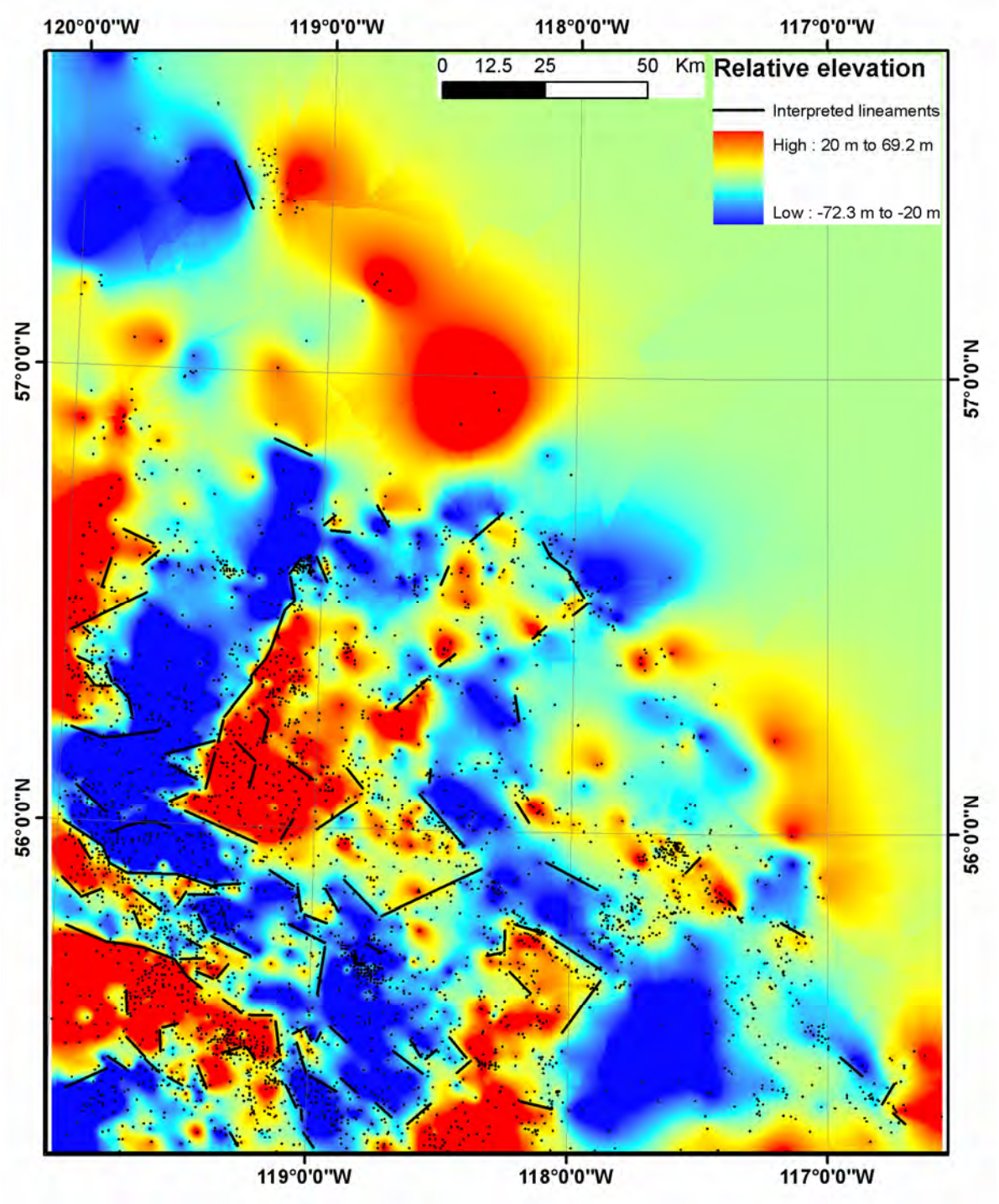

Figure 38. Lineaments interpreted from the top of the Triassic Montney Formation superimposed on the residual map of the top of the Montney Formation. Controlling wells are shown as black dots.

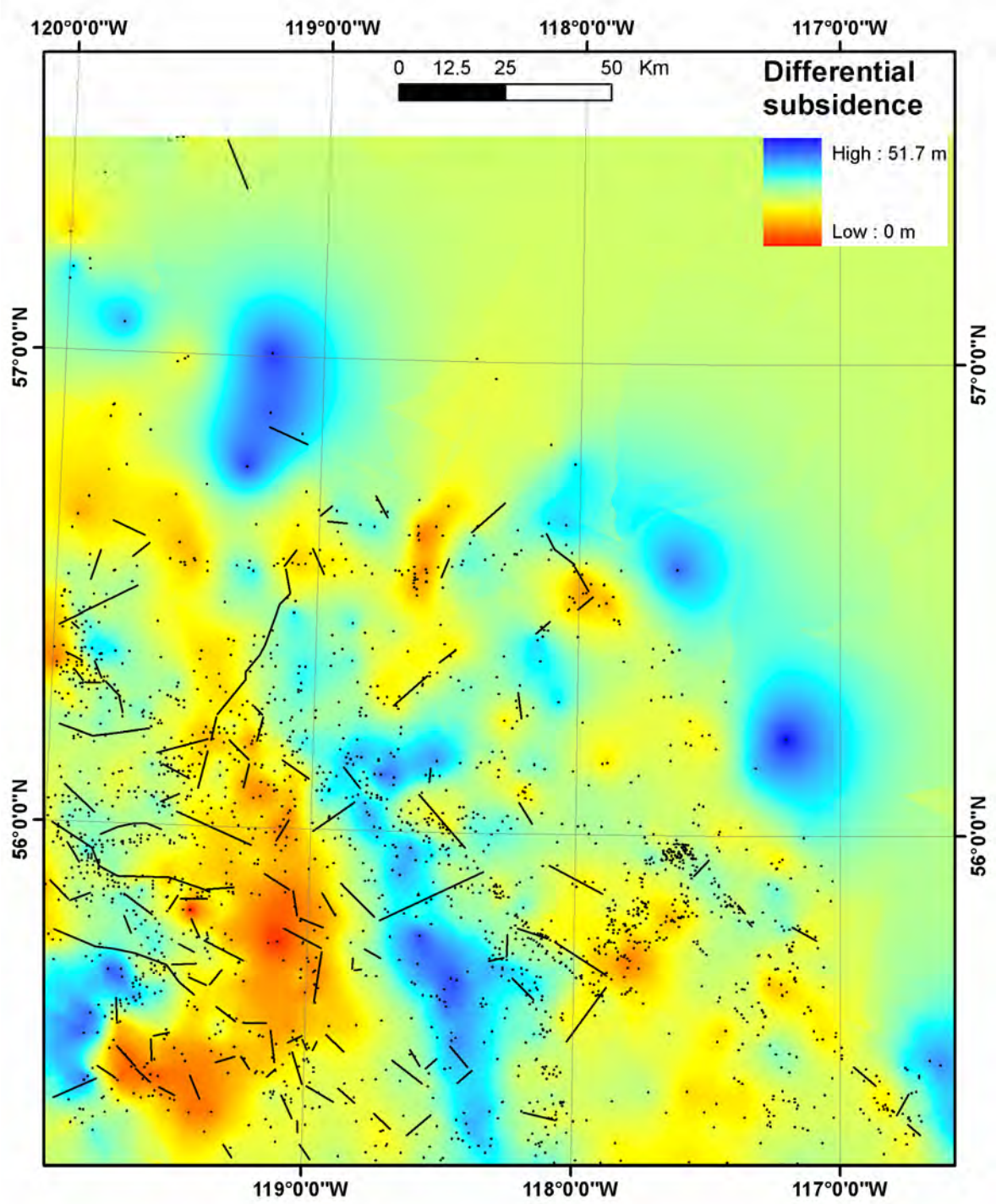

Figure 39. Lineaments interpreted from the top of the Triassic Montney Formation superimposed on the differential subsidence map of deposition from the top of the Belloy Formation to the top of the Montney Formation. Controlling wells are displayed as black points.

Figures 40 to 42 show lineaments interpreted from the top of the Permian Belloy Formation superimposed, respectively, on the local offset and residual maps of that top and the differential subsidence map of deposition from the top of the Mississippian Debolt Formation to the top of the Belloy Formation. Figures 43 to 45 show lineaments interpreted from the top of the Debolt Formation superimposed, respectively, on local offset and residual maps of that top and the differential subsidence

map of deposition from the top of the Banff Formation to the top of the Debolt Formation (i.e., the Rundle Group). These strata represent the tectonic stage of formation of the Dawson Creek Graben Complex (DCGC). Many of the faults are characterized by syndepositional growth faults, as indicated by the thickness/subsidence changes across the faults (*see* Figures 42, 45).

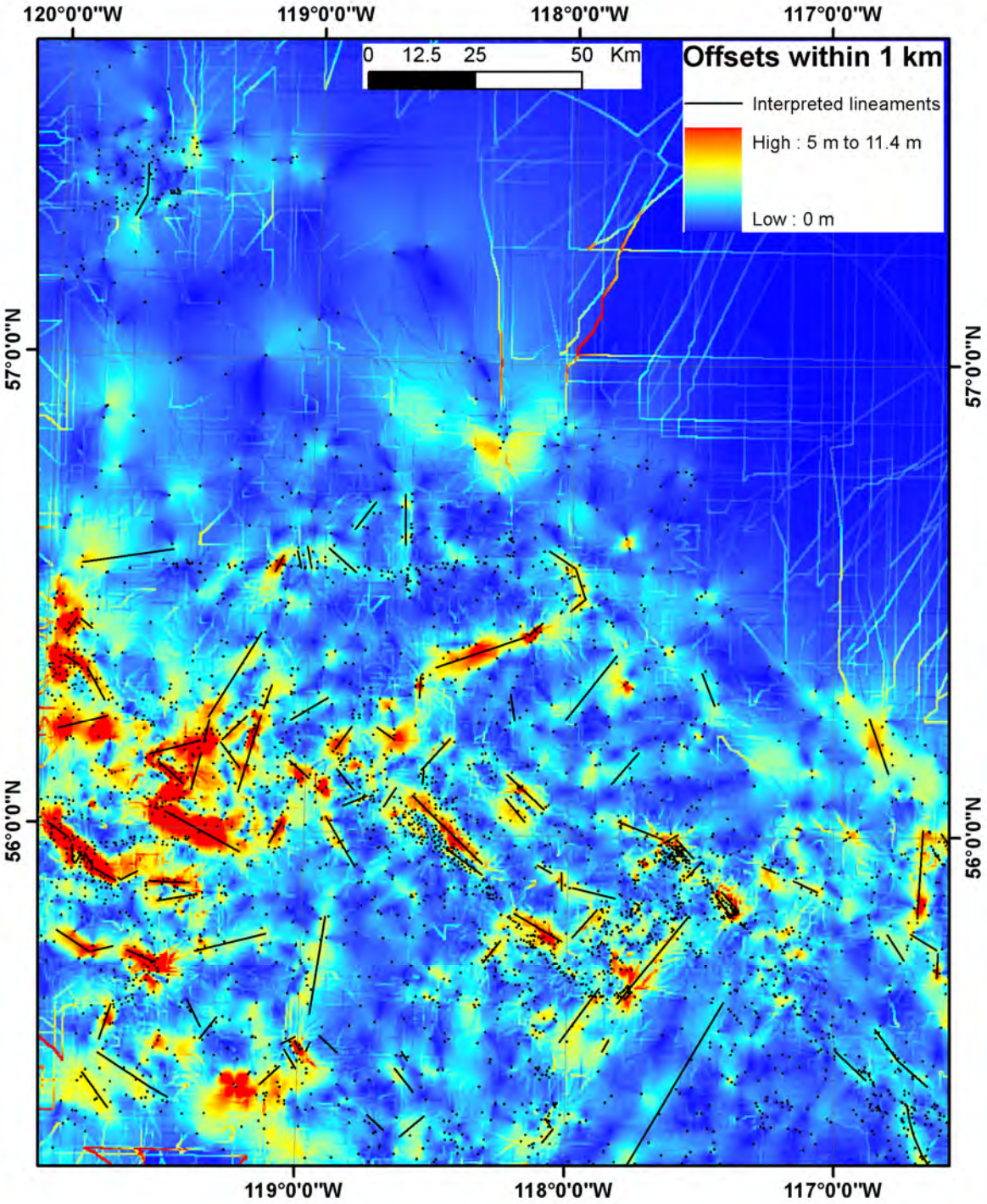

Figure 40. Lineaments interpreted from the top of the Permian Belloy Formation superimposed on the local offset map of the top of the Belloy Formation. Controlling wells are shown as black dots.

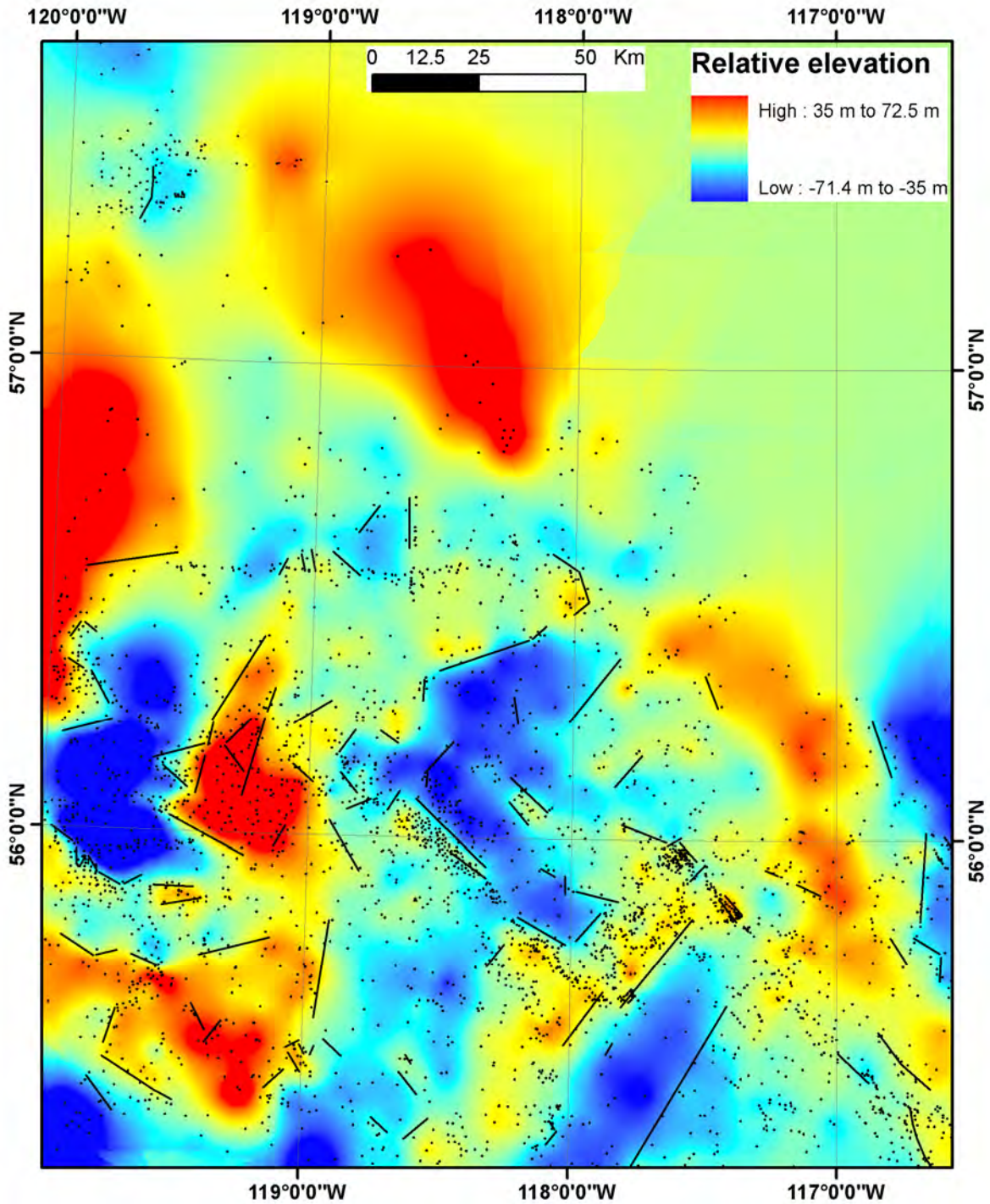

Figure 41. Lineaments interpreted from the top of the Permian Belloy Formation superimposed on the residual map of the top of the Belloy Formation. Controlling wells are shown as black dots.

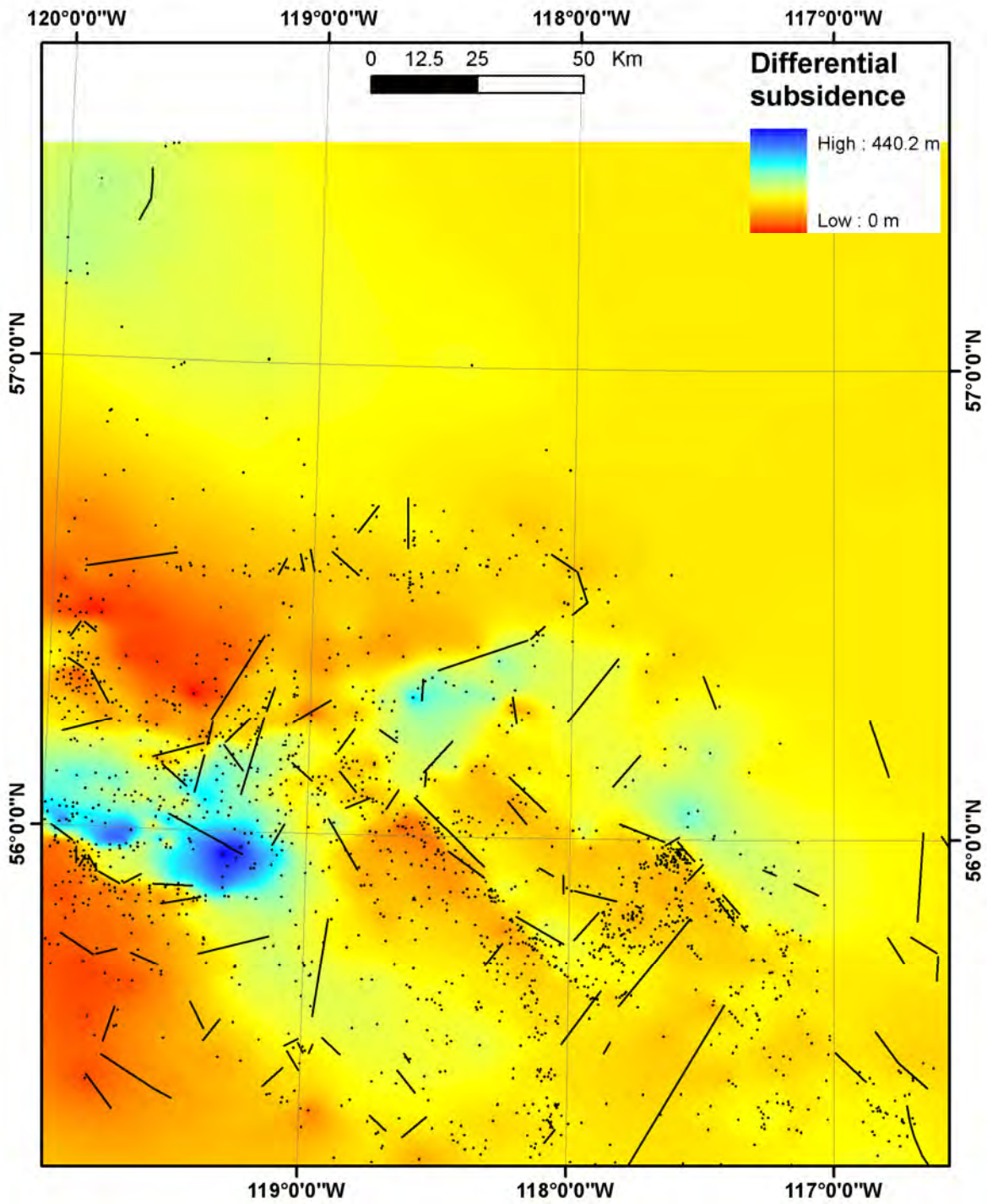

Figure 42. Lineaments interpreted from the top of the Permian Belloy Formation superimposed on the differential subsidence map of deposition from the top of the Belloy Formation to the top of the Debolt Formation. Controlling wells are displayed as black points.

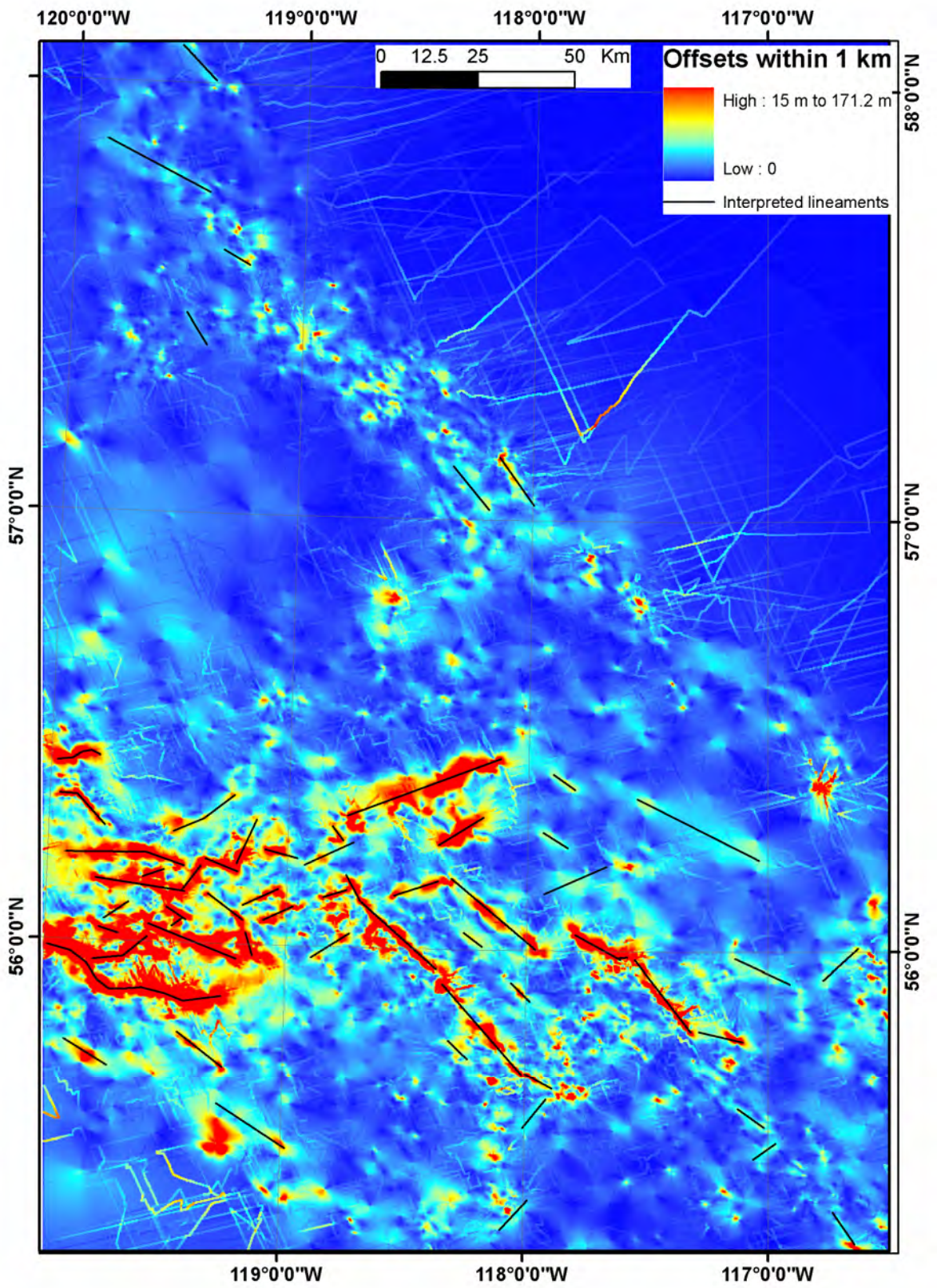

Figure 43. Lineaments interpreted from the top of the Mississippian Debolt Formation superimposed on the local offset map of the top of the Debolt Formation.

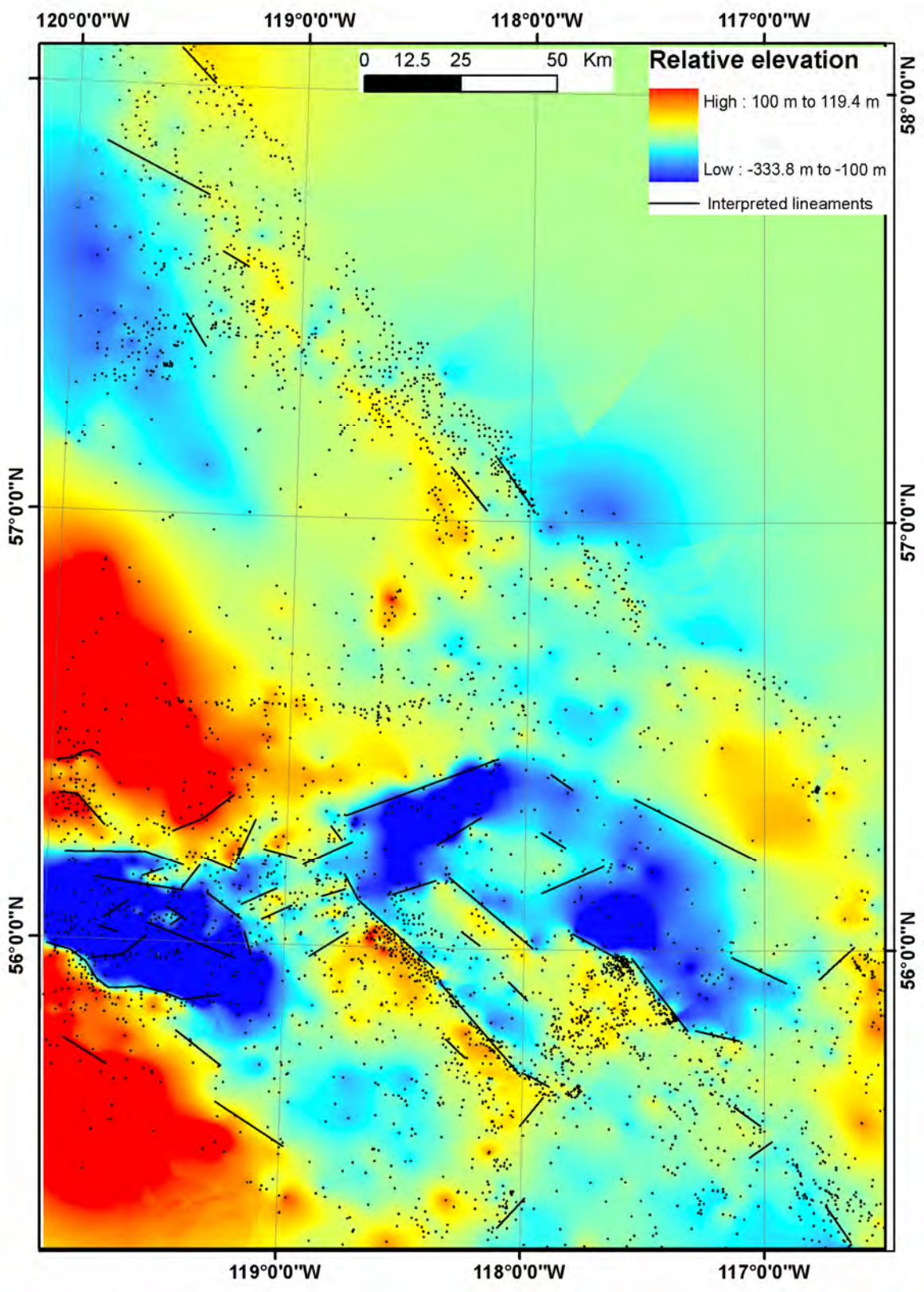

Figure 44. Lineaments interpreted from the top of the Mississippian Debolt Formation superimposed on the local offset map of the top of the Debolt Formation.

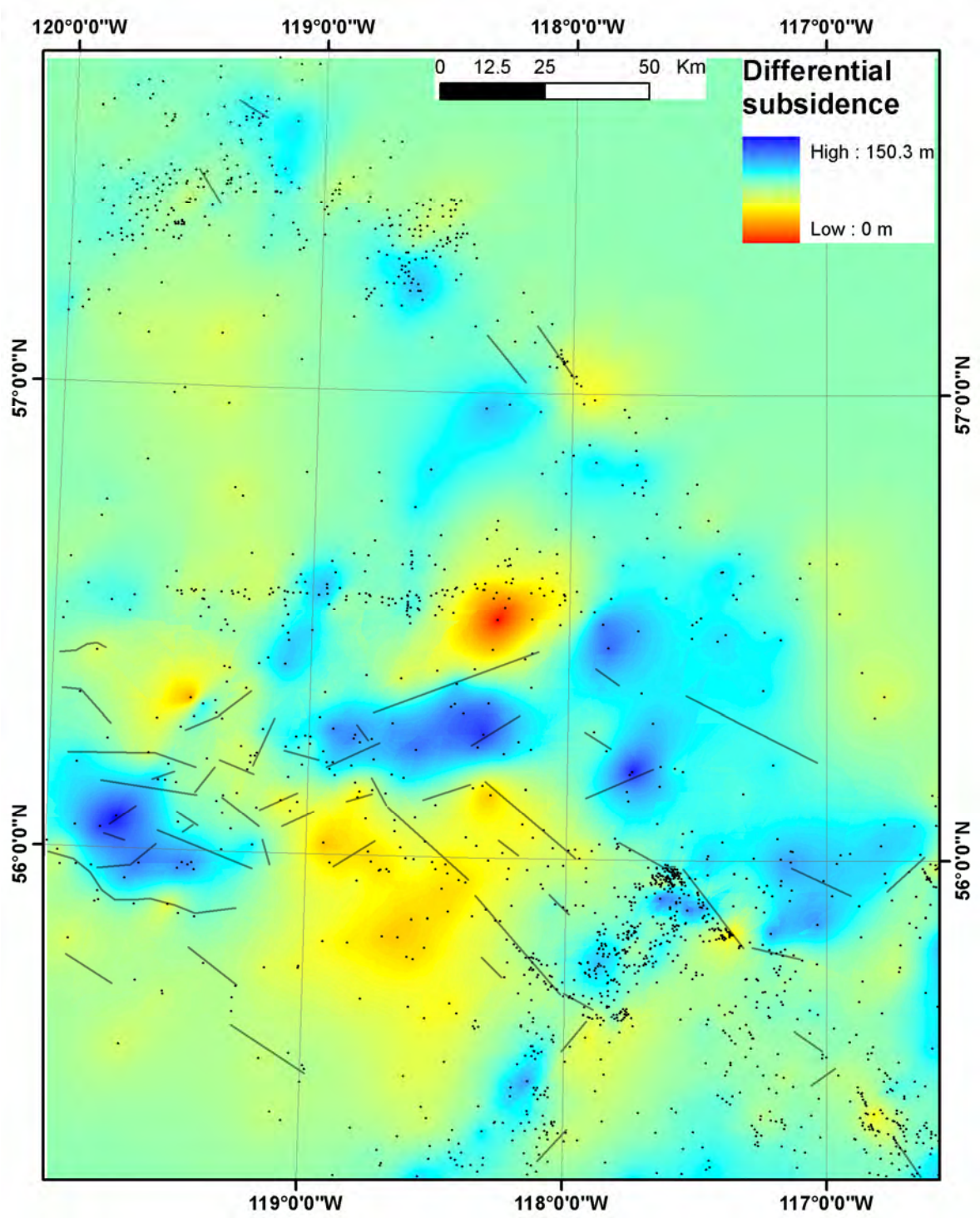

Figure 45. Lineaments interpreted from the top of the Mississippian Debolt Formation superimposed on the differential subsidence map of deposition from the top of the Banff Formation to the top of the Debolt Formation (i.e., the Rundle Group). Controlling wells are displayed as black points.

Figures 46 to 48 show lineaments interpreted from the top of the Carboniferous Banff Formation superimposed, respectively, on the local offset and residual maps of that top and the differential subsidence map of deposition from the top of the Wabamun Formation to the top of the Banff Formation. The faults interpreted from the top of the Banff Formation are typical postdepositional faults, as the

thickness/subsidence across them does not change (*see* Figure 48). The vertical offsets associated with these faults are greater than those interpreted from younger formations and are mainly confined to the area of the Dawson Creek Graben Complex. The residual map (Figure 47) also reveals a ridge-like structure that stands out in the northeast.

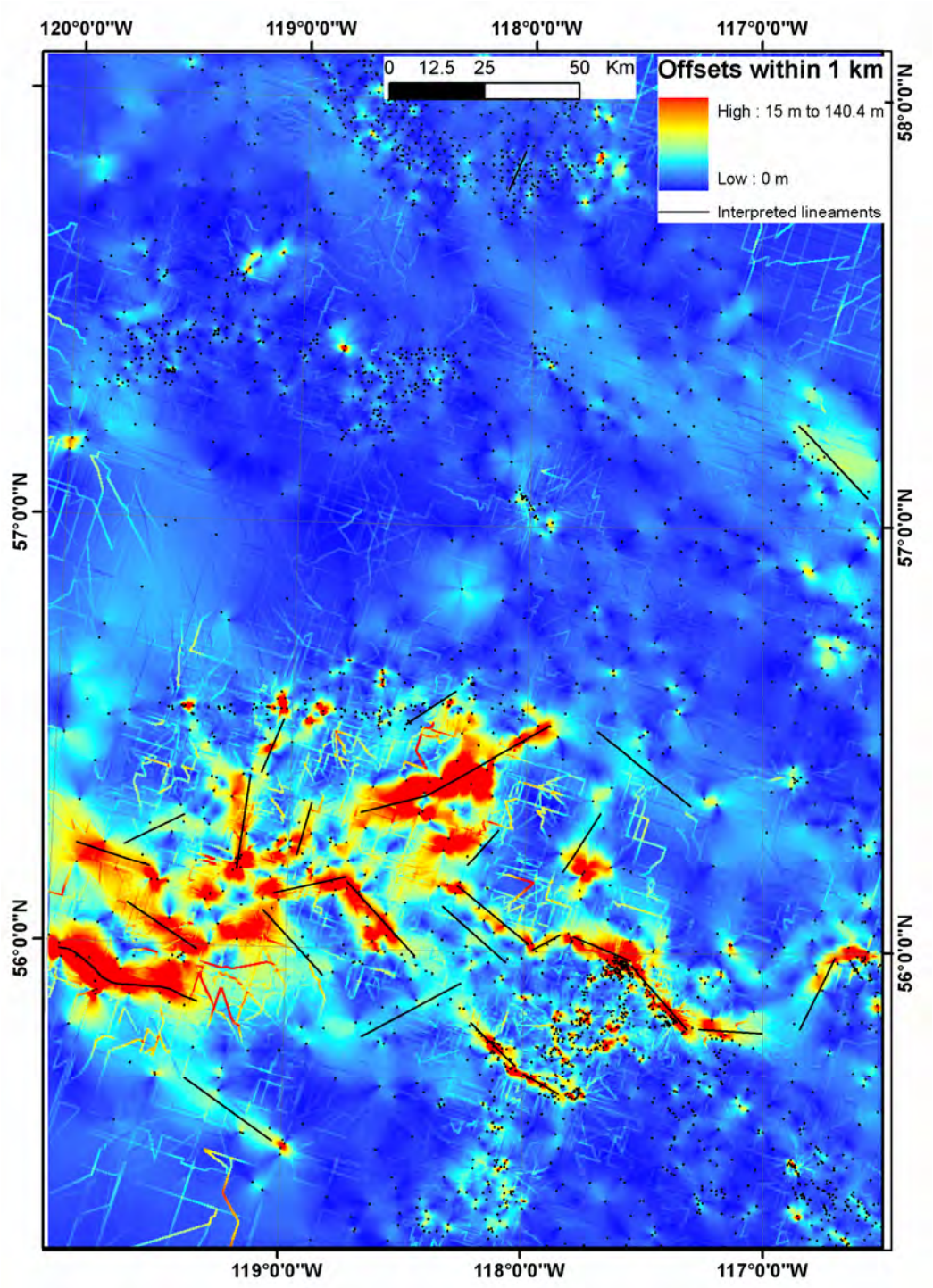

Figure 46. Lineaments interpreted from the top of the Carboniferous Banff Formation superimposed on the local offset map of the top of the Banff Formation. Controlling wells are shown as black dots.

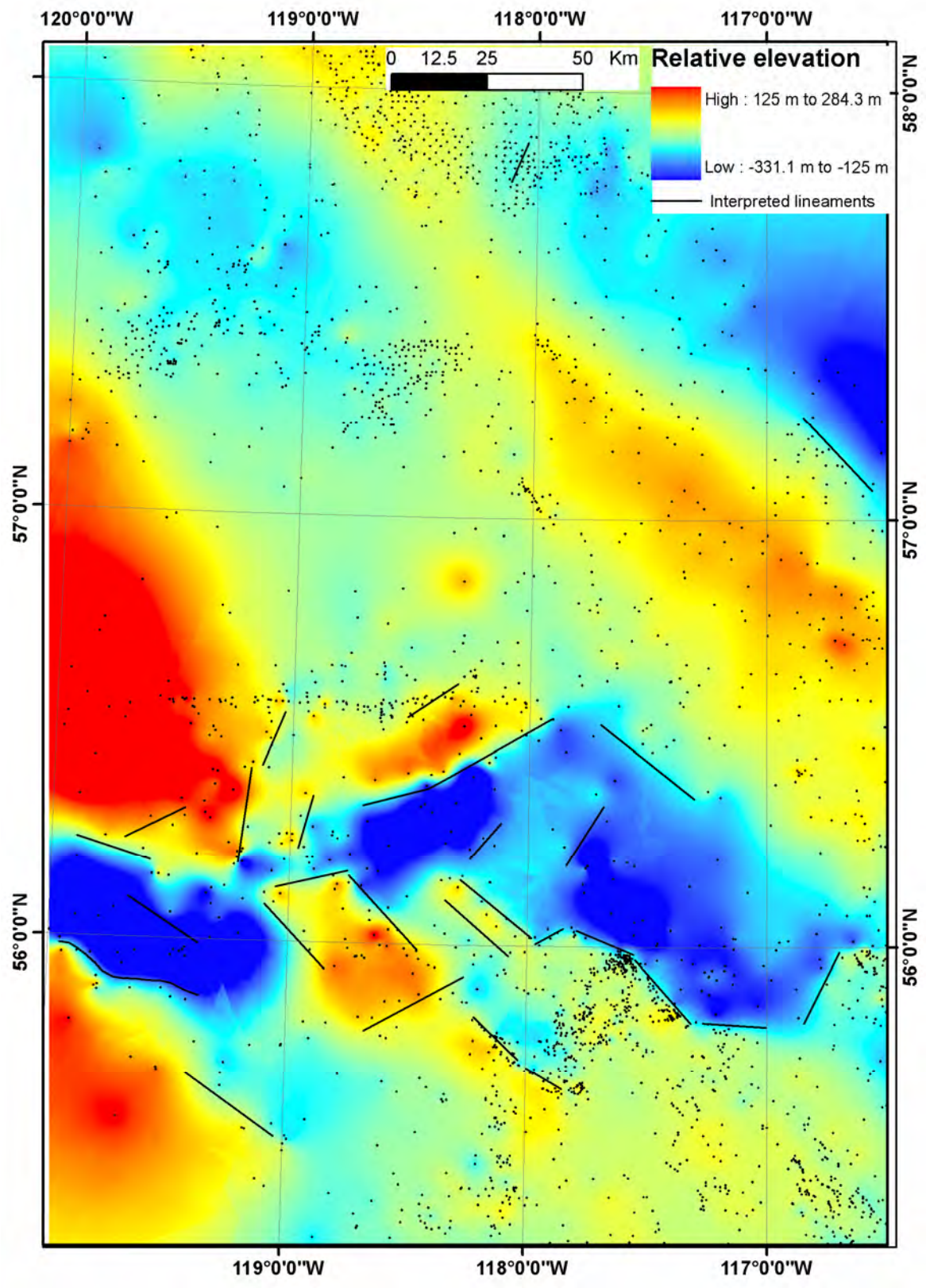

Figure 47. Lineaments interpreted from the top of the Carboniferous Banff Formation superimposed on the residual map of the top of the Banff Formation. Controlling wells are shown as black dots.

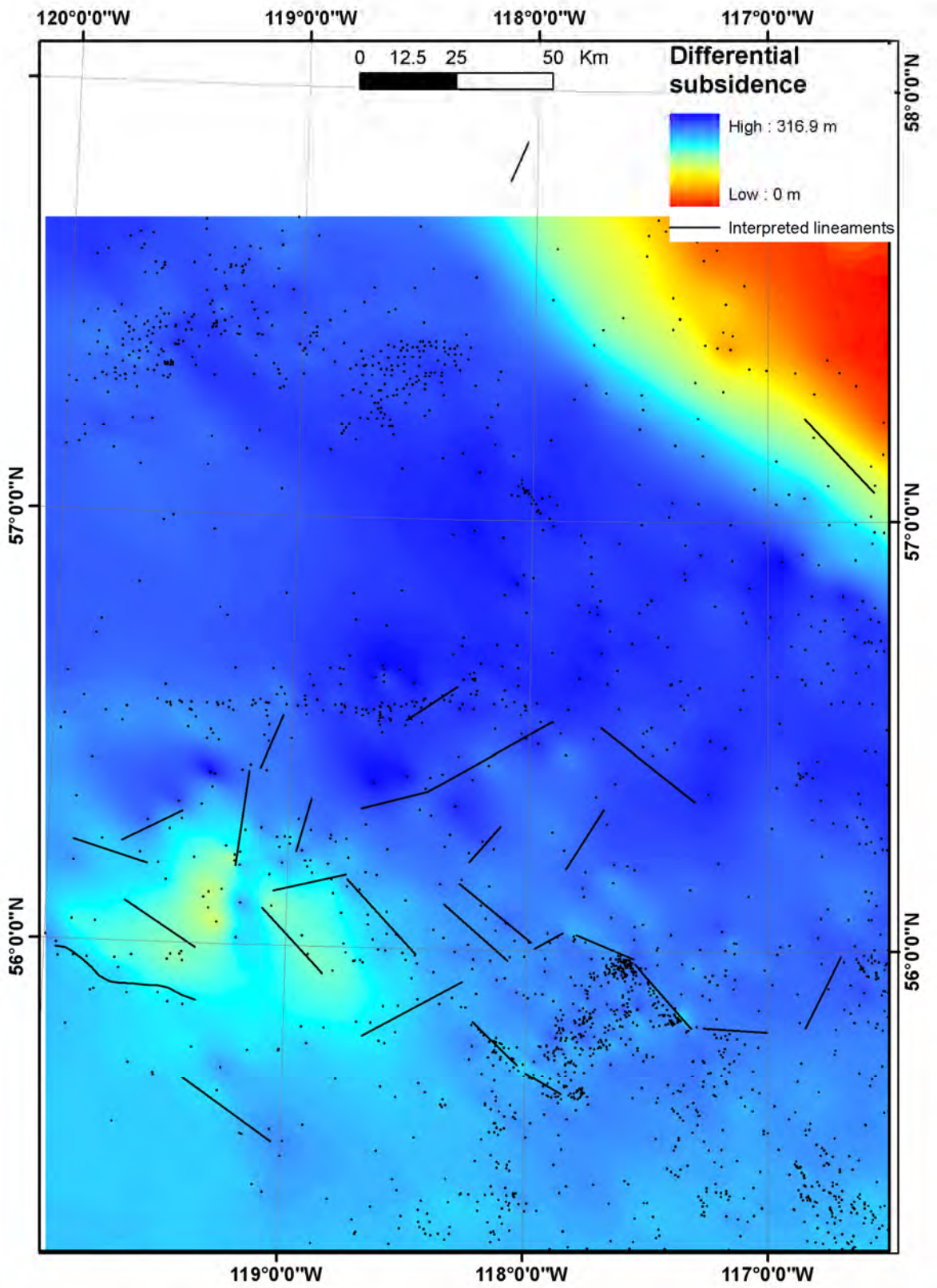

Figure 48. Lineaments interpreted from the top of the Carboniferous Banff Formation superimposed on the differential subsidence map of deposition from the top of the Wabamun Formation to the top of the Banff Formation. Controlling wells are displayed as black points.

Figures 49 and 50 show lineaments interpreted from the top of the Wabamun Formation superimposed, respectively, on the local offset and residual maps of that top. Together with the Banff Formation, it represents the latest stage of the Peace River Arch. The structures were enhanced by post-arch faulting.

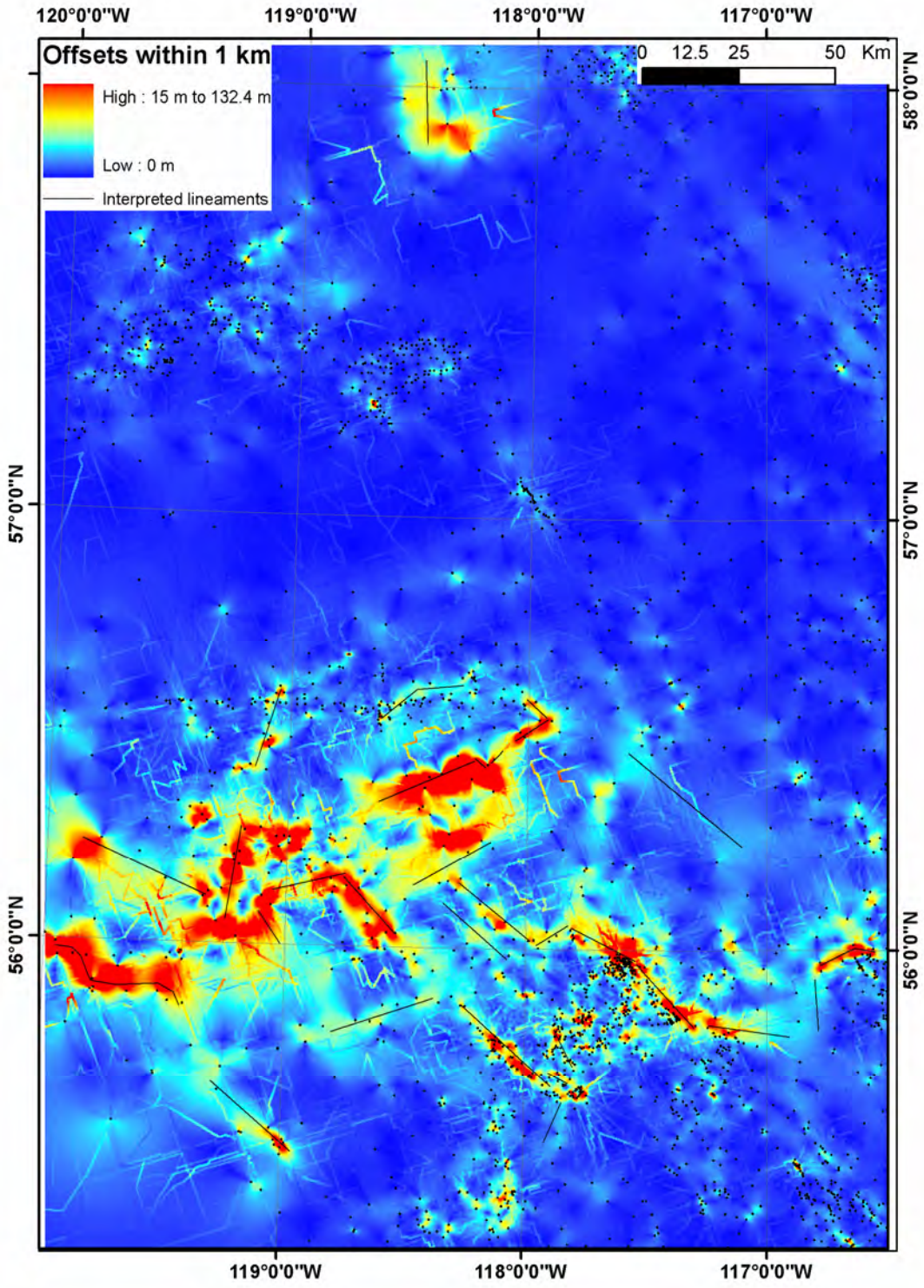

Figure 49. Lineaments interpreted from the top of the Wabamun Formation superimposed on the local offset map of the top of the Wabamun Formation. Controlling wells are shown as black dots.

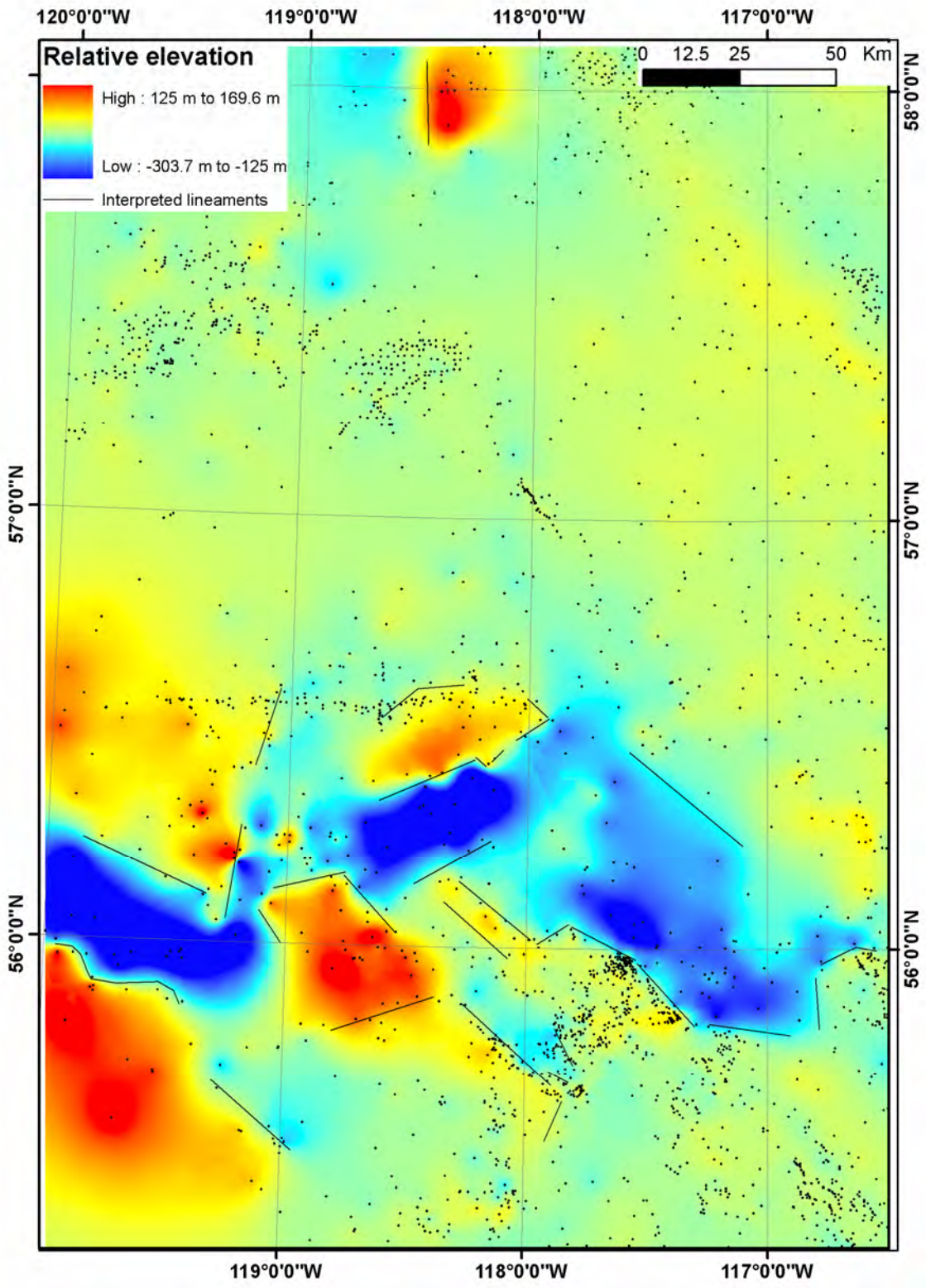

Figure 50. Lineaments interpreted from the top of the Wabamun Formation superimposed on the residual map of the top of the Wabamun Formation. Controlling wells are shown as black dots.

Figures 51 and 52 show, respectively, lineaments interpreted from the top of the Ireton/Fort Simpson Formation and the Slave Point Formation superimposed on residual maps of those tops. These two formations are not present over the Peace River Arch.

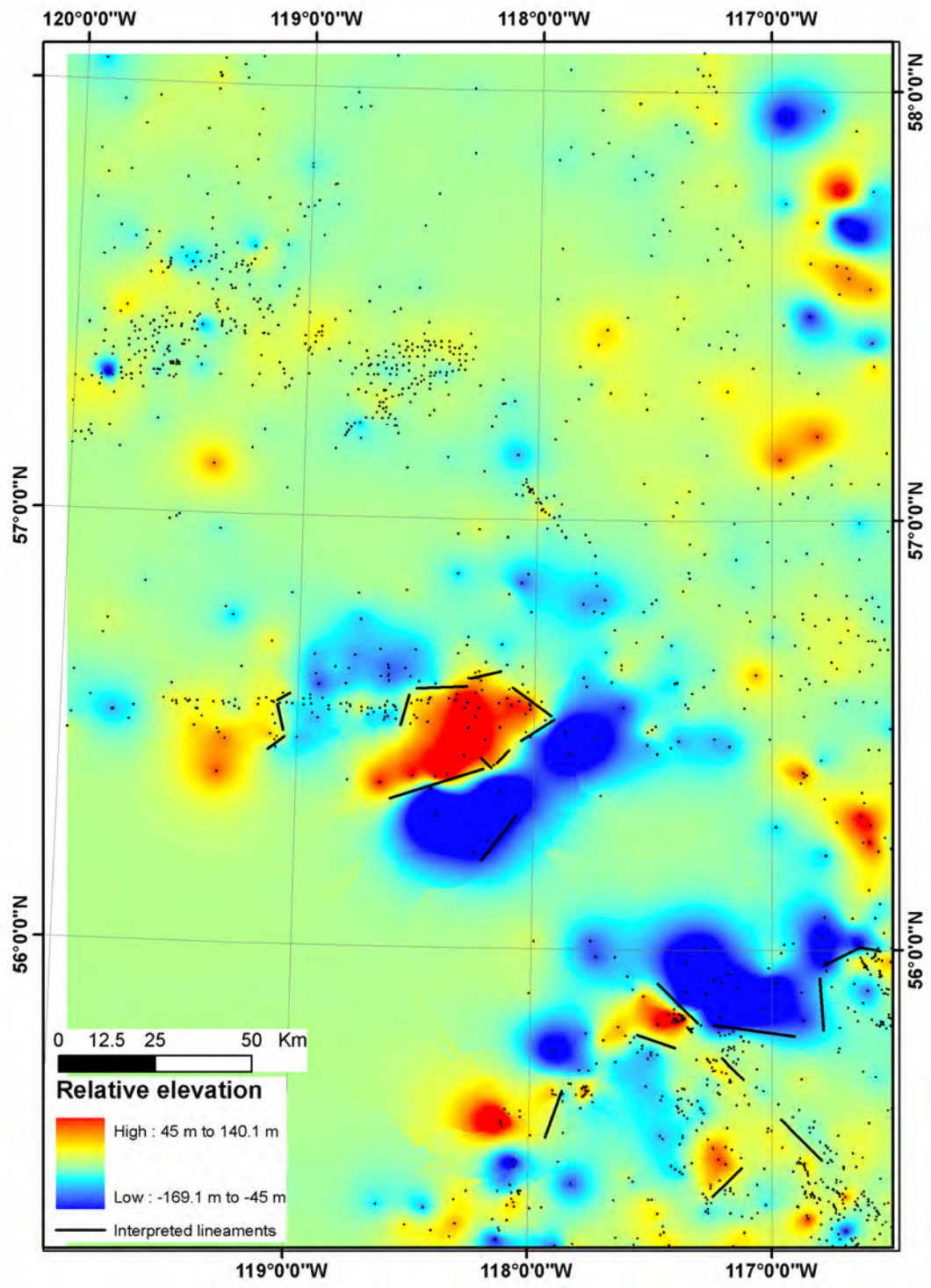

Figure 51. Lineaments interpreted from the top of the Ireton / Fort Simpson Formation superimposed on the residual map of the top of the Ireton / Fort Simpson Formation. Controlling wells are shown as black dots.

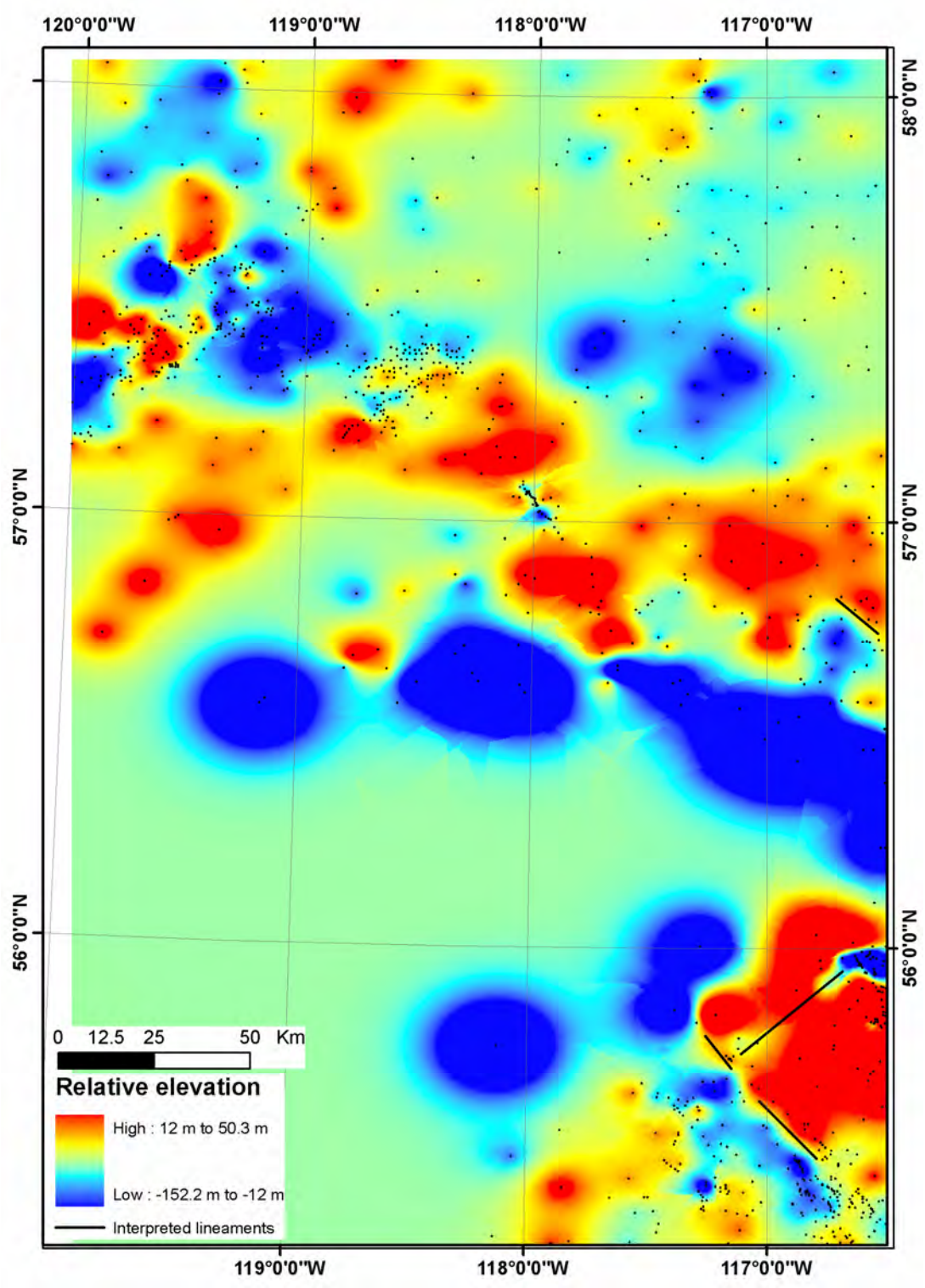

Figure 52. Lineaments interpreted from the top of the Slave Point Formation superimposed on the residual map of the top of the Slave Point Formation. Controlling wells are shown as black dots.

Figure 53 and 54 show lineaments interpreted from the top of the Precambrian superimposed, respectively, on the local offset and residual maps of that top. Although the penetrating wells have a

greater spacing, they are available over the Peace River Arch. This makes it possible to compare the structures from the Precambrian top surface to those from the sedimentary cover.

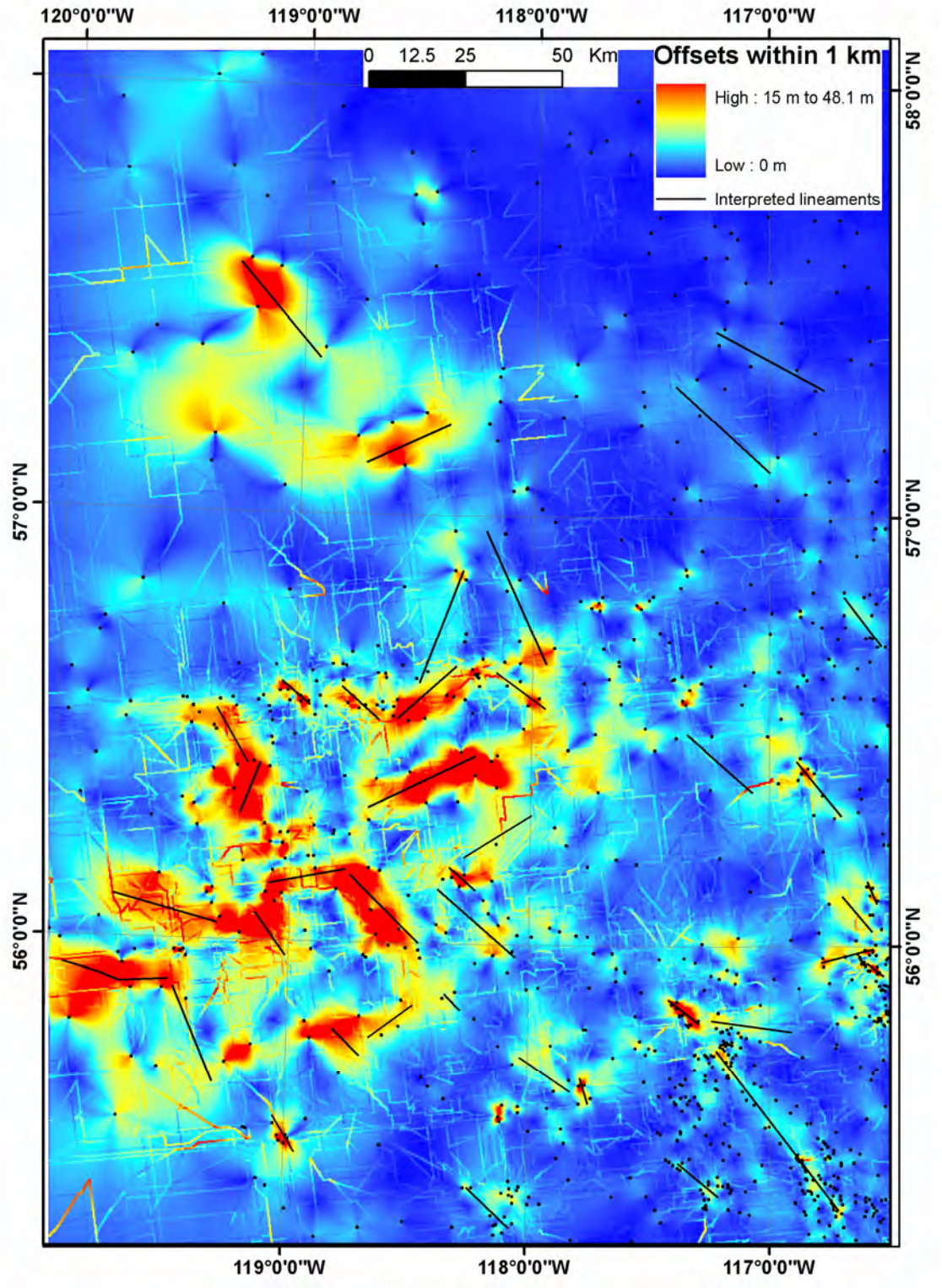

Figure 53. Lineaments interpreted from the top of the Precambrian superimposed on the local offset map of the top of the Precambrian. Controlling wells are shown as black dots.

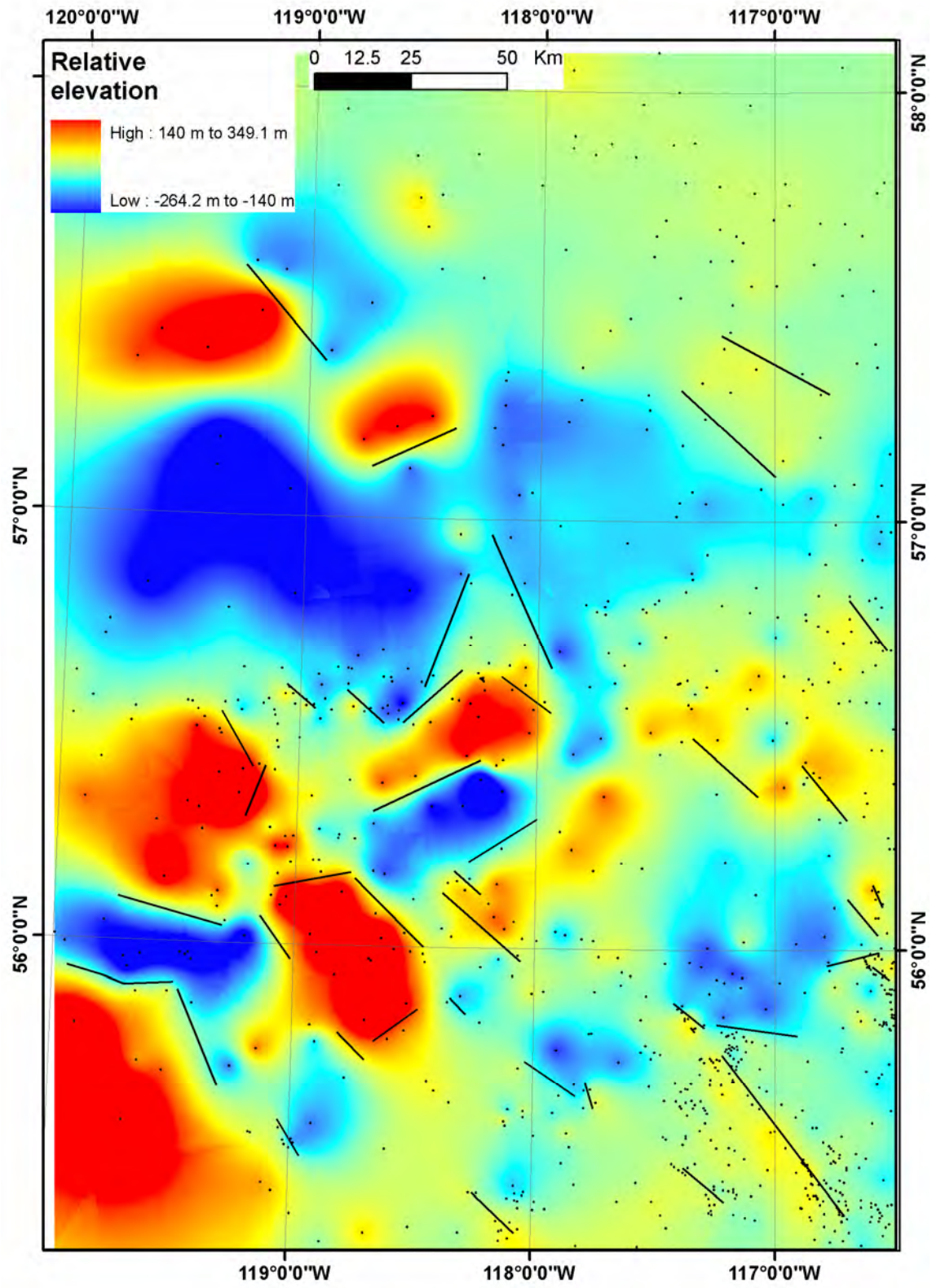

Figure 54. Lineaments interpreted from the top of the Precambrian superimposed on the residual map of the top of the Precambrian. Controlling wells are shown as black dots.

4.5 Compilation of Interpreted Lineaments/Faults

A fault has been routinely presented as a single line on a two-dimensional map, regardless of the fact that it is actually a three-dimensional surface. As indicated previously, the linear offset patterns of a specific formation top are digitized on screen as individual lines. These lines are initially termed lineaments. When a lineament is proven to be an expression of a fault on a specific formation top, then it represents a fault. The most convincing evidence to link a lineament to a fault is that the same or a similar offset pattern is repeatedly observed from several successive formation tops, as this indicates that the same fault has offset these formation tops. When a fault is nearly vertical, the linear offset patterns it caused on several formation tops more or less overlap on a two-dimensional map, and it is therefore straightforward to present it as a single line on a two-dimensional map. In many cases, however, faults are not vertical, which causes problems when trying to present them as single lines on a single two-dimensional map. When a fault with a consistent angle of dip offsets several formation tops, the linear offset patterns on the younger formation tops will shift toward the upthrown block, and the linear offset patterns on the older formation tops will shift toward the downthrown block. A listric fault will add more complexity.

In previous publications on structure in the Peace River region, lineaments/faults were interpreted from separate intervals, by different authors, at different times, from different maps (facies versus structure and isopach contour maps) and using different densities of data points and techniques (e.g., Sikabonyi and Rodgers, 1959; Jones, 1980; Cant, 1988; Barclay et al., 1990; Dix, 1990; O'Connell et al., 1990; Richards et al., 1994; Henderson et al., 1994; O'Connell, 1994). As a result, some of the faults are represented by multiple lineaments (*see* Figure 6) in the compilation of lineaments by Pană et al. (2001). The difference in location of the lineaments representing the same fault in the compilation is the collective result of the digitizing error, the fact that they are not vertical and the fact that they were interpreted from different formation tops, by different authors and with different data spacing and associated accuracy in both location and direction.

As demonstrated previously, lineaments are first interpreted from the residual and local offset maps created for each selected formation top. These lineaments are then compared across formation tops to identify the common linear patterns. Figure 55 shows all the lineaments interpreted from the selected formation tops and the Precambrian top. The linear patterns on this map are interpreted to be expressions of a fault on different formation tops. Most of the major faults in the study area are steep to nearly vertical, which makes the comparison task less difficult. The extent of overlap of the lineaments that represent the same fault on different formation tops is manifested by the darkness and width of the linear patterns (Figure 55). Generally speaking, the dark and narrow linear patterns represent steep to nearly vertical faults, and the wide linear patterns indicate faults with less steep dips. The locational differences of interpreted lineaments within a linear pattern are mainly caused by the dipping surface of the fault and some uncertainty in the position and direction of the fault during the on-screen digitizing. The isolated, light-colour and single-line patterns represent offsets that were identified only from a single formation top and therefore may not necessarily indicate faults, perhaps representing only local formation-top undulations.

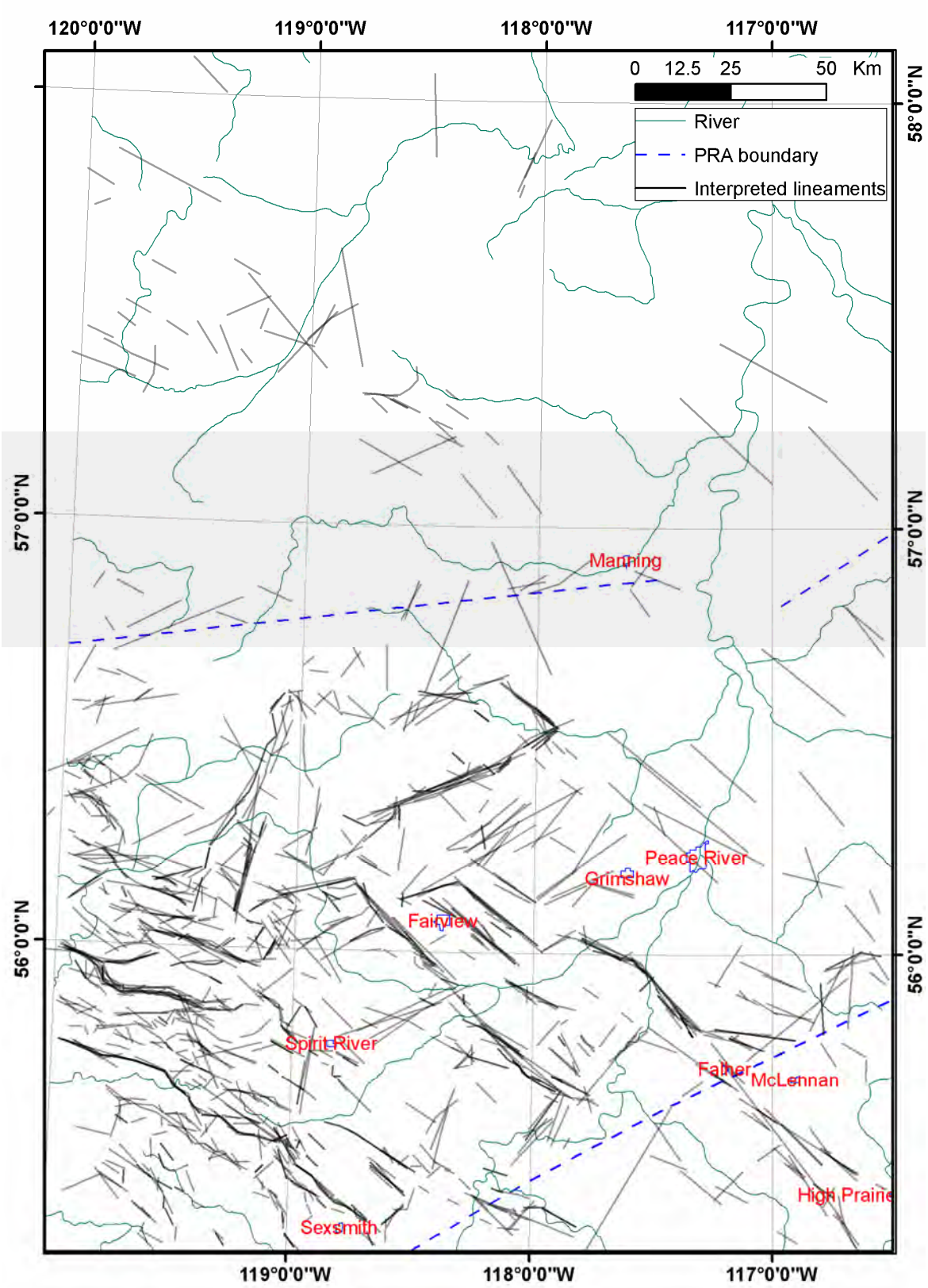

Figure 55. Linear patterns of formation-top offsets manifested by lineaments interpreted from all the selected formation tops and the Precambrian top.

A more detailed comparison of the overall structure pattern identifies three groups of similar patterns (Figure 56):

- Cretaceous formation tops, including the Basal Fish Scale Zone, the Peace River Formation, the Spirit River Formation and the Bluesky Formation
- the Lower Jurassic Nordegg Formation, the Triassic Montney Formation and the Permian Belloy Formation
- the Carboniferous Debolt and Banff formations, the Devonian Wabamun Formation and the Precambrian top

These groups represent different stages of tectonic evolution and will be discussed in more detail in the following section. Figure 57 shows the lineaments compiled for each of these three groups. During the compilation, the middle line of the linear pattern represented by similar and common lineaments from different formation tops within each group was digitized. Many of the interpreted lineaments are associated with the known faults of the DCGC (*see* below) and offset multiple formation tops. Figures 56 and 57 show that some of the faults offset the entire sedimentary cover sequence, whereas others are confined to only Permian and/or Mesozoic formations.

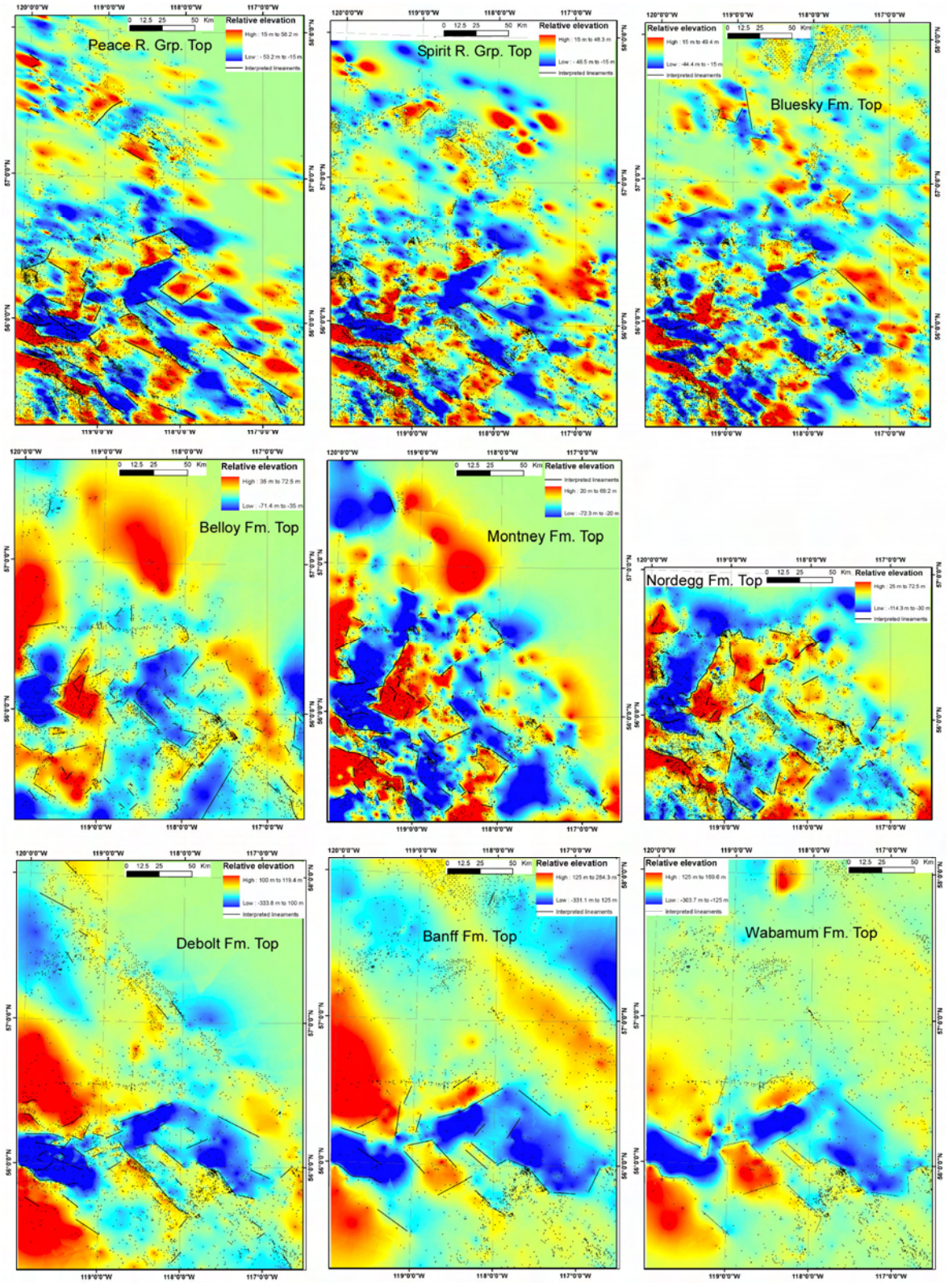

Figure 56. Summary of selected residual maps showing three groups of structure patterns.

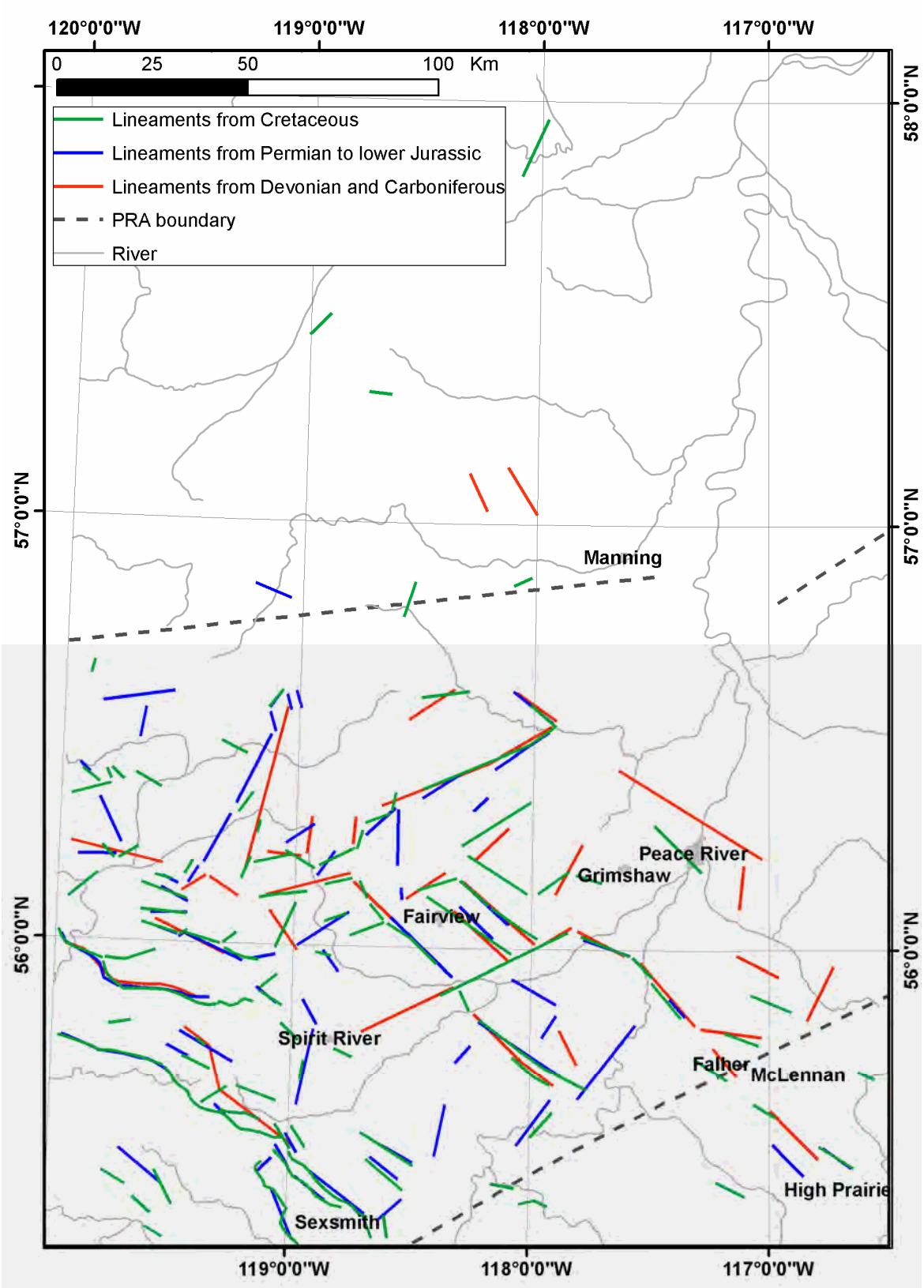

Figure 57. Lineaments compiled from Cretaceous, Permian to the Lower Jurassic, and Devonian to Carboniferous formations. Most of the lineaments can be associated with the known steep faults of the DCGC.

5 Discussion and Conclusion

The results presented above indicate that the structures within the sedimentary cover in the study area are concentrated in the area of the Peace River Arch (Figures 55 to 57). The structures associated with the Peace River Arch have been the focus of numerous studies (e.g., DeMille, 1958; Lavoie, 1958; Williams, 1958; Sikabonyi and Rodgers, 1959; Jones, 1980; Cant, 1988; Barclay et al., 1990; Dix, 1990; O'Connell et al., 1990; Richards et al., 1994; Henderson et al., 1994; O'Connell, 1994) and constitute the majority of faults in the sedimentary cover sequence of northern Alberta. The refined approach to structure mapping developed during the present study results in a higher resolution in capturing the linear offset patterns and higher accuracy in positioning the faults. It therefore results in refinements and updates of previously interpreted faults, as well as identification of possible new faults, especially from formations of Triassic to Cretaceous age. It is necessary to point out that the refined approach was applied to the existing AGS well database with only minimal control of data quality on formation-top picks, since more control was beyond the scope of this study. Nevertheless, the overall results are more accurate and have a higher resolution than previous interpretations (see below for more details).

Like any of the previous studies, the formation-top offset detected with the refined approach represents the final and total offset up to the present. A structure inversion has been detected around the mid-Cretaceous unconformity (compare Figures 25 and 29). It involves a hinge line that extends from the axis of the Hines Creek graben to roughly the north boundary of the Fort St. John graben (Figures 25 and 29). During deposition of the Peace River Formation, more subsidence occurred to the south of the hinge line (Figure 29), whereas, during deposition of the interval from the top of Peace River Formation to the BFSZ, more subsidence occurred to the north of the hinge line (Figure 25). It is expected that similar structure inversion may have occurred for some of the faults interpreted from formation-top offset patterns (*see* below). Detailed treatment of the inversion, however, is beyond the scope of the present study.

5.1 Refinements and Updates to the Dawson Creek Graben Complex

The Dawson Creek Graben Complex (DCGC), as defined by Barclay et al. (1990), forms the core of the structures in the Peace River Arch region. The interpreted faults related to the DCGC were presented by Richards et al. (1994) and Henderson et al. (1994); however, very few details were provided on how these faults were defined except to state that they were compiled from unpublished seismic and lithostratigraphic data. Barclay et al. (1990) defined the DCGC as including a large central Fort St. John Graben (FSJG) and three small satellite grabens, namely the Hines Creek, Whitelaw and Cindy grabens. Richards et al. (1994) and Henderson et al. (1994) recognized the FSJG and Hines Creek Graben on their maps, but the Whitelaw and Cindy satellite grabens were not confirmed by them. The present results agree with this latter interpretation.

The Fort St. John Graben (FSJG) was originally named by Sikabonyi and Rodgers (1959). Barclay et al. (1990, p. 123) adopted this name and defined it as enclosing the Stoddart Group and the thickest part of the Belloy Formation. Barclay et al. (1990, p. 123) believed that their FSJG included the FSJG and the Belloy Graben originally named by Sikobonyi and Rodgers (1959). They indicated that the FSJG and the Belloy Graben named by Sikobonyi and Rodgers (1959) are parts of the same graben, implying that the Belloy graben is the southeastern extension of the FSJG *sensu* Barclay et al. (1990). Richards et al. (1994) and Henderson et al. (1994) adopted the definition of FSJG proposed by Barclay et al. (1990), and both displayed the southeastern extension of FSJG *sensu* Barclay et al. (1990) as bounded by the Rycroft Fault on the southwestern side and the Dunvegan Fault on the northeastern side. They also showed the extension as a half graben, and the downthrown sides on both the Rycroft and Dunvegan faults as being toward the north.

The results of the present study provide a much more detailed and accurate picture of the DCGC on the Alberta side (e.g., *see* Figures 42, 44, 45, 47, 50, 54 and 56). In addition to confirming some of the major structures and faults, a close comparison of the present results with those presented by Barclay et al. (1990), Richards et al. (1994) and Henderson et al. (1994) reveals some discrepancies. One of the major discrepancies is that the present results clearly show a horst to the south of the Dunvegan fault, not a graben or half graben as presented by Richards et al. (1994) and Henderson et al. (1994). This led to a detailed examination of the literature related to the Fort St. John Graben. A close comparison of the maps created in the present study with those published by Sikabonyi and Rodgers (1959), Barclay et al. (1990), Richards et al. (1994) and Henderson et al. (1994) results in the following findings:

1) The Fort St. John Graben and the Belloy Graben were originally named by Sikabonyi and Rodgers (1959) for two structures recognized from a pre-Middle Devonian contour map (*see* Sikabonyi and Rodgers, 1959, Figures 3 and 4); the Fort St. John Graben extends northeast from the town of Fort St. John. Barclay et al. (1990), however, used the name Fort St. John Graben (FSJG) for the graben interpreted from the isopach and structure contour maps of the Stoddart Group and the Belloy Formation (Barclay et al., 1990, Figures 6 and 7), which extends southeast from the town of Fort St. John. Barclay et al. (1990) redefined the Fort St. John Graben to include both the Fort St. John Graben and the Belloy Graben *sensu* Sikabonyi and Rodgers (1959). The present study found that the structures of the Fort St. John Graben and the Belloy Graben interpreted by Sikabonyi and Rodgers (1959) are different from the structures of the Fort St. John Graben as redefined by Barclay et al. (1990), and they do not overlap in space on the Alberta side (*see* below for more details).

2) Sikabonyi and Rodgers (1959) recognized an unnamed, southeast-trending graben structure at about 56°N, 120°W (Sikabonyi and Rodgers, 1959, Figures 14, 15 and 20). This graben structure overlaps in space with the one interpreted from the isopach and structure maps of the Stoddart Group and the Belloy Formation and named as the Fort St. John Graben by Barclay et al. (1990, Figures 6 and 7). The same graben structure has also been clearly identified by the present study (*see* Figures 42, 44, 45, 47, 50, 54 and 56). Comparison of Figures 4, 14, 15 and 20 in Sikabonyi and Rodgers (1959) clearly shows that the unnamed, southeast-trending graben structure at 56°N, 120°W on Figures 14, 15 and 20 is not the same feature as the Fort St. John Graben displayed on Figure 4 of Sikabonyi and Rodgers (1959). For purposes of clarification and communication, this southeast-trending graben structure at 56°N, 120°W is renamed as the Fort St. John – Blueberry Graben.

3) Comparison of Figures 4, 14 and 15 in Sikabonyi and Rodgers (1959) also clearly shows that the Belloy Graben is not connected to the Fort St. John Graben *sensu* Sikabonyi and Rodgers (1959), or to the graben interpreted from the isopach and structure contour maps of the Stoddart Group and the Belloy Formation by Barclay et al. (1990, Figures 6 and 7). The Belloy Graben has been clearly identified, from the residual maps of Devonian to Cretaceous formations in the present study, as lying north of the Dunvegan Fault of Richards et al. (1994). It is not the southeastern extension of the Fort St. John Graben as redefined by Barclay et al. (1990).

4) The positions of the north flank of the FSJG shown on Figures 6 and 7 of Barclay et al. (1990) are not consistent, partly due to limitations in data spacing and contouring technology used at that time. Specifically, the positions shift around the location of the Rycroft Fault, as displayed on Figure 14.5 of Richards et al. (1994). This position has been consistently identified by the present study (e.g., Figures 42, 44, 45, 47, 50, 54 and 56), clearly indicating that the north flank of the southeastern extension of the Fort St. John Graben *sensu* Barclay et al. (1990) is located around the Rycroft Fault. The results of both Barclay et al. (1990) and the present study demonstrate that the southeastern extension of the Fort St. John Graben *sensu* Barclay et al. (1990) is located mainly to the southwest of the Rycroft Fault. Its south flank is located where Sikabonyi and Rodgers (1959, Figure 20) identified the Saddle Hill Fault. This means that Richards et al. (1994, Figure 14.5) misinterpreted and mislabelled the southeastern extension of the Fort St. John Graben *sensu* Barclay et al. (1990).

5) The present study demonstrates that the downthrown side on the Rycroft Fault is to the south, which agrees with the interpretation of Barclay et al. (1990). The present study also demonstrates that a horst lies between the Rycroft and Dunvegan faults, not a half graben as interpreted by Richards et al. (1994, Figure 14.5). This can also be confirmed from the seismic sections presented by Hope et al. (1999, Figure 8) and Eaton et al. (1999, Figure 4), regardless of the fact that the Rycroft Fault was interpreted as a faulted zone in both papers.

6) The Hines Creek graben of Barclay et al. (1990) and Richards et al. (1994) overlaps with the North Peace River Graben of Sikabonyi and Rodgers (1959, Figure 4); the Dunvegan Fault of Richards et al. (1994) was originally named the Belloy Fault by Sikabonyi and Rodgers (1959, Figures 15 and 16).

Figure 58 shows a refined version of the DCGC structures. The Clear River High and Pouce Coupe High could at times be parts/extensions of the Beaton High and the Sukunka Uplift, respectively, of Henderson et al. (1994, Figure 15.1). Further investigation may be necessary to confirm this.

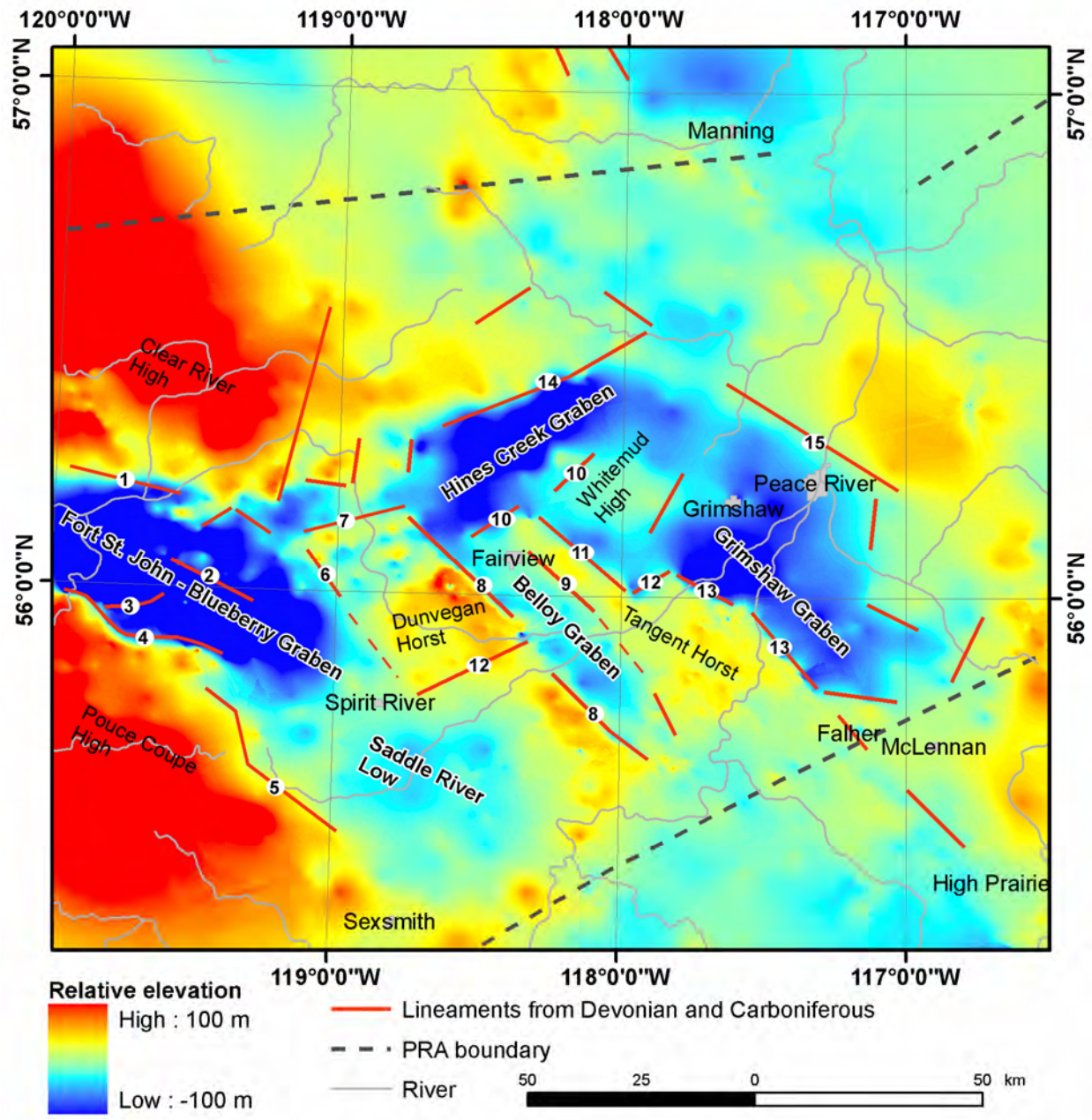

Figure 58 Refined interpretation of the Dawson Creek graben complex (DCGC), superimposed on the residual map for the top of the Debolt Formation. Major faults: 1, Bear Canyon; 2, Josephine Creek; 3, Farmington; 4, Gordondale; 5, Saddle Hills; 6, Rycroft; 7, George; 8, Belloy (Dunvegan); 9, Fairview; 10, Whitemud; 11, Bluesky; 12, Berwyn; 13, Normandville (Tangent); 14, Hines Creek; 15, Peace River.

Table 2 provides a comparison of different names used by different authors for structures of the DCGC. 'North Peace River Graben,' 'Belloy Fault' and 'Normandville Fault' have historical precedence over 'Hines Creek Graben,' 'Dunvegan Fault' and 'Tangent fault,' respectively. In the present paper, 'Hines Creek Graben' is used because it was more clearly defined, overlaps with the location of Hines Creek and has been well accepted by the industry; 'Belloy (Dunvegan) Fault' and 'Normandville (Tangent) Fault' are used because 'Belloy Fault' and 'Normandville fault' have the precedence in history and the town of

Dunvegan and the town of Tangent are father away from the named faults, but 'Dunvegan fault' and 'Tangent fault' are more popular with industry.

Table 2. Comparison of names for structures of the Dawson Creek Graben Complex (DCGC).

Structures	Sikabonyi and Rodgers (1959)	Barclay et al. (1990)	Richards et al. (1994)	Present paper
Fort St. John Graben *sensu* Sikabonyi and Rodgers (1959)	Originally named on p. 197, Figure 4	No equivalent	No equivalent	No equivalent
Fort St. John Graben *sensu* Barclay et al. (1990)	Unnamed graben, recognized on Figs. 14, 15 and 20	Fort St. John Graben	Fort St. John Graben, but misplaced	Fort St. John–Blueberry Graben
Saddle Hills Fault	Originally named on p. 197, Figure 4	Equivalent to southwestern flank of Fort St. John Graben *sensu* Barclay et al. (1990)	Not recognized	Saddle Hills Fault
Rycroft Fault	Not recognized	Equivalent to southeastern flank of the Fort St. John Graben *sensu* Barclay et al. (1990)	Misinterpreted as the southwestern flank of the Fort St. John Graben *sensu* Barclay et al. (1990)	Rycroft Fault
Dunvegan Horst	Not recognized	Not recognized	Mislabelled as graben	Dunvegan Horst
Belloy Fault	Originally named on p. 207, Figure 16	Not recognized	Dunvegan Fault	Belloy (Dunvegan) Fault
Bluesky Fault	Unnamed fault, recognized on Fig. 15	Not recognized	Unnamed fault, recognized on p. 223, Fig. 14.5	Bluesky Fault
Berwyn Fault	Not recognized	Not recognized	Originally named on p. 223, Fig. 14.5	Berwyn Fault
Normandville Fault	Plan view location first displayed on Figs. 4, 10, 13–16; originally named by Lavoie (1958)	Not recognized	Tangent (Normandville) Fault	Normandville (Tangent) Fault
North Peace River Graben	Originally named on p. 197, Fig. 4	Hines Creek Graben	Hines Creek Graben	Hines Creek Graben

5.2 Clear River Graben

As demonstrated previously, the DCGC was formed mainly during the Late Carboniferous and offset the underlying formation tops from the Early Carboniferous to the top of the Precambrian. It was followed by a stage of infilling of the grabens and tectonic stability toward the end of Permian (Barclay et al., 1990).

The tops of the Lower Triassic Montney Formation and the Lower Jurassic Nordegg Formation are offset by a structure pattern that is different from that of the DCGC. Unlike the DCGC faults, which are mostly syndepositional, a comparison with the local subsidence map indicates that the faults offsetting the tops of the Montney and Nordegg formations are mostly postdepositional. In addition to those features associated with the DCGC below and those identified from the Cretaceous formation tops above, a new graben structure has been identified around the Clear River (Figure 59). This graben, which appears

confined to the Triassic and Lower Jurassic formations, trends northeast and is herein named the 'Clear River Graben.' It connects to the southeast-trending Fort St. John–Blueberry Graben. The Fort St. John–Blueberry graben is separated from the Hines Creek Graben by a new structure herein named the 'Forth Creek High.' The northeast-trending Hines Creek Graben is connected to the southeast-trending Belloy Graben. As a result, the formation-top offset patterns of the Montney and Nordegg formations demonstrate a fishbone-like structure pattern (Figure 59).

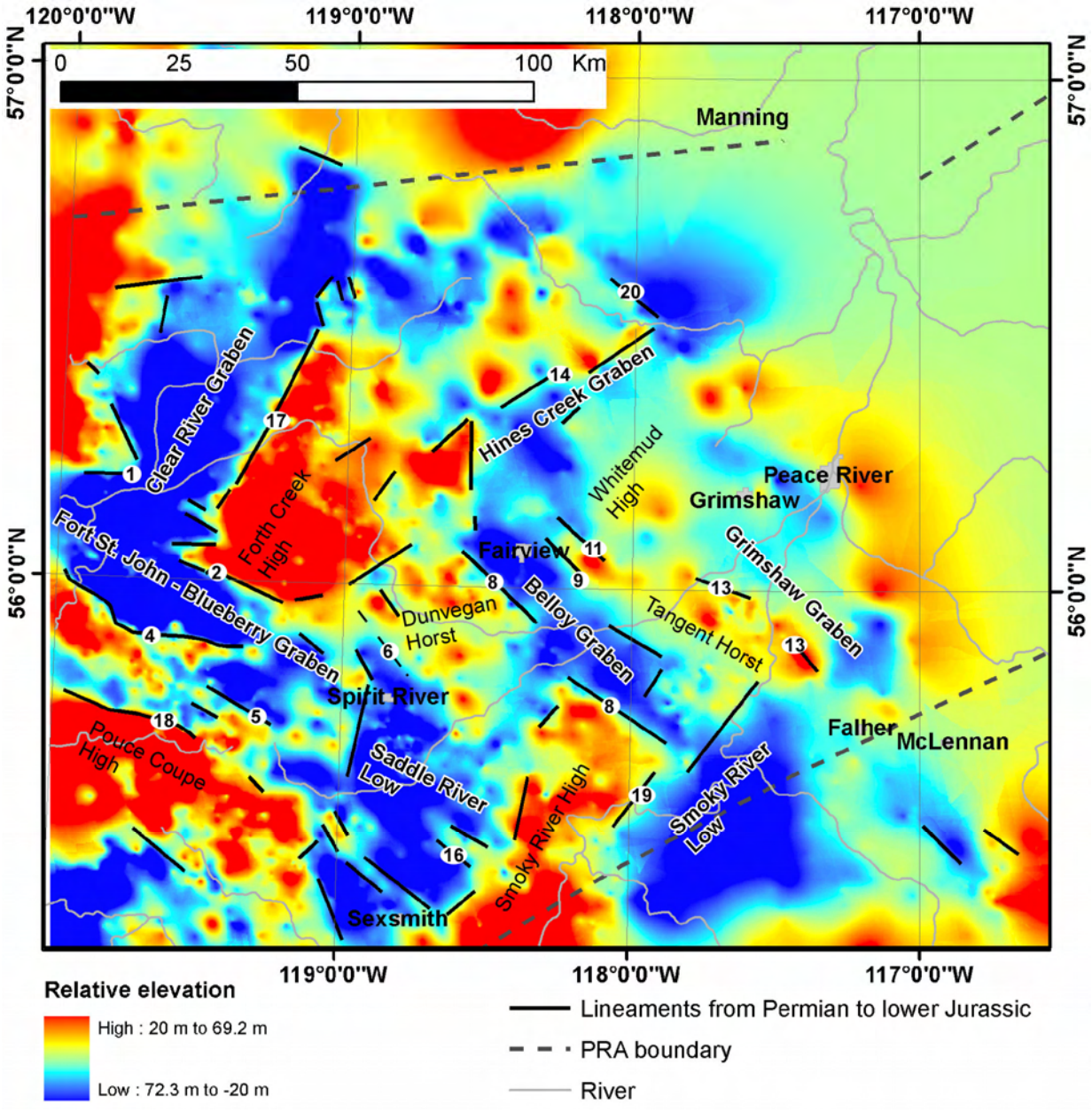

Figure 59. Clear River Graben and other structures, including those related to the Dawson Creek Graben Complex (DCGC), superimposed on the residual map for the top of the Montney Formation. Major faults: 1, Bear Canyon; 2, Josephine Creek; 4, Gordondale; 5, Saddle Hills; 6, Rycroft; 8, Belloy (Dunvegan); 9, Fairview; 11, Bluesky; 13, Normandville (Tangent); 14, Hines Creek; 16, Teepee; 17, fault on the eastern flank of the Clear River graben; 18, Pouce Coupe; 19, Smoky River; 20, Beaton Creek.

Previously, the tectonic evolution of this region was divided into three distinct phases (Cant, 1988; O'Connell et al., 1990; Eaton et al., 1999): the Peace River Arch (PRA, *sensu stricto*) during pre-Late Devonian, the Peace River Embayment (PRE) during the Carboniferous to Triassic, and a downwarping phase during the Jurassic and Cretaceous. The fishbone structure pattern recognized from the Montney and Nordegg formation tops in the present study, including the Clear River Graben and the Forth Creek High, clearly identifies an independent stage of tectonic evolution for this region probably related to some form of intraplate stress. However, a detailed study of the formation of the structures related to the Clear River graben is beyond the scope of this study.

5.3 Tectonic Reactivation during the Late Cretaceous

It has been suggested that the basement faults have commonly influenced the distribution of hydrocarbon traps and mineralization zones in the WCSB (Edwards et al., 1995, 1998; Leblanc and Morris, 1999; Lyatsky et al., 1998, 1999), and these faults may have reactivated during the Cretaceous (O'Connell et al., 1990; O'Connell, 1994; Donaldson et al., 1998; Eccles et al., 2002). A comparison of the offset patterns of Cretaceous formation tops (Figure 60) with the refined DCGC (Figure 58) reveals that part of the Fort St. John Graben between the Josephine Creek Fault and the Gordondale Fault, the Hines Creek Graben, the Belloy Graben and the Grimshaw Graben can also be recognized from the Cretaceous formation tops. The associated faults also offset these formation tops, but with a lower average amount of offset. These can be regarded as direct evidence that the DCGC structures reactivated at least after the deposition of the BFSZ. Additional faults associated with the reactivation were also identified, of which the most prominent feature is the Pouce Coupe Fault. This fault broke the Pouce Coupe High into a graben to the north. It also offset the underlying Nordegg and Montney formation tops, although it did not offset the Paleozoic formation tops. It is noteworthy that the Fort St. John–Blueberry graben remains separated from the Hines Creek graben, based on the Cretaceous formation tops.

Edwards and Brown (1994) and Burwash et al. (2000) suggested that the low-angle shear zones and/ or faults recognized in the Precambrian basement indicate an extensional sense of movement and exerted a fundamental control on block faulting in the overlying Paleozoic cover rocks. Burwash et al. (2000) concluded that these low-angle faults have undergone hydrothermal alteration and are longstanding zones of weakness. They remain susceptible to reactivation whenever crustal extension or compression occurs. This model of basement-controlled faulting proposed by Edwards and Brown (1994) and Burwash et al. (2000) could be used to explain the tectonic reactivation in the Late Cretaceous, as suggested by Donaldson et al. (1998). Donaldson et al. (1998) interpreted four faults based on the distribution of the Upper Cretaceous Coniacian Bad Heart Formation on the southern flank of the Peace River Arch (Figure 60): the southwestern limit to the Bad Heart sandstone (fault 1), the abrupt thinning of the Bad Heart Formation (fault 2), and two erosional edges of the Bad Heart sandstone (faults 3 and 4). These faults were interpreted as a series of drape faults, forming 5–20 m of topography that controlled the preservation and facies of the Bad Heart sandstone (Donaldson et al., 1998, Figure 11). They were attributed to the reactivation of the Paleozoic faults that occurred in response to subtle extension on the low-angle shear zones in the Proterozoic basement. These faults, identified by Donaldson et al. (1998), are roughly linear extensions of the Pouce Coupe Fault, the Wenham Fault recognized by Burwash et al. (2000), the Belloy (Dunvegan) Fault and the Normandville (Tangent) Fault (Figure 60). Identification of the DCGC related faults in the upper Cretaceous formations in this study provided direct evidence for the tectonic reactivation in this region during the Late Cretaceous.

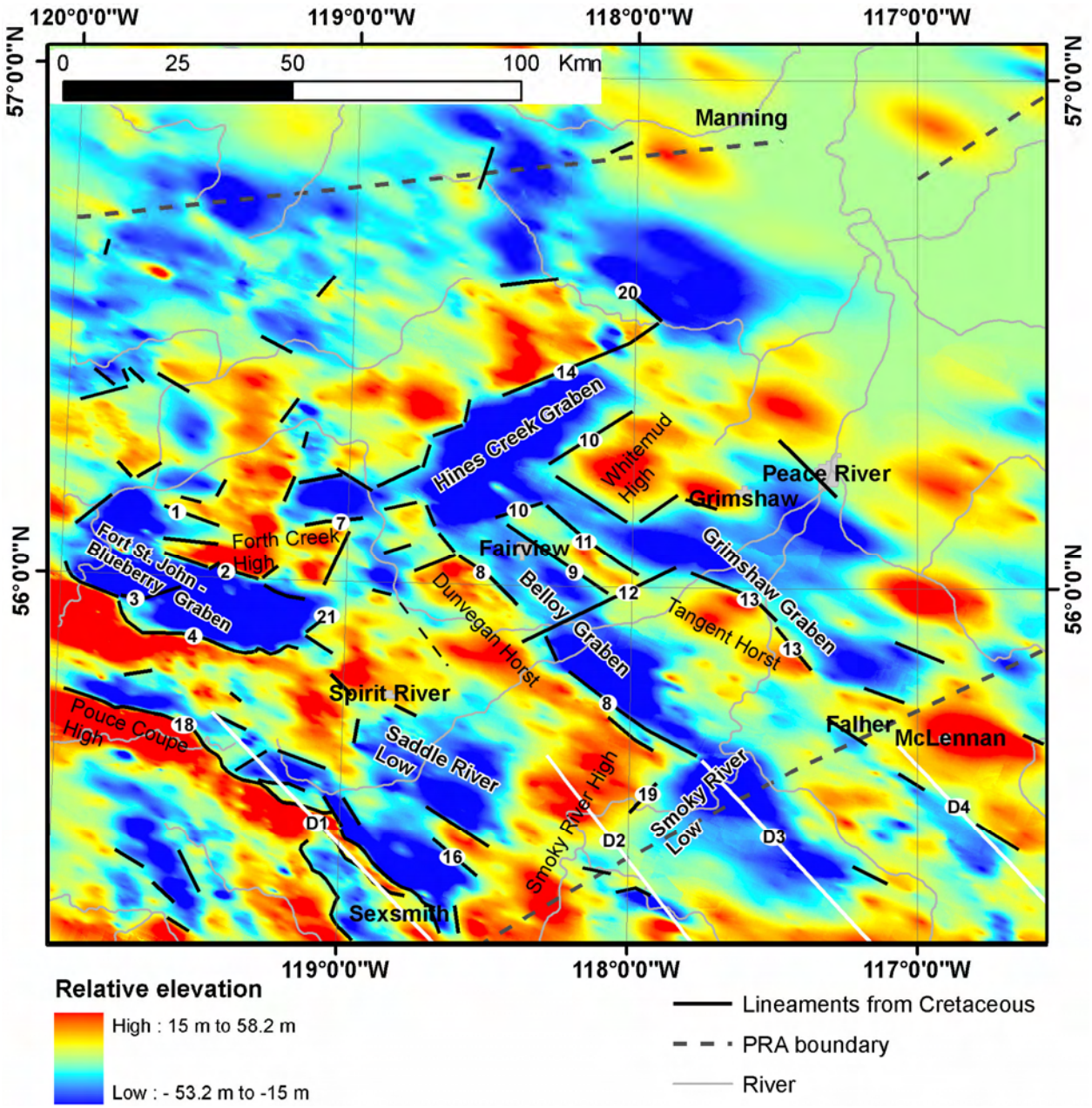

Figure 60. Formation-top offset pattern and interpreted faults of Cretaceous formations, superimposed on the residual map for the Basal Fish Scale Zone (BFSZ). Major faults: 1, Bear Canyon; 2, Josephine Creek; 3, Farmington; 4, Gordondale; 7, George; 8, Belloy (Dunvegan); 9, Fairview; 10, Whitemud; 11, Bluesky; 12, Berwyn; 13, Normandville (Tangent); 14, Hines Creek; 16, Teepee; 18, Pouce Coupe; 19, Smoky River; 20, Beaton Creek; 21, Blueberry. D1–D4, the four faults interpreted by Donaldson et al. (1998).

5.4 Possible Conduits/Pathways for the Hydrothermal Fluid Venting Hypothesis

As mentioned previously, it has been suggested that the deposition, geometry and grades of the Upper Cretaceous Bad Heart Formation ooidal ironstones may have been controlled by reactivation of the Precambrian faults (e.g., Donaldson et al., 1998, 1999; R.A. Olson et al., work in progress, 2005). It has also been postulated that upward movement of hypersaline brines and related hydrothermal venting along the reactivated Precambrian faults may have resulted in the local deposition of the ferruginous ooidal

facies (Olson et al., 1999; Collom, 2001; Collom and Johnston, 2001). Evidence for this hypothesis could be the faults that extend from the basement throughout the sedimentary cover, as they could serve as the conduits for venting hydrothermal fluid. Identification of such faults was one of the goals in the present study.

As demonstrated previously, faults can be traced from the Upper Cretaceous all the way down to the top of the Precambrian by examining slices of local offset-pattern maps generated from multiple formation tops (e.g., Figure 56). Figure 61 shows the lineaments interpreted from Cretaceous, Permian to Lower Jurassic, Devonian and Carboniferous formations, as well as the outline of the Bad Heart Formation, superimposed on the satellite image of the study area. The majority of the interpreted lineaments can be associated with the known faults of the Dawson Creek Graben Complex, including the Josephine Creek, Farmington, Gordondale, Belloy (Dunvegan), Fairview, Bluesky, Berwyn, Normandville (Tangent), Whitemud, Hines Creek and Blueberry faults, all of which are steep faults and offset formation tops from the Upper Cretaceous through the Paleozoic down to the top of Precambrian (also compare Figure 54 with Figure 55, or with Figures 58–60). Figure 61 also indicates that each of these faults shifts slightly in location on different formation tops, which can be attributed to the fact that each of them is probably a steep listric fault as illustrated by Hope et al. (1999). These faults could all be possible conduits or pathways for the hydrothermal venting hypothesis regarding origin of the ooidal ironstone deposit of the Bad Heart Formation. Among them, the Hines Creek Faults has been found to be associated with magnetization by vertical fluid flow and exotic geochemistry (Peirce et al., 1998b).

If the hydrothermal venting hypothesis can be proven, then the amount and grade of ooidal ironstone within the Bad Heart Formation should be theoretically related to the location of the possible pathways/conduits. Unfortunately, most of the faults mentioned above underlie the core area of Peace River Arch, where the Bad Heart Formation has been eroded (Figure 61). Previously, four separate 'ore reserve' blocks, named 'Rambling River,' 'North Whitemud River,' 'South Whitemud River' and 'Worsley' (Figure 61), were identified in the early 1960s (Bertram and Mellon, 1975). It was estimated that these four blocks together contain net recoverable 'reserves' of 206 million tonnes proven and 814 million tonnes probable and possible combined (Hamilton, 1980). They are located along the eastern and southern slopes of the Clear Hills, which represents a structurally stable area according to the present study (Figure 61). Comparison of the grade and volume of ooidal ironstone in these blocks with those overlying the structurally active core area of the PRA is not possible because of the erosion. As a result, it is not clear whether the grade and volume of ooidal ironstone can be related to proximity to the possible pathways/conduits, due to very limited information on the distribution of grade and geometry of the ooidal ironstone deposits in this region (R.A. Olson et al., work in progress, 2005).

In addition, the faults mentioned above formed mainly during the Carboniferous and Permian (Barclay et al., 1990; Richards et al., 1994; Henderson et al., 1994). Although it is clear that they offset the top of the Precambrian and were reactivated in the late Cretaceous, it is difficult to trace them in the basement due to limited seismic resolution. Burwash et al. (2000, Figure 10) inferred that the Belloy Fault (Dunvegan fault of Richards et al., 1994) extends into the basement to a depth of about 14 km. They identified a zone of the ^{18}O depletion, named the 'Kimiwan isotope anomaly' (KIA), beneath and parallel to the Normandville Fault. The KIA was interpreted to have originated through high-temperature interaction with surface-derived fluids in an extensional tectonic setting ca. 1800 Ma. Two low-angle basement faults, the Fahler and Kimiwan faults, were identified as intersecting the Phanerozoic-Precambrian unconformity at the location of the KIA from the seismic reflection profiles acquired during the LITHOPROBE Alberta Basement Transect (Burwash et al., 2000, Figure 10). It was suggested that periodic reactivation of these basement structures during the Phanerozoic played an important role in the development of faults (e.g., the Normandville (Tangent) Fault) in the overlying sedimentary basin.

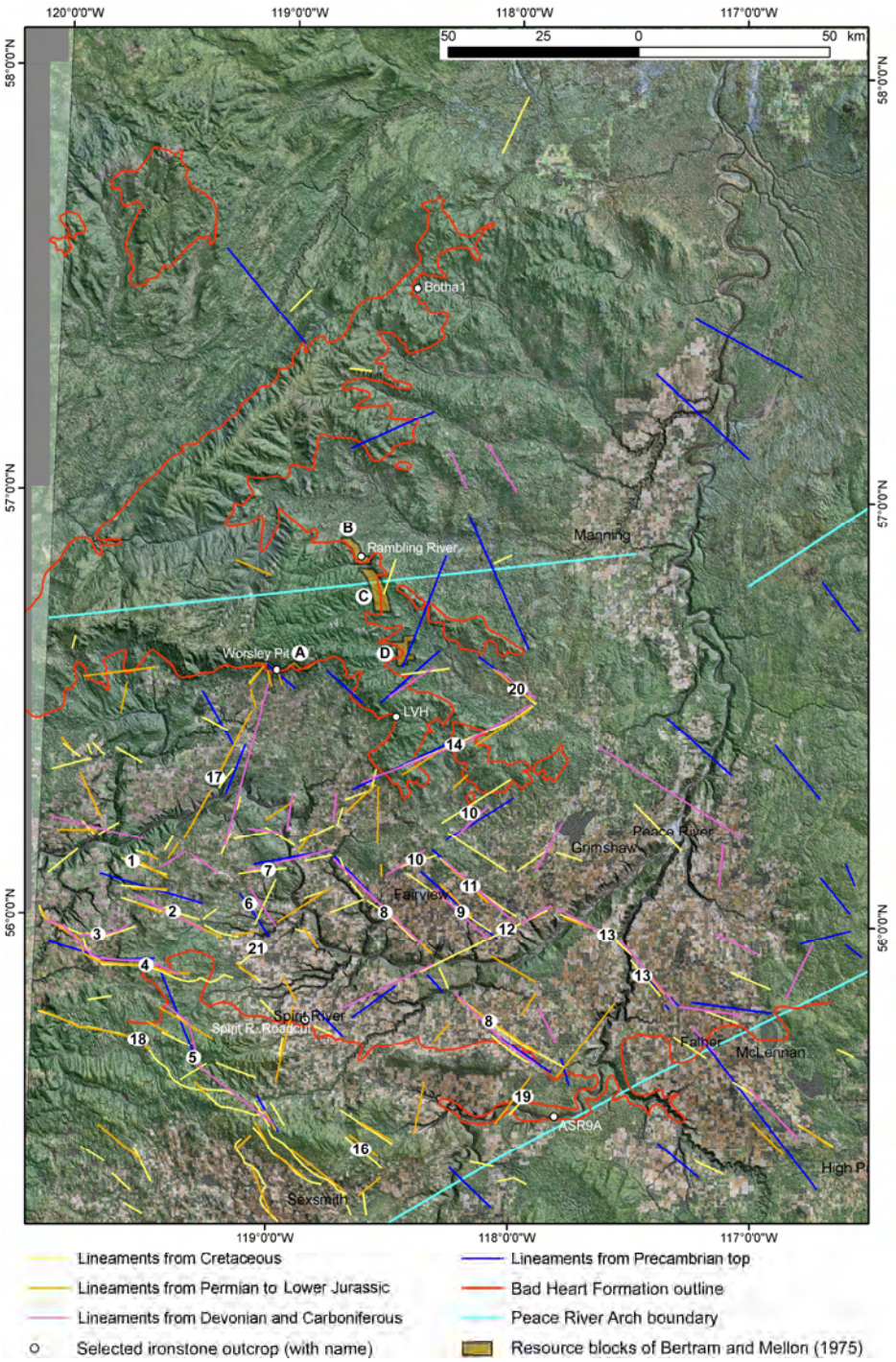

Figure 61. Interpreted lineaments/faults superimposed on the image of study area (Figure 2). Major faults: 1, Bear Canyon; 2, Josephine Creek; 3, Farmington; 4, Gordondale; 5, Saddle Hills; 6, Rycroft; 7, George; 8, Belloy; 9, Fairview; 10, Whitemud; 11, Bluesky; 12, Berwyn; 13, Normandville; 14, Hines Creek; 16, Teepee; 17, fault on the east flank of the Clear River graben; 18, Pouce Coupe; 19, Smoky River; 20, Beaton Creek; 21, Blueberry. Ironstone resource blocks identified by Bertram and Mellon (1975): A, Worsley; B, Rambling River; C, North Whitemud River; D, South Whitemud River.

5.5 Comparison of the Refined Approach to Subsurface Structure Mapping with Seismic sections and Aeromagnetic Data

The refined approach to structure mapping follows the same workflow as the conventional approach that uses formation picks and seismic sections. The difference is that the refined approach is developed by incorporating the trend-surface analysis and geostatistical modelling into the workflow of the conventional approach. Table 3 gives a brief comparison of the refined and conventional approaches.

Table 3. Comparison of the refined approach with the conventional approach.

Workflow	Conventional approach	Refined approach
Identify syndepositional faults	Isopach contour map (e.g., Barclay, 1990, Fig. 6)	Residual Isopach (differential subsidence) surface (e.g., this report, Fig. 42, 45 and 48)
Identify postdepositional faults	Structure-top contour map (e.g., Barclay, 1990, Fig. 7)	Residual formation-top surface (e.g., this report, Fig. 41, 44, 47 and 50)
Trace offset of a fault vertically	Cross-section, seismic-section (e.g., Richards et al., 1994, Fig. 14.6; Hope et al., 1999, Fig. 8; Eaton et al., 1999, Fig. 4)	Slices from multiple formation tops (e.g., this report, Fig. 56)
Digitizing fault locations	Faults drawn by hand from contour maps	Linear offset pattern extracted statistically (e.g., this report, Fig. 40, 43, 46 and 49)

Comparison of the maps generated by the refined approach with those of the conventional approach indicates that the refined approach has higher resolution and accuracy than the conventional contour-map approach. It also has a higher resolution in tracing the offset by faults throughout the sedimentary cover. This leads to identification of numerous new faults with metre-scale offsets in the Triassic to Upper Cretaceous, as demonstrated previously. The refined approach is also able to trace the major faults (e.g., Josephine Creek, Farmington, Gordondale, Belloy, Fairview, Bluesky, Berwyn, Normandville, Whitemud, Hines Creek and Beaton Creek faults) all the way from the Precambrian top to the Upper Cretaceous. However, it is difficult to trace these faults in the stratigraphic interval above the Permian on the seismic sections (*see* Richards et al., 1994, Figure 14.6; Hope et al., 1999, Figures 8 and 9; Eaton et al., 1999, Figure 4) due to limited seismic resolution. The residual maps created during the present study indicate that the offset detected increases from commonly less than 30 m in the BFSZ (Figure 16) to as much as 300 m at the top of Precambrian (Figure 54). This explains why formation top offset can be recognized on seismic sections only from the stratigraphic interval below the Permian when the offset is great enough to be detected by available seismic resolution. In the Permian, the offset is commonly less than 70 m (Figure 41).

A comparison of the refined approach with that of aeromagnetic data interpretation indicates that the refined approach is superior in identifying faults of the sedimentary cover. Aeromagnetic maps are dominated by Precambrian ductile orogenic structures. These Precambrian structures contrast with brittle basement faults that could offset the Phanerozoic section, including the basement-cover contact. The ductile structures include faults and shear zones that formed during the collisional assembly of the basement in the Precambrian and can be mapped with both regional aeromagnetic anomaly data and crustal reflection profiles. However, these structures are rarely reactivated in the Phanerozoic Alberta Basin (Ross and Eaton, 1999). The brittle basement faults are often steep and, if ever detectable in potential-field maps, usually extremely subtle (Lyatsky et al., 1999). Ross and Eaton (1999) concluded that the Phanerozoic faults exhibit little spatial co-location with antecedent fabrics within the basement and are associated only locally with an offset of the basement-cover contact. This can be confirmed with Figure 62, which shows all the lineaments interpreted from the sedimentary cover superimposed on the map of the first vertical derivative of the residual total field aeromagnetics. In this figure, except that a few lineaments overlie and/or parallel parts of the Ksituan-Chinchaga and Chinchaga-Buffalo Head

terrane boundaries, the orientations of interpreted faults in the sedimentary section do not appear to coincide with the underlying basement structures.

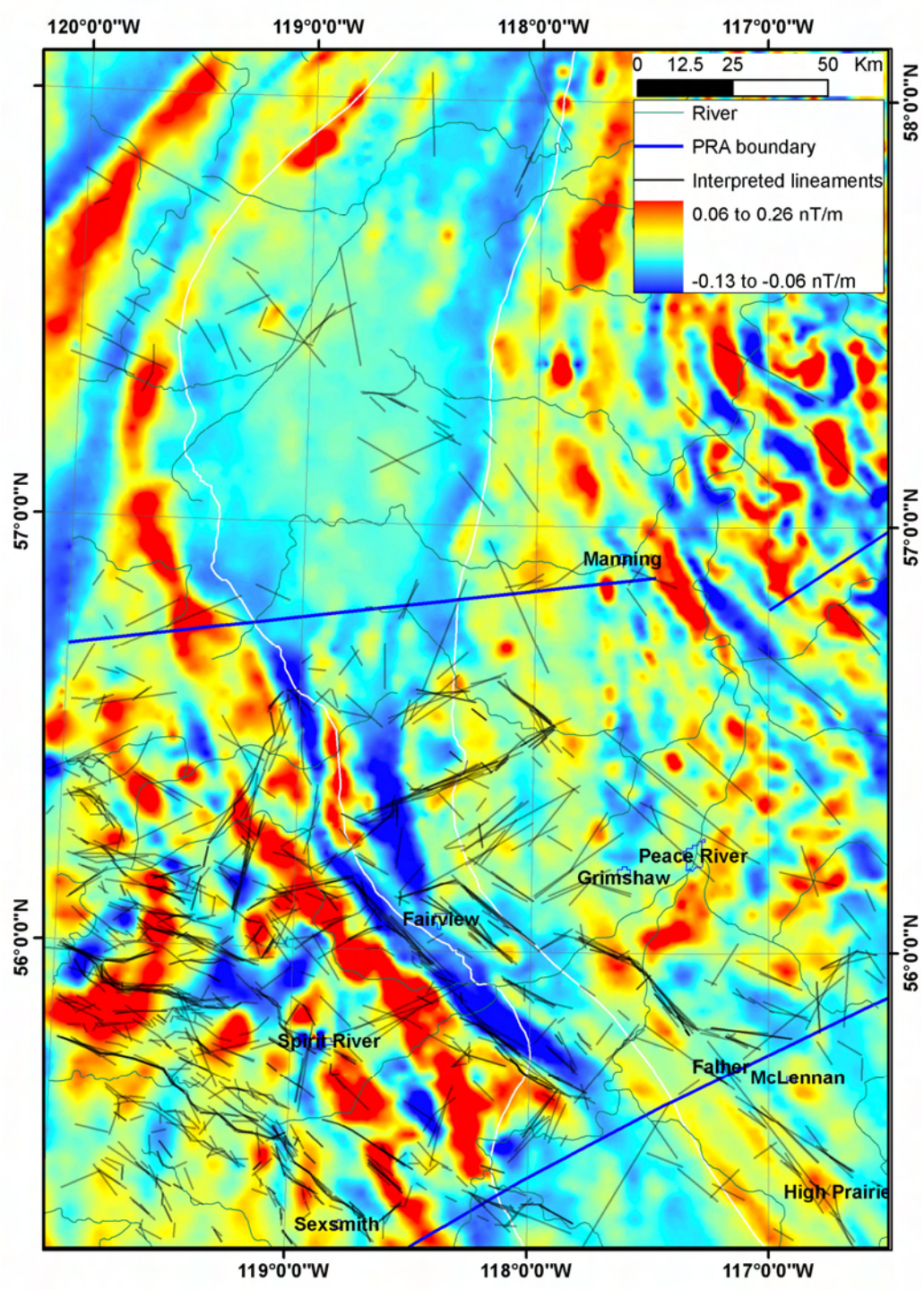

Figure 62. Interpreted lineaments superimposed on the first vertical derivative of the residual total field aeromagnetics. The Ksituan-Chinchaga and Chinchaga–Buffalo Head terrane boundaries are indicated as the left and right thin white lines, respectively. The aeromagnetic data were obtained from the Geoscience Data Repository (GDR) for Geophysical and Geochemical Data, Geological Survey of Canada (http://gdr.nrcan.gc.ca/index_e.php).

Various filtering techniques, including band-pass filters have been applied to total field aeromagnetic data to accentuate the internal structure and edges of magnetic sources. Depending on the wavelength of the filter used, some of the distracting effects of depth and extent of a magnetic source can be reduced and the contributions of the interval of interest enhanced. Combined with modern acquisition method, these technologies result in high-resolution aeromagnetic surveys (HRAM; Peirce et al., 1998a; Leblanc and Morris, 1999). It was suggested that HRAM data can be processed to resolve magnetic anomalies originating in the sedimentary cover. Except in cases associated with hydrothermal precipitation (e.g., Peirce et al., 1998b), however, the HRAM approach is incapable of detecting 1) basement faults on the basis of displacement at the basement-sediment interface, and 2) the offset by faults in the sedimentary cover as well.

In conclusion, the refined subsurface-structure-mapping approach developed in the present study has a higher resolution in detecting formation-top offsets caused by faults and higher accuracy in digitizing fault locations compared to the conventional contour-map, seismic-section and aeromagnetic-data interpretation techniques in structure mapping for the sedimentary cover. Furthermore, it can be applied to the entire Western Canada Sedimentary Basin.

6 References

Alberta Energy and Utilities Board (2002): Table of Formations, Alberta.

Barclay, J.E., Krause, F.F., Campbell, R.I. and Utting J. (1990): Dynamic casting of a graben complex: basin infill and differential subsidence during the Permo–Carboniferous, Peace River Embayment, western Canada; Bulletin of Canadian Petroleum Geology, v. 38A, p. 115–145.

Barss, D.L., Copland, A.B. and Ritchie, W.D. (1970): Geology of Middle Devonian reefs, Rainbow area, Alberta, Canada; *in* Geology of Giant Petroleum Fields, Symposium, American Association of Petroleum Geologists Memoir, v. 14, p. 19–49.

Beaumont, C., Quinlan, G. and Stockmal, G.S. (1993): The evolution of the western interior basin: causes, consequences and unsolved problems; *in* Geodynamic Evolution of the Western Interior Basin, W.G.E. Caldwell and E.G. Kauffman (ed.), Geological Association of Canada, Special Paper 39, p. 97–117.

Bertram, E.F. and Mellon, G.B. (1975): Peace River iron deposits; Alberta Research Council, Alberta Geological Survey, Information Series 075, 53 p.

Boerner, D.E., Kurtz, R.D., Craven, J.A. and Jones, F.W. (1997): Towards a synthesis of electromagnetic results from the Alberta Basement LITHOPROBE Transect; LITHOPROBE Report No. 59, p. 55–67.

Burk, C.F. (1970): Devonian reefs in west-central Alberta as revealed by structural analysis of shallow Cretaceous horizons (abstract); Bulletin of the American Association of Petroleum Geologists v. 54(5), p. 839.

Burwash, R.A., Chacko, T., Muehlenbachs, K. and Bouzidi, Y. (2000): Oxygen isotope systematics of the Precambrian basement of Alberta: implications for Paleoproterozoic and Phanerozoic tectonics in northwestern Alberta; Canadian Journal of Earth Science, v. 37, no. 11, p. 1611-1628.

Burwash, R.A., McGregor, C.R. and Wilson, J.A. (1994): Precambrian basement beneath the Western Canada Sedimentary Basin; *in* Geological Atlas of the Western Canada Sedimentary Basin, G.D. Mossop and I. Shetsen (comp.), Canadian Society of Petroleum Geologists and Alberta Research Council, Special Report 4, p. 49–56.

Calvert, W. L. (1974): Sub-Trenton structure of Ohio, with views on isopach maps and stratigraphic sections as basis for structural myths in Ohio, Illinois, New York, Pennsylvania, West Virginia, and Michigan; American Association of Petroleum Geologists Bulletin, v. 58, p. 957–972.

Cant, D. J. (1984): Development of shoreline-shelf sand bodies in a Cretaceous epeiric sea deposit; Journal of Sedimentary Petrology, v. 54, p. 541–556.

Cant, D.J. (1988): Regional structure and development of the Peace River Arch, Alberta: a Paleozoic failed-rift system?; Bulletin of Canadian Petroleum Geology, v. 36, p. 284–295.

Cant, D.J. and Abrahamson, B. (1996): Regional distribution and internal stratigraphy of the Lower Mannville; Bulletin of Canadian Petroleum Geology, v. 44, p. 508-529.

Cecile, M.P., Morrow, D.W. and Williams, G.K. (1997): Early Paleozoic (Cambrian to Early Devonian) tectonic framework, Canadian Cordillera; Bulletin of Canadian Petroleum Geology, v. 45, p. 54–74.

Collom, C.J. (2001): Systematic palaeontology, biostratigraphy and paleoenvironmental analysis of the Upper Cretaceous Wapiabi Formation and equivalents, Alberta and British Columbia, western Canada; Ph.D. thesis, University of Calgary, 817 p.

Collom, C.J. and Johnston, P.A. (2001): Ooidal ironstones, products of exhalative paleoenvironments in shallow epeiric seas (abstract); *in* Earth Systems Processes – Abstracts with Programs, Geological Society of America and Geological Society of London, p. 104.

Cook, A.C. (1969): Trend-surface analysis of structure and thickness of the Bulli seam, Sydney Basin, N.S.W; Journal of the International Association for Mathematical Geology, v.1(1), p. 53-78.

Davis, J.C. (1973): Statistical and Data Analysis in Geology; John Wiley and Sons, New York, 550 p.

Davis, J.C. (1986): Statistical and Data Analysis in Geology (2nd edition); John Wiley and Sons, New York, 646 p.

Davis, J. C. (2002): Statistical and Data Analysis in Geology (3rd edition); John Wiley and Sons, New York, 638 p.

DeMille, G. (1958): Pre-Mississippian history of the Peace River Arch; Journal of the Alberta Society of Petroleum Geologists, v. 6, p. 61–68.

Dix, G.R. (1990): Stages of platform development in the Upper Devonian (Frasnian) Leduc Formation, Peace River Arch, Alberta; Bulletin of Canadian Petroleum Geology, v. 38A, p. 66–92.

Doveton, J.H. (1970): Trend analysis of a thin sedimentary sequence within the Upper Carboniferous of Ayrshire, Scotland; Journal of the International Association for Mathematical Geology, v.2(1), p. 47-62.

Donaldson, W.S., Plint, A.G. and Longstaffe, F.J. (1998): Basement tectonic control on distribution of the shallow marine Bad Heart Formation, Peace River Arch area, northwest Alberta; Bulletin of Canadian Petroleum Geology, v. 46, no. 4, p. 576-598.

Donaldson, W.S., Plint, A.G. and Longstaffe, F.J. (1999): Tectonic and eustatic control on ore deposition and preservation of Upper Cretaceous ooidal ironstone and associated facies: Peace River Arch area, NW Alberta, Canada; Sedimentology, v. 46, p. 1159-1182.

Dyke, A.S. (2004): An outline of North American deglaciation with emphasis on central and northern Canada; *in* Quaternary Glaciations — Extent and Chronology, Part II: North America, J. Ehlers and P.L. Gibbard (ed.), Elsevier, Developments in Quaternary Science, p. 373–424.

Eaton, D.W., Ross, G.M. and Hope, J. (1999): The rise and fall of a cratonic arch: a regional perspective on the Peace River Arch, Alberta; Bulletin of Canadian Petroleum Geology, v. 47, no. 4, p. 346-361.

Eccles, D.R., Grunsky, E.C., Grobe, M. and Weiss, J. (2002): Structural emplacement model for kimberlitic diatremes in northern Alberta; Alberta Energy and Utilities Board, EUB/AGS Earth Sciences Report 2000-01, 106 p.

Edwards, D.J. and Brown, R.J. (1994): Tectonic heredity in west central Alberta: recognition and significance; *in* Alberta Basement Transects, G.M. Ross (ed.), Lithoprobe Report 37, p. 164–194.

Edwards, D.J., Lyatsky, H.V. and Brown, R.J. (1995). Basement fault control on Phanerozoic stratigraphy of the Western Canada Sedimentary Province: integration of potential field and lithostratigraphic data; *in* Alberta Basement Transects, G.M. Ross (ed.), Lithoprobe Report 47, p. 181–224.

Edwards, D.J., Lyatsky, H.V. and Brown, R.J. (1998): Regional interpretation of steep faults in the Alberta Basin from public-domain gravity and magnetic data: an update; Canadian Society of Exploration Geophysicists, Recorder, v. 23, no. 1, p. 15-24.

Elliot, D. (1965): The quantitative mapping of directional minor structures; Journal of Geology, v. 73, p. 865–880.

Evenick, J.C., Jacobi, R.D., Baker, G.S. and Mitchell, C.E. (2005): Subsurface evidence for faults in the Appalachian basin, western New York State; Northeastern Geology and Environmental Sciences, v. 2791, p. 1–17.

Forgotson, J.M. (1963): How computers help find oil; Oil and Gas Journal, v. 61(11), p. 100–109.

Gehrels, G.E., Dickinson, W.R., Ross, G.M., Stewart, J.H. and Howell, D.G. (1995): Detrital zircon reference for Cambrian to Triassic miogeoclinal strata of western North America; Geology (Boulder), v. 23, no. 9, p. 831–834.

Gehrels, G.E. and Ross, G.M. (1998): Detrital zircon geochronology of Neoproterozoic to Permian miogeoclinal strata in British Columbia and Alberta; Canadian Journal of Earth Sciences, v. 35, no. 12, p. 1380–1401.

Geiger, D. and Cook F.A. (2001): Analyses of crustal structure from bandpass and directionally filtered potential-field data: an example from Western Canada; Canadian Journal of Earth Sciences, v. 38, no. 6, p. 953–961.

Gibson, D.W. (1992): Stratigraphy, sedimentology, coal geology and depositional environments of the Lower Cretaceous Gething Formation, northeastern British Columbia and west-central Alberta; Geological Survey of Canada, Bulletin 431, 127 p.

Green, R. and Mellon, G.B. (1962): Geology of the Chinchaga River and Clear Hills (north half) map-areas, Alberta; Alberta Research Council, Alberta Geological Survey, Preliminary Report 62-8, 18 p.

Green, R. and Mellon, G.B. (1970): Bedrock geology of northern Alberta; Alberta Research Council, Alberta Geological Survey, Map 24, scale 1:50 000.

Hamilton, W.N. (1980): Clear Hills iron deposit geology, mineralogy and ore reserves; Alberta Research Council, Alberta Geological Survey, Open File Report 1982-13, 43 p.

Hamilton, W.H., Langenberg, W., Price, M.C. and Chao, D.K., comp. (1999): Geological map of Alberta; Alberta Energy and Utilities Board, EUB/AGS Map 236, scale 1:1 000 000.

Hart, B. S. and Plint, A.G. (1990): Upper Cretaceous warping and fault movement on the southern flank of the Peace River Arch, Alberta; Bulletin of Canadian Petroleum Geology, v. 38A, p. 190–195.

Henderson, C.M., Richards, B.C. and Barclay, J.E. (1994): Permian strata of the Western Canada Sedimentary Basin; *in* Geological Atlas of the Western Canada Sedimentary Basin, G.D. Mossop and I. Shetsen (comp.), Canadian Society of Petroleum Geologists and Alberta Research Council, Special Report 4, p. 251–258.

Hope, J., Eaton, D.W. and Ross, G.M. (1999): Lithoprobe seismic transect of the Alberta Basin: compilation and overview; Bulletin of Canadian Petroleum Geology, v. 47, no. 4, p. 331-345.

Jones, R.M.P. (1980): Basinal isostatic adjustment faults and their petroleum significance; Bulletin of Canadian Petroleum Geology, v. 28, p. 211–251.

Kiernan, J.P. (1996): Tectonic controls on sedimentation and erosion in the Upper Cretaceous Lower Kaskapau Formation, Peace River region, Alberta; B.Sc. thesis, University of Western Ontario, 77 p.

Krumbein, W.C. (1962): Computer analysis of stratigraphic maps (abstract); Bulletin of the American Association for Petroleum Geology, v. 46(2), p. 270-271.

Lavoie, D.H. (1958): The Peace River Arch during Mississippian and Permo–Pennsylvanian time; Journal of the Alberta Society of Petroleum Geologists, v. 6, p. 69–74.

Leblanc, G. and Morris, W.A. (1999): Aeromagnetics of southern Alberta within areas of hydrocarbon accumulation; Bulletin of Canadian Petroleum Geology, v. 47, no. 4, p. 439-454.

Leckie, D. (1986): Rates, controls and sand-body geometries of transgressive-regressive cycles: Cretaceous Moosebar and Gates formations, British Columbia; American Association of Petroleum Geologists Bulletin, v. 70, p. 516–535.

Leckie, D., Staniland, M.R. and Hayes, B.J. (1990): Regional maps of the Albian Peace River and lower Shaftsbury formations on the Peace River Arch, northwestern Alberta and northeastern British Columbia; Bulletin of Canadian Petroleum Geology, v. 38A, p. 176–189.

Lemmen, D.S., Duk-Rodkin, A. and Bednarski, J. (1994): Late glacial drainage systems along the northwestern margin of the Laurentide ice sheet; Quaternary Science Reviews, v. 13, p. 805–828.

Lyatsky, H.V., Dietrich, J.R. and Edwards, D.J. (1998): Analysis of gravity and magnetic horizontal-gradient vector data over the buried Trans-Hudson Orogen and Churchill-Superior boundary zone in southern Saskatchewan and Manitoba; Geological Survey of Canada, Open File 3614, 34 p.

Lyatsky, H.V., Friedman, G.M. and Lyatsky, V.B. (1999): Principles of Practical Tectonic Analysis of Cratonic Regions; lecture Notes in Earth Sciences, v. 84, Springer-Verlag, 369 p.

Massey, N.W.D., MacIntyre, D.G., Desjardins, P.J. and Cooney, R.T. (2005): Digital geology map of British Columbia; British Columbia Ministry of Energy, Mines and Petroleum Resources, GeoFile 2005-1, scale 1:250 000, URL <http://www.em.gov.bc.ca/Mining/Geolsurv/Publications/catalog/bcgeolmap.htm> [Apr 2005].

Mathews, W.H. (1980): Retreat of the last ice sheets in northeastern British Columbia and adjacent Alberta; Geological Survey of Canada, Bulletin 331, 22 p.

McMechan, M.E. (1990): Upper Proterozoic to Middle Cambrian history of the Peace River Arch: evidence from the Rocky Mountains; Bulletin of Canadian Petroleum Geology, v. 38A, p. 36–44.

Merriam, D.F. (1964): Use of trend-surface residuals in interpreting geological structure; Stanford Publications in Geological Science, v. 9, p. 686-692.

Merriam, D.F. and Lippert, R.H. (1966) Geologic model studies using trend-surface analysis; Journal of Geology, v. 74, p. 334-357.

Mossop, G.D. and Shetsen, I., comp. (1994): Geological atlas of the Western Canadian Sedimentary Basin; Canadian Society of Petroleum Geologists and Alberta Research Council, Special Report 4, 510 p.

Norford, B.S. (1990): Ordovician and Silurian stratigraphy, palaeogeography and depositional history of the Peace River Arch area, Alberta and British Columbia; Bulletin of Canadian Petroleum Geology, v. 38A, p. 45–54.

O'Connor, M. J. and Gretener, P. E. (1974): Differential compaction within the Woodbend Group of central Alberta; Bulletin of Canadian Petroleum Geology, v. 22, p. 269-304.

O'Connell, S.C. (1992): Parasequence development in a Lower Cretaceous transgressive systems tract: the Gething and Bluesky formations of northwestern Alberta, Canada; *in* Mesozoic of the Western Interior, Society of Economic Paleontologists and Mineralogists Theme Meeting, Ft. Collins, Colorado, Abstracts, p. 51.

O'Connell, S.C. (1994): Geological history of the Peace River Arch; *in* Geological Atlas of the Western Canada Sedimentary Basin, G.D. Mossop and I. Shetsen (comp.), Canadian Society of Petroleum Geologists and Alberta Research Council, Special Report 4, p. 431–438.

O'Connell, S.C., Dix, G.R. and Barclay, J.E. (1990): The origin, history and regional structural development of the Peace River Arch, Western Canada; Bulletin of Canadian Petroleum Geology, v. 38A, p. 4–24.

Olson, R.A., Eccles, D.R. and Collom, C.J. (1999): A study of potential co-product trace elements within the Clear Hills iron deposits, northwestern, Alberta; Alberta Energy and Utilities Board, EUB/AGS Special Report 8, 190 p.

Pană, D., Waters, E.J. and Grobe, M. (2001): GIS compilation of structural elements in northern Alberta, release 1.0; Alberta Energy and Utilities Board, EUB/AGS Earth Sciences Report 2001-01, 60 p.

Peirce, J.W., Ebner, E. and Marchand, N. (1998a): High resolution aeromagnetic interpretation over Sierra and Yoyo reefs, northeastern British Columbia; *in* Geologic Applications of Gravity and Magnetics: Case Histories, R.I. Gibson and P.S. Milligan (ed.)., American Association of Petroleum Geologists, Studies in Geology, no. 43, p. 93-101.

Peirce, J.W., Abercrombie, H.J., Depaoli, G.R., Goussev, S.A. and Charters, R.A. (1998b): Intrasedimentary magnetization by vertical fluid flow and exotic geochemistry; The Leading Edge, v. 17, p. 89-92.

Poulton, T.P., Tittemore, J. and Dolby, G. (1990): Jurassic stratigraphy, northwestern Alberta and northeastern British Columbia; Bulletin of Canadian Petroleum Geology, v. 38A, p. 159–175.

Price, R.A. (1994): Cordilleran tectonics and the evolution of the Western Canada Sedimentary Basin; *in* Geological Atlas of the Western Canada Sedimentary Basin, G.D. Mossop and I. Shetsen (comp.), Canadian Society of Petroleum Geologists and Alberta Research Council, Special Report 4, p. 13–24.

Read, W.A. and Merriam, D.F. (1966): Trend-surface analysis of stratigraphic thickness data from some Namurian rocks east of Stirling, Scotland; Scottish Journal of Geology, v. 2(1), p. 96-100.

Richards, B.C., Barclay, J.E., Bryan, D., Hartling, A., Henderson, C.M. and Hinds, R.C. (1994): Carboniferous strata of the Western Canada Sedimentary Basin; *in* Geological Atlas of the Western Canada Sedimentary Basin, G.D. Mossop and I. Shetsen (comp.), Canadian Society of Petroleum Geologists and Alberta Research Council, Special Report 4, p. 221–250.

Ross, G.M., Broome, J. and Miles, W. (1994): Potential fields and basement structure – Western Canada Sedimentary Basin; *in* Geological Atlas of the Western Canada Sedimentary Basin, G.D. Mossop and I. Shetsen (comp.), Canadian Society of Petroleum Geologists and Alberta Research Council, Special Report 4, p. 41–47.

Ross, G.M. and Eaton, R.J. (1999): Basement reactivation in the Alberta Basin: observational constraints and mechanical rationale; Bulletin of Canadian Petroleum Geology, v. 47, no. 4, p. 391–411.

Ross, G.M., McNicoll, V.J., Geldsetzer, H.J., Parrish, R.R., Carr, S.D. and Kinsman, A. (1993): Detrital zircon geochronology of Siluro–Devonian sandstones, Rocky Mountains, northeastern British Columbia; Bulletin of Canadian Petroleum Geology, v. 41, no. 3, p. 349–357.

Ross, G.M. and Villeneuve, M.E. (1997): U-Pb geochronology of stranger stones in Neoproterozoic diamictites, Canadian Cordillera: implications for provenance and ages of deposition; *in* Current Research, 1997-F, Geological Survey of Canada, p. 141–155.

Sikabonyi, L.A. and Rodgers, W.J. (1959): Paleozoic tectonics and sedimentation in the northern half of the west Canadian basin; Journal of the Alberta Society of Petroleum Geologists, v. 7, p. 193–216.

Smith D.G. (1994). Paleogeographic evolution of the Western Canada foreland basin; *in* Geological Atlas of the Western Canada Sedimentary Basin, G.D. Mossop and I. Shetsen (comp.), Canadian Society of Petroleum Geologists and Alberta Research Council, Special Report 4, p. 277–296.

Smith, D.G., Zorn, C.E. and Sneider, R.M. (1984): The paleogeography of the Lower Cretaceous of western Alberta and northeastern British Columbia in and adjacent to the Deep Basin of the Elmworth area; *in* Elmworth – Case Study of a Deep Basin Gas Field, J.A. Masters (ed.), American Association of Petroleum Geologists, Memoir 38, p. 153–172.

Stevenson, D.L. (1970): Trend-surface analysis of the structure of the Ste. Genevieve Limestone in the Effingham, Illinois, area; Illinois Geological Survey, Circular 454, 12 p.

Stott, D.E. (1973): Lower Cretaceous Bullhead Group between Bullmoose Mountain and Tetsa River, Rocky Mountain Foothills, northeastern British Columbia; Geological Survey of Canada, Bulletin 219, 228 p.

Williams, G.K. (1958): Influence of the Peace River Arch on Mesozoic strata; Journal of the Alberta Society of Petroleum Geologists, v. 6, p. 74–81.

Wright, G.N., McMechan, M.E. and Potter D.E.G. (1994): Structure and architecture of the Western Canada Sedimentary Basin; *in* Geological Atlas of the Western Canada Sedimentary Basin, G.D. Mossop and I. Shetsen (comp.), Canadian Society of Petroleum Geologists and Alberta Research Council, Special Report 4, p. 25–40.